Agglomeration and Defluidisation Behaviour of High-Sodium, High-Sulphur South Australian Lignite under Fluidised Bed Gasification Conditions

Daniel Peter McCullough

Thesis submitted for the degree of

Doctorate of Philosophy

School of Chemical Engineering

The University of Adelaide

January 2007

CHAPTER 5

EFFECT OF INORGANIC INTERACTIONS ON AGGLOMERATION AND DEFLUIDISATION DURING SPOUTED BED GASIFICATION OF A SOUTH AUSTRALIAN LIGNITE

5.1 Introduction

Findings from Chapter 4 indicate that defluidisation in a spouted bed gasifier is a result of uncontrolled particle growth. This particle growth is primarily due to operational factors, including high temperature and/or low superficial velocity, but is also affected by the proportion of steam in the gasification environment. While physical mechanisms for agglomeration and defluidisation were subsequently analysed, the chemical mechanisms behind the phenomena have yet to be established. The following chapter investigates the chemical reactions responsible for molten ash formation, and hence the cause of particle growth, during the gasification of high-sodium, high-sulphur lignite.

5.2 Objectives

The objectives of the work presented in this chapter include:

- Determining the distribution of the various inorganic species throughout the gasifier; and
- Identifying the key inorganic species in the ash contributing to particle growth.

These objectives will be achieved by conducting elemental and mineralogical analyses on targeted samples from each experiment. In particular, distribution of chemical species in

agglomerate structures will be analysed in order to determine the mode of formation of the various chemical compounds in the ash. Satisfying these objectives will provide data for comparison with findings by Kosminski (2001) regarding inorganic transformations in gasification ash that are typical for high-sodium, high-sulphur lignite. This knowledge will allow control strategies to be developed for achieving stable gasification of South Australian low-rank coal in a fluidised bed.

5.3 Ash behaviour and Agglomeration

5.3.1 Introduction

Determining the distribution of inorganics in the char throughout the gasification system is important in identifying key inorganic components involved in agglomeration. Inorganic matter from the coal becomes distributed throughout the system in a number of forms. These forms primarily include:

- Inorganic matter retained in the char;
- Cyclone dust;
- Agglomerates and coated mineral particles in the bed; and
- Deposited ash.

Bed char, cyclone dust, ash deposits, and agglomerates were collected at the completion of each run and subjected to elemental and mineralogical analysis. Bed char was sieved to exclude material exceeding 3.35 mm in diameter – predominantly large agglomerates in defluidisation experiments. Investigating the inorganic composition of each manifestation provides valuable clues to the inorganic reactions contributing to agglomeration and defluidisation. Each form is examined in the following sections.

For the purposes of analysis, experiments are separated into a number of different categories, which include:

- typical steam gasification runs (i.e. < 20 wt% of steam in the fluidising gas), which are subdivided into the following categories:
    - stable runs;
    - runs showing stable operation for the 4-hour operating period, with observed particle growth in the bed indicating possible defluidisation beyond 4 hours; and

- defluidisation runs.

- high steam gasification runs (i.e. approximately 90 wt% steam in the fluidising gas).

Grouping experiments in this way will aid in determining the effect of ash chemistry on behaviour of the bed in each case, in particular when referring to runs indicating possible defluidisation beyond the 4-hour operating period.

5.3.2 Bed Char Inorganics

The composition of inorganics in the bed char was found to vary based on whether agglomeration occurred, and also with the amount of steam in the fluidising gas. Results of bed char elemental analysis via X-ray Fluorescence (XRF) are presented in Figure 5.1, with distinction made between the four groups of experiments identified in Section 5.3.1. Analyses are reported in oxide form. Calculated data used to derive each plot is presented in Appendix D.

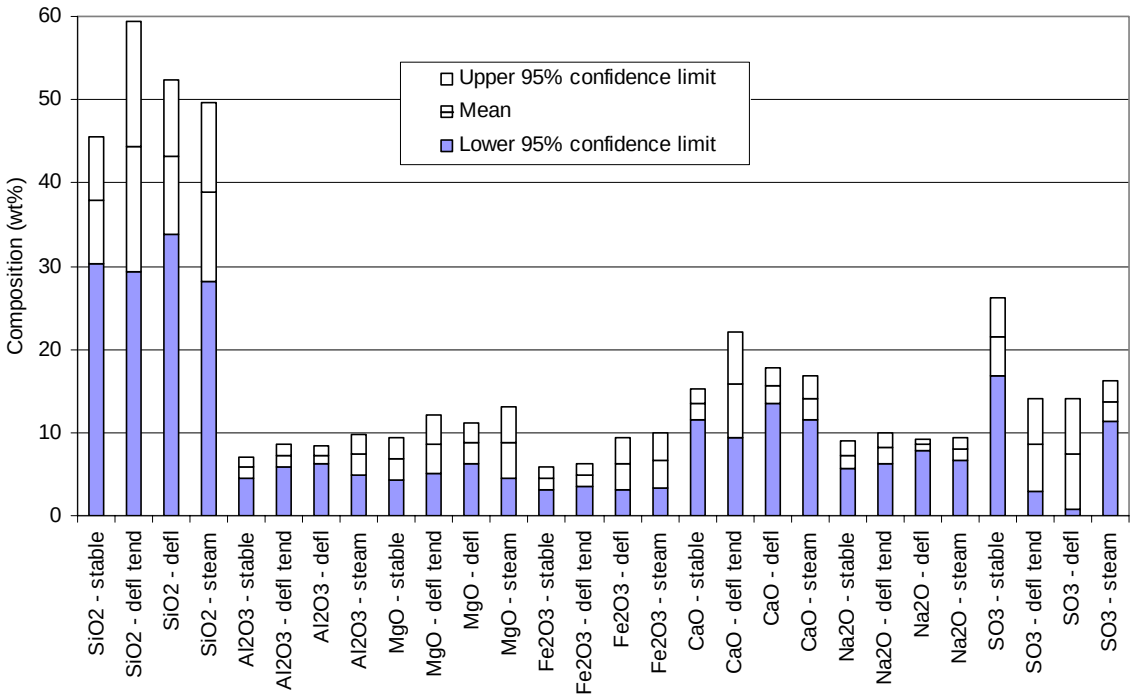

Figure 5.1. Averaged results of XRF analyses for (i) runs showing stable spouting for the duration of the run ('stable'); (ii) runs which showed no sign of defluidisation, but showed significant particle growth within the bed ('defl tend'); (iii) runs that showed defluidisation behaviour ('defl'); and (iv) runs operated with high (90 wt%) steam content in the fluidising gas ('steam').

Typical Steam Gasification Conditions

In general, SiO_2 dominates bed composition, with average compositions ranging from approximately 38 to 44 wt% of the total inorganic content across each experimental group. Furthermore, average SiO_2 composition of the bed char shows an increase from approximately 38 wt% in stable runs to 43 wt% in runs in which possible or actual defluidisation was identified. Although the averages indicate an increase, the 95% confidence limits calculated for the small number of experiments suggest that this increase is not statistically significant.

Other major elements, including Al_2O_3, CaO, MgO, Na_2O, and Fe_2O_3, are relatively consistent in bed char composition across the four groups of experiments. Only iron shows a significant increase from stable to defluidisation runs: average of 4.5 wt%, with a standard deviation of 0.7 wt%, in stable runs; 4.9±0.7 wt% in stable runs that showed particle growth; and 6.3±1.6 wt% in runs that defluidised. In comparison, the iron composition of the raw coal ash is approximately 4.1 wt%, indicating enrichment of iron in the gasification ash, particularly in the defluidisation runs.

The reason for the elevated content of iron in the bed char under certain conditions appears related to corrosion of the stainless steel spouted bed vessel. In defluidisation runs, the elevated content of iron coincides with an increased content of nickel and chromium in the bed inorganic matter. These species are common inclusions in stainless steel, but not present in coal to a significant extent. Instead, chromium is present in beds of defluidisation runs in quantities up to 14,000 ppm, while nickel is present up to 6,000 ppm. As shown in Figure 5.2, the compositions of nickel and chromium vary relatively linearly with iron, suggesting that these elements enter the ash via an independent source to the coal. Note that the Cr and Ni contents in the char of stable spouting runs remain relatively constant with increasing Fe content, remaining below 600 ppm Cr, and 200 ppm Ni, for Fe contents up to 5.0 wt% of the char ash. Only at approximately 5.4 wt% Fe does the Ni and Cr contents of the char from stable spouting runs increase to 930 ppm and 3,250 ppm, respectively. The relatively constant contents of Cr and Ni in char from stable spouting runs suggests the possibility that the deposition of molten ash on the walls of the reactor facilitates leaching of steel components into the ash.

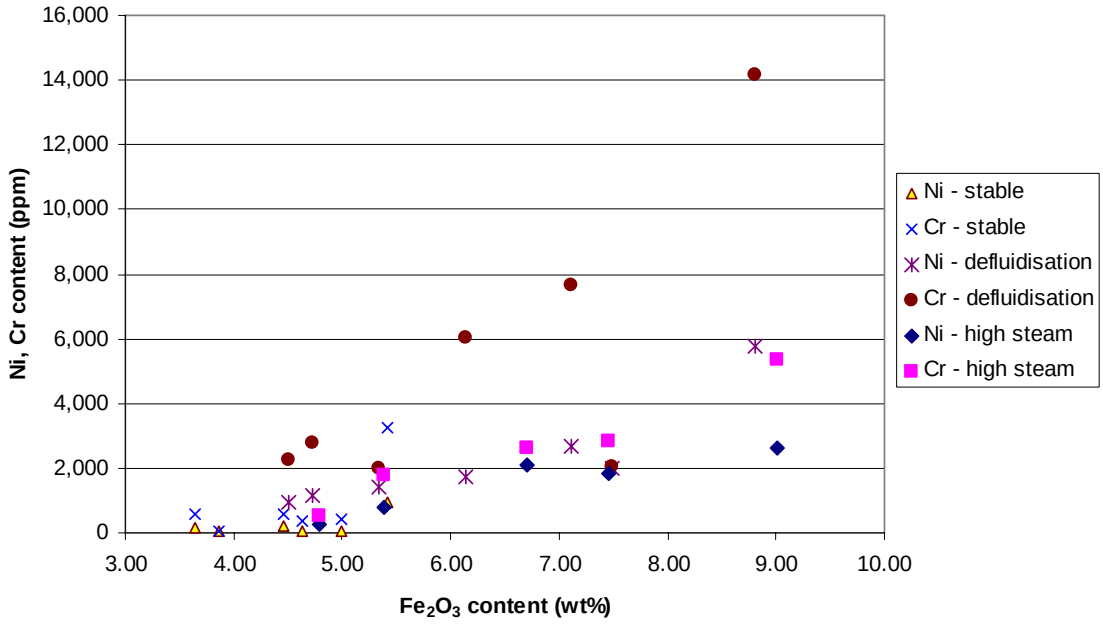

Figure 5.2. Variation of Fe_2O_3 with trace elements Cr and Ni in bed char samples. Results for agglomeration and defluidisation runs, and high steam runs, are shown.

Sulphur shows the most significant variation in bed char composition from stable to defluidisation runs. Sulphur is present at 21.5±2.4wt% under stable conditions, 8.6±2.8wt% in stable runs exhibiting significant particle growth, and 7.4±3.3wt% under defluidisation conditions. The reason for this trend may be due to the temperature of the bed in each case, with agglomeration runs generally being operated at higher temperatures than stable spouting runs. Figure 5.3 shows the sulphur content of each char bed versus the corresponding maximum average bed temperature. This shows that all of the stable runs, ranging from 789°C to 872°C maximum bed temperature, have sulphur contents ranging from 18.7 to 25.3 wt%. On the other hand, runs in which particle growth was observed and/or defluidisation occurred were operated at 844 to 967°C, and possessed sulphur contents in the range 1.3 to 11.5 wt%. These trends suggest that the higher temperatures result in more sulphur leaving the bed in gaseous form, although this was not confirmed by analysis of the flue gas.

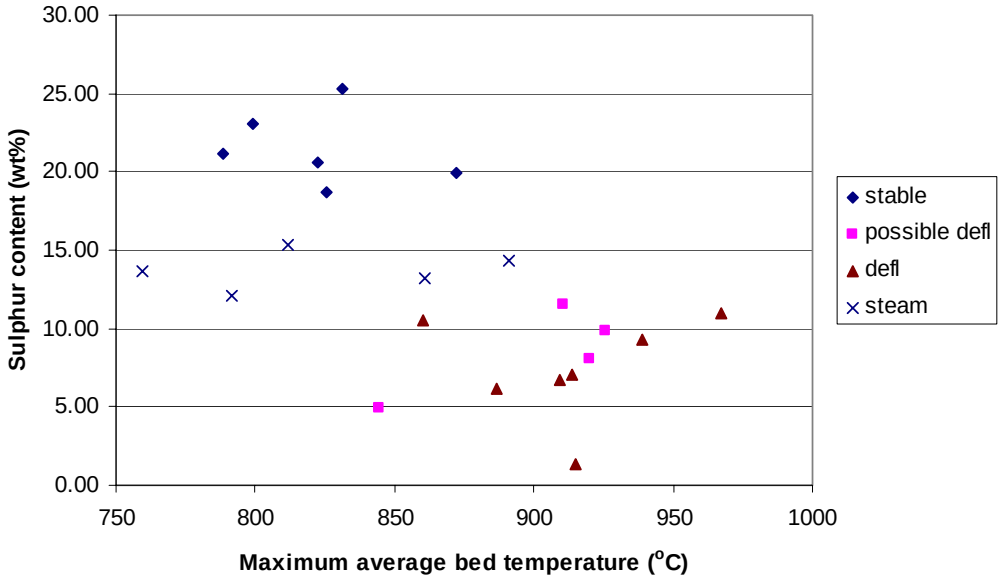

Figure 5.3. Variation of bed char sulphur content versus maximum average bed temperature. Runs distinguished by stable runs; stable runs exhibiting particle growth; defluidisation runs; and high S/F runs.

The mineralogy of each char bed was determined using X-ray Diffraction (XRD), and is shown in Table 5.1. The minerals identified using XRD were also assigned semi-quantitative descriptors based on the approximate prevalence of each mineral in the field of analysis. These descriptors include:

- Dominant/co-dominant, indicating the phase (or sum of co-dominant phases) represents 60% or greater of all the mineral species identified;
- Sub-dominant, indicating the phase (or sum of sub-dominant phases) represents 20 to 60% of the mineral phases identified;
- Minor, indicating the phase (or sum of minor phases) represents 5 to 20% of the mineral phases identified; and
- Trace, indicating the phase (or sum of trace phases) represents less than 5% of all identified mineral species.

Mineral forms in the bed char show a tendency towards silicate formation as defluidisation begins to impact upon gasifier operation. Quartz is the dominant mineral detected in each char bed. Other mineral phases vary in quantity, reflecting the elemental analysis in Figure 5.1.

Table 5.1. XRD analysis results of char beds from all experiments.

Run	Dominant/ Co-dominant	Sub-dominant	Minor	Trace
B01	Quartz	Gehlenite	Oldhamite, anhydrite, amorphous	Sodalite, halite, nepheline, magnetite
B02	Quartz, gehlenite-akermanite	-	Augite, anhydrite, monticellite, amorphous	Thenardite, hematite
B03	Quartz	Gehlenite	Oldhamite, anhydrite, magnetite	Halite, nepheline, augite, mayenite[1], monticellite[1]
B05	Quartz	Gehlenite	Oldhamite, anhydrite, magnetite, amorphous, augite	Halite, nepheline, monticellite[1]
B06	Quartz	-	Oldhamite, anhydrite, gehlenite	Halite, nepheline, magnetite, sodalite, monticellite[1]
B07	Quartz	Gehlenite	Oldhamite, magnetite, monticellite[1]	Anhydrite, halite, nepheline, sodalite, augite, mayenite[1]
B08	Quartz	Oldhamite	Anhydrite, gehlenite-akermanite, periclase	Amorphous, augite, monticellite, mayenite, magnetite
B09	Quartz	-	Anhydrite, monticellite, oldhamite, amorphous	Gehlenite-akermanite, augite, periclase
B10	Quartz	Oldhamite, periclase	Augite, amorphous	Anhydrite, gehlenite-akermanite, monticellite, mayenite, sodalite
B11	Quartz	Oldhamite, periclase	Anhydrite, monticellite, amorphous	Augite, gehlenite-akermanite, mayenite, sodalite
B12	Quartz, gehlenite	-	Periclase, augite	Anhydrite, magnetite, nepheline, monticellite, sodalite[1]
A01	Quartz	Gehlenite, augite	Oldhamite	Nepheline, monticellite, thenardite
A02	Quartz	Gehlenite, augite	Nepheline	Thenardite
A03	Quartz, gehlenite	Augite	Nepheline, forsterite, magnetite	Hematite, monticellite
A04	Quartz	Gehlenite, augite	Nepheline, magnetite	Monticellite, thenardite, hematite, anhydrite
A05	Quartz	Augite	Gehlenite, magnetite	Nepheline, thenardite, hematite, anhydrite
A06	Quartz	Augite	Gehlenite, magnetite, nepheline, calcite	Thenardite, hematite, anhydrite
C01	Quartz, amorphous, oldhamite	-	Periclase, gehlenite-akermanite	Anhydrite, magnetite, nepheline, monticellite
C02	Quartz	Oldhamite	Anhydrite, amorphous	Periclase, magnetite, gehlenite-akermanite, nepheline
C03	Quartz	Oldhamite	Periclase, amorphous	Anhydrite, magnetite, gehlenite-akermanite, nepheline, monticellite
C04	Amorphous	-	Quartz, periclase, oldhamite	Anhydrite, magnetite, gehlenite-akermanite, nepheline
C05	Quartz, oldhamite	-	Anhydrite, periclase, amorphous, calcite	Magnetite, gehlenite-akermanite, nepheline, monticellite, hematite

[1] Possible detection of species.

Under stable conditions, oldhamite (CaS) is one of the major minerals present in the bed, at sub-dominant to minor proportions. Anhydrite ($CaSO_4$) is also present in minor to trace

proportions to make up the sulphur minerals in the bed char. Gehlenite/Akermanite ($Ca_2(Al,Mg)_2SiO_7$), monticellite ($CaMgSiO_4$) and augite ($Ca(Mg,Fe)Si_2O_6$) are the main silicate phases present. Gehlenite/Akermanite is present in sub-dominant proportions in two runs, and in trace amounts in the remainder. Monticellite and augite are present in minor to trace quantities. Calcium is also detected in trace quantities as mayenite ($Ca_{12}Al_{14}O_{33}$). Periclase (MgO) is present in sub-dominant quantities in two runs, and in trace amounts in one other run. This suggests that magnesium is remaining largely unreacted at the temperatures of the stable runs. Iron is also detected in minor to trace amounts as magnetite (Fe_3O_4).

Sodium is detected in trace amounts only, in the forms of sodalite ($Na_4Al_3Si_3O_{12}Cl$), nepheline ($NaAlSiO_4$) and halite (NaCl). The presence of sodalite indicates a potential intermediate product between halite and nepheline. As shown by Kosminski (2001), halite reacts with aluminosilicates from clay to form nepheline. Nepheline is a higher melting point mineral than sodium disilicate, and the preferred mineral form of sodium to avoid agglomeration and defluidisation. A possible reaction mechanism is as follows:

$$4NaCl + 3AlSiO_4 \rightarrow Na_4Al_3Si_3O_{12}Cl + 1.5Cl_2 \quad (5.1)$$

$$Na_4Al_3Si_3O_{12}Cl \rightarrow 3NaAlSiO_4 + NaCl \quad (5.2)$$

No sodium disilicate is detected within any sample. However, it is well documented that sodium silicate species can exist as non-crystalline glasses. In particular, mixtures containing silica contents greater than the sodium disilicate-quartz eutectic composition are difficult to crystallise from a glass state (Morey and Bowen, 1924). The presence of a glass phase in the bed char would produce an amorphous XRD pattern indistinguishable from the XRD pattern produced by the organic fraction of the char. Note in Table 5.1 that an amorphous phase was detected in minor amounts in a number of char samples, which would consist mostly of the organic fraction of the char, but may also include glass fractions of the ash.

Runs that did not show defluidisation behaviour, but indicated significant bed particle growth, show a higher content of silicates and a reduced quantity of sulphur minerals in the bed char than under stable conditions. Oldhamite was only detected in two runs in minor amounts. Sulphate content varied depending on the conditions of the run. Under ‘low’ steam gasification runs (i.e. 10 to 13 wt% steam in the fluidising gas, in Runs A01 to A06), thenardite (Na_2SO_4) was detected in trace amounts. Under ‘medium’ steam gasification

runs (i.e. 14 to 17 wt% steam in the fluidising gas, in Runs B01 to B12), anhydrite was detected in minor to trace amounts. This suggests that the more oxidising conditions of the low steam gasification runs was conducive to sodium reacting with sulphur in addition to silicates.

Gehlenite was detected in co-dominant (i.e. sum with quartz greater than 60% of mineral phases) to sub-dominant amounts in bed char from 'possible defluidisation' runs, being the most prevalent of the silicates in the char. Augite was detected in sub-dominant amounts in low steam gasification runs, with minor to trace amounts detected in medium steam gasification conditions. Augite formation appears to be related primarily to temperature, sub-dominant amounts produced in the runs exceeding 920°C maximum bed temperature (Runs A01 and A02), with minor amount detected at 910°C (Run B12), and trace amounts detected at 844°C (Run B03). This is reflected in periclase formation, with only minor amounts detected in one run (Run B12). Monticellite was detected only in trace amounts.

Sodium minerals were more prevalent in the 'possible defluidisation' runs compared to stable runs, in particular under low steam gasification conditions. Nepheline was present in minor to trace amounts under low steam gasification conditions (refer to Runs A01 to A06). Under these conditions, no chloride minerals were detected. As mentioned previously, thenardite was also present in trace amounts under these conditions. Under medium steam gasification conditions (refer to Runs B01 to B12), nepheline was only present in trace amounts, with both halite and sodalite also present in trace amounts. Kosminski (2001) found that sodium in chloride form only reacts with silica in a steam atmosphere. Thus, the higher S/F ratios used in the medium steam gasification runs may result in sodium chloride reacting more extensively with silica in preference to aluminosilicate. This condition would lead to the preceding observation of smaller amounts of sodium aluminosilicate under the medium steam in comparison to low steam gasification conditions, with more of the sodium present in the amorphous phase.

Mineral composition of char beds from agglomeration and defluidisation runs was similar to those from potential defluidisation runs, with experimental conditions appearing to impact upon the various mineral forms and quantities produced. Oldhamite was not detected in any experiment run at low steam gasification conditions, but was detected in sub-dominant to minor amounts in runs under medium steam gasification conditions.

Anhydrite was detected only in trace amounts under the high temperature conditions (> 900°C) of the low steam runs, but detected in minor to trace quantities under the more typical steam conditions of Runs B01 to B12. Thenardite was also present in trace quantities in 3 of 4 low steam gasification runs, while only present in one medium steam gasification run (i.e. Run B02, at 914°C).

Gehlenite/akermanite was present in dominant to minor quantities under all conditions, with high quantities coinciding with higher temperature conditions i.e. dominant in Runs A03 (939°C) and B02 (914°C), and minor in B08 (887°C). Augite was detected in dominant quantities in low steam gasification conditions, while present in only minor to trace quantities in medium steam gasification experiments (i.e. Runs B01 to B12). Conversely, monticellite was present in trace to non-detected quantities under low steam conditions, and minor to trace quantities under medium steam gasification runs. The detections of these silicates suggest that augite formation is preferred over monticellite at higher temperature and/or lower steam conditions. The reason for this is unclear, but may be due to iron entering the silicate matrix more readily at higher temperatures, thereby forming augite instead of monticellite.

Sodium mineral formation exhibits a major difference between possible and actual defluidisation runs. No halite, or any other chlorine compound, is detected in any of the beds, suggesting that the majority of chlorine in the coal is volatilised at these gasification conditions. Nepheline on the other hand is detected in similar quantities to the possible defluidisation runs, at minor to trace levels under low steam conditions, yet only in one medium steam run at trace conditions. In addition, an amorphous phase was detected in minor to trace quantities. While this amorphous phase is likely to be mostly organic fraction of the char bed, this raises the possibility that some of the amorphous phase is sodium silicate glass. This may be an indication that sodium disilicate-quartz eutectic formation is occurring, resulting in the agglomeration and defluidisation observed in the relevant runs.

<u>High Steam Gasification Conditions</u>

Bed char from high steam gasification conditions show several distinct differences in composition to those collected under typical steam gasification conditions (refer to Figure 5.1). Sulphur composition of the bed was greater than either possible or actual

defluidisation runs, with an average composition of 13.7 wt% and a standard deviation of 1.2 wt%, although was still reduced in comparison to stable runs under typical steam gasification conditions. SiO_2 was also reduced in comparison to defluidisation runs, at 38.9±5.4 wt%. Iron content of the bed char was greater than either stable or possible defluidisation runs from typical steam gasification runs, but was consistent with actual defluidisation runs, at 6.7±1.7 wt%. Again, iron content in the char under high steam gasification conditions appears to be related to leaching of stainless steel from the reactor, with nickel and chromium content significantly higher than expected for coal ash composition (refer to Figure 5.2). Leaching of the steel components in the high steam gasification runs is expected, given the high moisture, highly reducing conditions provided by these gasification conditions. Other major elements in the char were consistent with runs from typical steam gasification conditions.

Referring to Table 5.1, oldhamite was detected in the bed char in dominant to sub-dominant quantities under high steam gasification conditions, even though agglomerates were collected from each run. Conversely, oldhamite was detected in minor amounts in the lowest temperature run for the experimental set, which was the only run that did not yield agglomerates (i.e. Run C04). Anhydrite was present in a more constant composition across the experiments, at minor to trace quantities.

Silicate formation was a major difference from low to high steam conditions in the char beds. Gehlenite/akermanite was present in trace quantities (one run in minor quantity), while monticellite was also present in trace amounts, but only above approximately 800°C maximum bed temperature, and not detected below this temperature. No augite was present in the bed char. Nepheline was detected in every bed, but only in trace quantities. No other sodium species was detected in the char.

Magnetite (Fe_3O_4) was detected in the bed in trace quantities throughout the runs, possibly reflecting the iron content from the stainless steel reactor vessel. Hematite (Fe_2O_3), at a higher oxidation state than magnetite, was also detected in trace quantities, but only at the highest temperature run (C05 at 891°C). Periclase was detected in minor quantities (1 run as trace) under high steam conditions, a contrast to agglomeration and defluidisation runs from typical steam gasification runs, which showed no detection of periclase. Evidence of calcite ($CaCO_3$) was also detected in minor amounts in one run (C05). The presence of

both periclase and calcite in significant amounts suggests that reaction rates of calcium and magnesium are not as high in high steam conditions as for typical steam gasification conditions.

5.3.3 Cyclone Dust Inorganics

Inorganics in the cyclone dust varied based on the occurrence of agglomeration and the amount of steam in the gasification environment, as for bed char. Figure 5.4 shows the corresponding elemental analysis of cyclone dust.

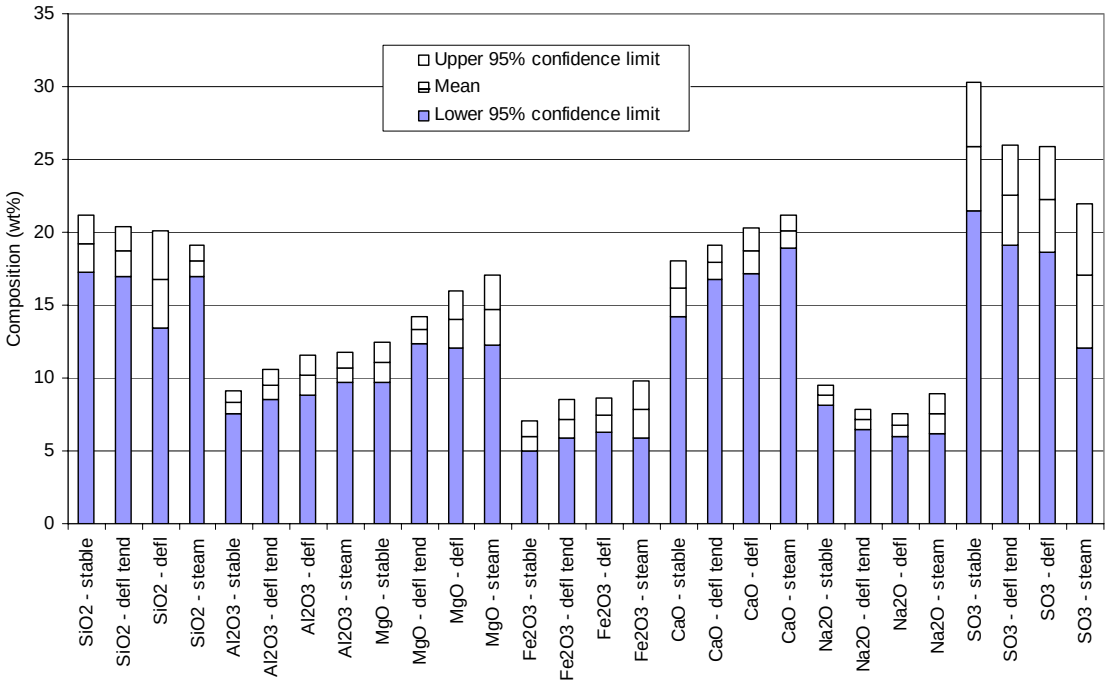

Figure 5.4. Elemental composition of cyclone dust from stable runs that showed no defluidisation behaviour; stable runs that showed significant bed particle growth; runs which defluidised; and runs from high steam gasification conditions.

Typical Steam Gasification Conditions

Silica and sulphur form the major components of the inorganic phase in the cyclone dust (refer to Figure 5.4). Average SiO_2 content in cyclone dust varies between 17 to 19 wt%. This is significantly lower than silica composition of the bed char, indicating that silica is not elutriated from the bed to a significant extent. The average SiO_2 composition decreases marginally from approximately 19 wt% under stable conditions to 17 wt% under agglomeration and defluidisation conditions. Sulphur composition shows a minor

decreasing trend in the cyclone dust, from an average of 25.9 wt%, with a standard deviation of 2.2 wt%, under stable conditions, to 22.5±1.7 wt% in the dust from stable runs exhibiting particle growth, and 22.3±1.8 wt% under defluidisation conditions.

The preceding analyses further serve to indicate that increasing amounts of silica are retained in the bed as agglomeration becomes an issue to operation. The relatively higher sulphur content in the cyclone dust in comparison to the char beds of defluidisation and possible defluidisation runs suggests that much of the sulphur in these cases is elutriated from the bed rather than take a major part in agglomerate formations. However, the corresponding decrease of sulphur in the cyclone dust suggests that the sulphur is not being elutriated from the bed in larger amounts from stable to defluidisation runs. The possibility exists that sulphur is being released from the bed into the gaseous phase rather than in solid form in the ash, but this cannot be confirmed by flue gas analysis. The other major elements (i.e. Al_2O_3, CaO, MgO, Na_2O, and Fe_2O_3) are marginally enriched in the cyclone dust compared to char bed material, although this is expected with the reduced content of SiO_2 in the cyclone dust.

Compositions of the species Al_2O_3, CaO, MgO and Fe_2O_3 tend to increase from stable runs to defluidisation runs under typical steam gasification conditions for all of these elements. In contrast, Na_2O shows a decrease from stable to defluidisation runs. However, the compositions of these species are affected by the behaviours of the more prevalent species in the cyclone dust, namely sulphur and silicon. Thus, the compositions of the remaining elements were recalculated after removing the silica and sulphur compositions from each set of analyses, as shown in Figure 5.5. This figure indicates that the major elements (except sodium) remain proportionally constant in cyclone dust under all types of conditions. However, sodium decreases from a corrected average of 17.5 wt%, with a standard deviation of 0.7 wt%, in stable runs, to 11.8±0.7 wt% under defluidisation conditions. This suggests that as silica is increasingly retained in the bed due to agglomerate formation, sodium is also retained. Note however that a corresponding increase of sodium in bed char is not specifically indicated in the results.

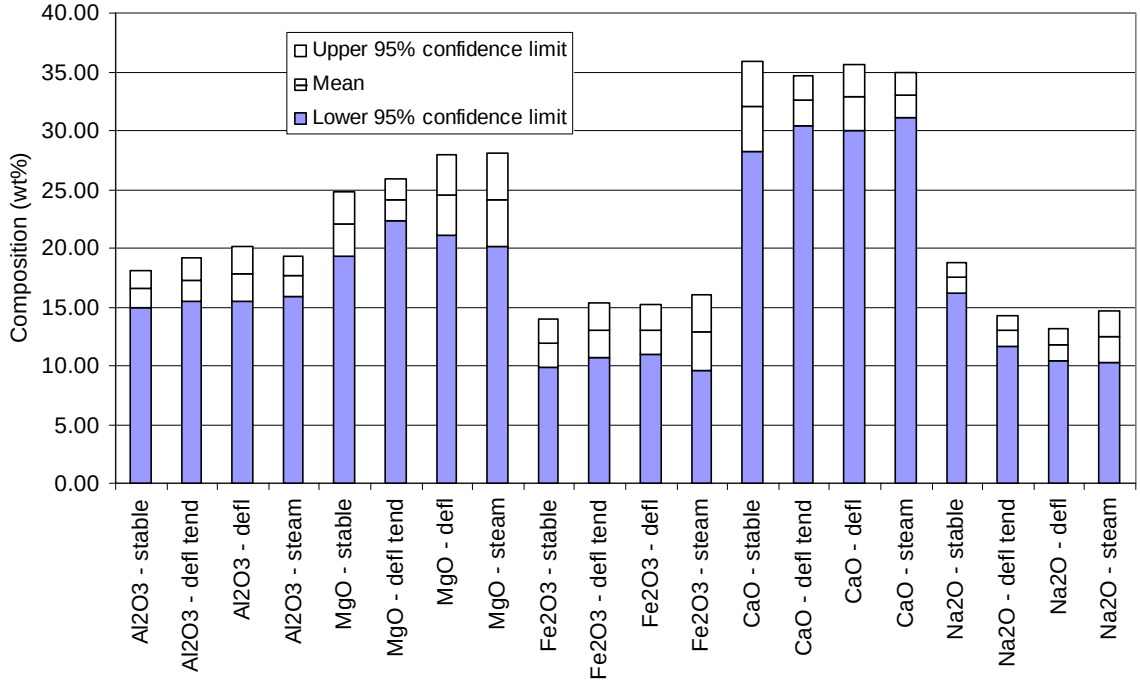

Figure 5.5. Major elemental compositions of cyclone dust, normalised against SiO_2 and SO_3.

Minerals in the cyclone dust show a tendency towards silicate formation as agglomeration and defluidisation occurs. The mineralogy of cyclone dust compositions is shown in Table 5.2. Cyclone dust from stable runs is dominated by an amorphous phase, constituting the organic fraction of the char. Compositions between cyclone and bed char are generally similar, with oldhamite detected in sub-dominant to minor amounts, gehlenite detected in sub-dominant to minor amounts, and sodium minerals such as nepheline and halite in trace amounts, with one run (B01) containing halite in minor quantities. Quartz content is the major difference between bed and cyclone matter, detected in minor to trace amounts only, suggesting further that quartz has a low elutriation rate from the bed. Sodalite is also not detected in the cyclone dust, suggesting that reaction between halite and aluminosilicate is only occurring within the higher temperature conditions of the bed.

Table 5.2. XRD analysis results of cyclone dust samples from all experiments.

Run	(Co-)Dominant	Sub-dominant	Minor	Trace
B01	Amorphous	Gehlenite, periclase	Quartz, oldhamite, anhydrite, halite	Nepheline, magnetite, mayenite[1], monticellite[1]
B02	Amorphous	-	Periclase, oldhamite, calcite	Quartz, anhydrite, magnetite, halite, nepheline[1], qypsum
B03	Amorphous	Gehlenite, periclase	Quartz, oldhamite, anhydrite, magnetite	Halite, nepheline, mayenite[1], monticellite[1]
B05	Amorphous	Gehlenite, periclase	Quartz, anhydrite, magnetite	Oldhamite, halite, nepheline, mayenite[1], monticellite[1]
B06	Amorphous	Periclase	Quartz, anhydrite, gehlenite, magnetite	Oldhamite, halite, nepheline, eugsterite, monticellite[1]
B07	Amorphous	Gehlenite, periclase	Quartz, oldhamite, anhydrite	Halite, nepheline, magnetite, monticellite[1]
B08	Amorphous	Gehlenite, periclase	Oldhamite, anhydrite	Quartz, halite, nepheline, magnetite, mayenite[1], monticellite[1]
B09	Amorphous	-	Quartz, anhydrite, periclase, oldhamite	Magnetite, halite, monticellite
B10	Amorphous	Oldhamite	Periclase	Quartz, anhydrite, halite, nepheline, mayenite[1]
B11	Amorphous	Oldhamite	Quartz, periclase	Anhydrite, halite, monticellite, nepheline
B12	Amorphous, gehlenite		Quartz, anhydrite, periclase	Magnetite, halite, mayenite, nepheline, monticellite, oldhamite
A01	Gehlenite, amorphous	-	Periclase, oldhamite	Quartz, anhydrite, halite, mayenite, nepheline, monticellite
A02	Gehlenite, amorphous	-	Periclase, oldhamite	Quartz, anhydrite, halite, mayenite, nepheline, monticellite
A03	Gehlenite, amorphous	-	Quartz, anhydrite, periclase, oldhamite	Magnetite, halite, mayenite, nepheline, monticellite
A04	Anhydrite, gehlenite, amorphous	-	Quartz, periclase, oldhamite	Magnetite, halite, mayenite, nepheline, monticellite, gypsum
A05	Gehlenite, amorphous	-	Quartz, anhydrite, periclase, oldhamite	Magnetite, halite, mayenite, nepheline, monticellite
A06	Gehlenite, amorphous	-	Anhydrite, periclase, oldhamite	Quartz, magnetite, halite, mayenite, nepheline, monticellite
C01	Amorphous	Calcite	Quartz, nepheline	Magnetite, gehlenite-akermanite, gypsum, aragonite, vaterite
C02	Amorphous	Calcite	Quartz, nepheline	Magnetite, gehlenite-akermanite, gypsum, aragonite, vaterite
C03	Amorphous	Calcite	Nepheline	Quartz, anhydrite, magnetite, gehlenite-akermanite, gypsum, aragonite, vaterite
C04	Amorphous	Calcite	Nepheline, gypsum	Quartz, anhydrite, magnetite, gehlenite-akermanite, aragonite, vaterite
C05	Amorphous, calcite	-	Nepheline, aragonite	Anhydrite, gehlenite-akermanite, gypsum, vaterite

[1] Species is possibly present in trace amounts based on X-ray diffractograms, but cannot be confirmed with certainty due to the small quantity of phase present.

In stable runs exhibiting significant particle growth, cyclone dust compositions are similar to char bed compositions, with the exception of quartz dominance. Interestingly, quartz content in low steam gasification conditions (i.e. 10 to 13 wt% steam content in the fluidising gas, from Runs A01 to A06) appears lower than that for the medium steam gasification runs (i.e. 14 to 17 wt% steam in the fluidising gas, in Runs B01 to B12); quartz is present at trace quantities under low steam conditions, and minor quantities under medium steam gasification conditions. There also appears to be a greater content of unreacted magnesium in the cyclone under the medium steam conditions, at sub-dominant to minor quantities, compared with only minor quantities at low steam conditions. These differences indicate that more quartz is reacting to form silicates under the lower steam gasification conditions, thereby remaining in the bed rather than becoming elutriated from the reactor. Thus, it can be inferred that particle growth in the bed is affected by the formation of silicates and aluminosilicates in the ash.

Cyclone dust composition for agglomeration and defluidisation runs is again similar to bed char composition, with a number of exceptions. Quartz is present only in minor to trace amounts. Periclase is present in sub-dominant to minor quantities under medium steam gasification conditions, while present in minor quantities only in the low steam gasification runs. Halite is also present in trace quantities for all runs. Both halite and periclase represent unreacted minerals elutriated from the bed, with less periclase in particular found under the higher temperature conditions, suggesting more complete reaction in the bed.

<u>High Steam Gasification Conditions</u>

A significant amount of unreacted calcium is present in the cyclone dust from high steam experiments. Calcite is present in dominant to sub-dominant quantities in the cyclone dust, with vaterite and aragonite (both forms of $CaCO_3$) also present in trace quantities. No CaS is detected in any of the cyclone samples, but anhydrite and gypsum ($CaSO_4.2H_2O$) are both detected in trace amounts. Gehlenite/akermanite was only detected in trace amounts for all high steam runs. No other calcium silicate minerals were detected in the cyclone dust. The significant levels of unreacted calcium compounds, and the corresponding low quantities of calcium silicate minerals in the bed, infers that calcium is being elutriated from the bed instead of reacting with silica to form silicates and aluminosilicates. Implied by this is that high melting temperature calcium rich compounds are not forming to as large an extent as in typical gasification conditions, which indicates that other silicate

compounds, which are not detectable by XRD (i.e. amorphous compounds), may be forming in preference.

Nepheline is present in minor quantities in the cyclone dust, higher than the amount of nepheline retained in the bed material (i.e. trace). This again infers that nepheline is preferentially being elutriated from the bed rather than taking part in bed ash reactions. With this high melting point sodium compound being removed from the char ash chemistry, this suggests the possibility that sodium retained in the char may be present in another form, which would likely be responsible for the formation of the molten phase in the ash that contributes to particle growth.

5.3.4 Ash Agglomerates and Coated Mineral Particles

Agglomerates were obtained by sieving each char bed and retaining the size fraction greater than 3.35 mm. These agglomerates were subjected to elemental and mineralogical analyses, which are shown in Figure 5.6 and Table 5.3, respectively. Agglomerate analyses are differentiated with respect to the experimental set i.e. 10 to 13 wt% steam in the fluidising gas (Runs A01 to A06); 14 to 17 wt% steam in the fluidising gas (Runs B01 to B12), and 90 wt% steam gasification (Runs C01 to C05). In each case, agglomerate composition is dominated by silica, with other elements varying depending on the gasification environment used.

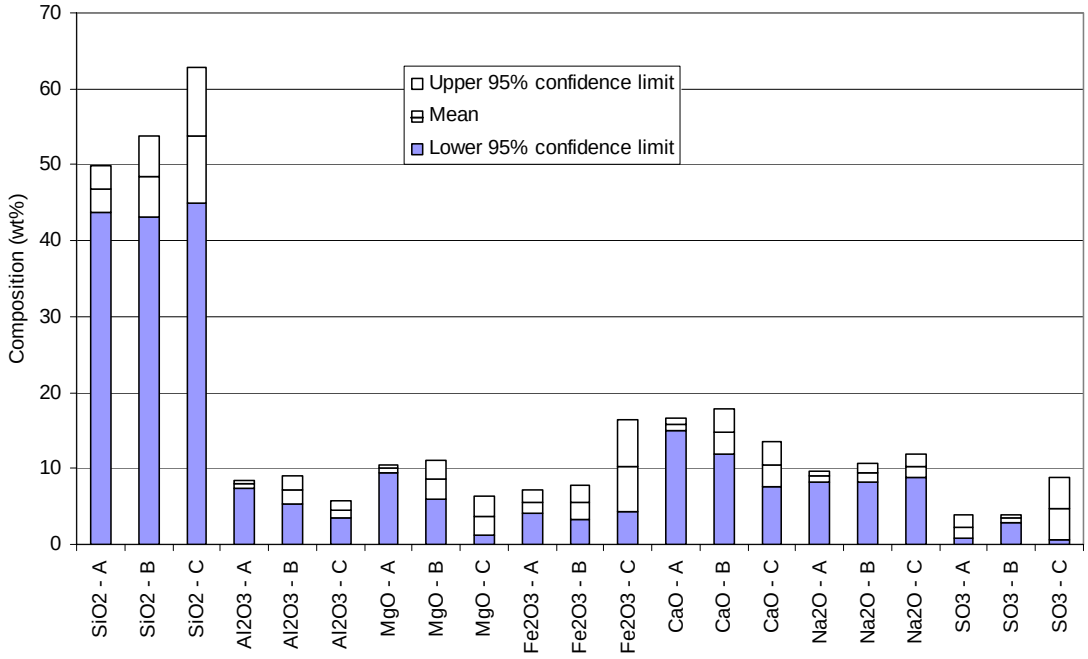

Figure 5.6. Elemental composition of agglomerates from gasification runs operating with 10 to 13 wt% steam in the fluidising gas ('A'); gasification runs operating with 14 to 17 wt% steam in the fluidising gas ('B'); and gasification runs operating with 90 wt% steam in the fluidising gas ('C').

Table 5.3. XRD analysis results of agglomerate samples from all experiments.

Run	(Co-)Dominant	Sub-dominant	Minor	Trace
B02	Gehlenite-akermanite	Augite	Quartz, monticellite, thenardite	Anhydrite, periclase, oldhamite[1], nepheline
B05	Quartz	Gehlenite	Magnetite, augite, amorphous	Oldhamite, anhydrite, periclase, monticellite[1], lime
B08	Quartz	Gehlenite	Augite, lime, amorphous	Oldhamite, anhydrite, periclase, magnetite, monticellite[1], magnesite[1]
A03	Quartz, gehlenite	-	Nepheline, augite, forsterite, magnetite	Thenardite, hematite
A04	Gehlenite	Quartz, forsterite	Nepheline, augite, magnetite, monticellite	-
A05	Quartz, gehlenite	Forsterite	Nepheline, augite, magnetite	-
A06	Quartz, gehlenite	Augite, forsterite	Nepheline, magnetite	-
C01	Quartz, amorphous	-	Magnetite, gehlenite-akermanite, oldhamite, augite	Nepheline, monticellite
C02	Quartz, amorphous	-	Magnetite, gehlenite-akermanite, augite	Nepheline, oldhamite, hematite
C03	Quartz	-	Anhydrite, magnetite, amorphous	Thenardite, gehlenite-akermanite, nepheline, oldhamite, augite, hematite
C05	Quartz	Amorphous	Anhydrite, magnetite, oldhamite	Periclase, gehlenite-akermanite, nepheline, monticellite, augite, hematite, lime

[1] Possible detection of species.

Silica appears to increase from low steam (10 to 13 wt% steam in the fluidising gas) to high steam (90 wt% steam) gasification conditions; silica is present at 46.9±1.5 wt% under low steam conditions, 48.5±2.7 wt% under medium steam gasification environments (i.e. 14 to 17 wt% steam in the fluidising gas), and 53.8±4.5 wt% under high steam conditions. Note however that as the average composition increases, the variation in results also increases, so statistically the differences from low to high steam environment are not substantial. Calcium, magnesium, and aluminium contents vary significantly from typical gasification conditions to high steam gasification. Magnesium composition under medium steam gasification experiments is 8.6±1.3 wt%, compared to 3.7±1.3 under high steam conditions. Similarly, calcium composition is 14.9±1.5 wt% under medium steam gasification experiments, compared with 10.5±1.5 wt% under high steam gasification. Aluminium content also decreases, from 7.2±1.0 wt% under medium steam gasification conditions, to 4.6±0.6 wt% under high steam gasification conditions. These differences correspond with the compositional changes observed in bed char and cyclone composition, indicating less reaction of calcium and magnesium, and subsequently less aluminosilicate formation, under the higher steam, lower temperature conditions.

Iron content shows a significant increase from typical steam gasification (<20 wt% steam in the fluidising gas) to high steam gasification environments, from 5.6±1.1 wt% under typical steam gasification conditions, to 10.3±3.0 wt% under high steam gasification conditions. Note that nickel and chromium compositions of the agglomerates are also high – as for the bed char composition – indicating this higher content of iron is due to enhanced leaching of iron from the stainless steel reactor. The higher moisture gasification environment is the likely cause of the higher degree of iron corrosion indicated by the presence of Ni and Cr in the ash.

Sulphur shows a marginal increase from low steam to high steam gasification conditions; at 2.3±0.8 wt% under low steam gasification conditions; 3.4±0.2 wt% under medium steam gasification conditions; and 4.7±2.1 wt% under high steam gasification conditions. This trend is reflected in bed char composition examined previously, which showed that sulphur compounds, such as CaS and $CaSO_4$, were slightly enriched in the bed char of medium steam gasification conditions from that of low steam gasification conditions, and even more so in char produced under high steam conditions. This indicates that sulphur may

have a role in the agglomeration mechanism, even if not dominating the agglomerate composition.

Sodium remains relatively consistent across the various gasification conditions. However, the ratios of sodium to calcium, magnesium and aluminium vary. Phase diagrams indicate that increasing the amount of sodium with respect to these components results in a decrease of melting temperature of the mineral mixture (Hall and Insley, 1947). Thus, this is of critical importance for determining the agglomeration temperature of the ash. Ratios of significant elements are shown in Table 5.4. Statistical analysis of the data reveals that ash composition of agglomerates differs between those formed under typical gasification conditions, and those formed under high steam conditions. Na/Si ratio is seen to remain relatively consistent for agglomerates formed under all conditions, at 0.19±0.03. However, Na/Ca ratio increases from 0.60±0.08 at high A/F conditions to 0.99±0.07 at high S/F conditions. Na/Al ratio is also shown to increase from 1.22±0.19 at high A/F to 2.28±0.12 at high S/F. Correspondingly, the Al/Si ratio decreases from 0.16±0.02 under 10 to 13 wt% steam gasification conditions to 0.09±0.02 at 90 wt% steam gasification conditions.

Table 5.4. Significant elemental (oxide) ratios of agglomerates analysed with XRF, including mean and 95% confidence interval values.

Run	Na/Si	Na/Ca	Na/Al	Al/Si
A03	0.18	0.52	1.05	0.17
A04	0.20	0.56	1.12	0.18
A05	0.19	0.61	1.17	0.16
A06	0.19	0.58	1.20	0.16
B02	0.20	0.63	1.14	0.18
B05	0.20	0.75	1.62	0.12
B08	0.18	0.54	1.24	0.15
Mean (Set A+B)	0.19	0.60	1.22	0.16
95% confidence	0.02	0.15	0.38	0.04
C01	0.22	0.91	2.18	0.10
C02	0.20	1.01	2.35	0.09
C03	0.15	1.08	2.42	0.06
C05	0.20	0.95	2.17	0.09
Mean (Set C)	0.19	0.99	2.28	0.09
95% confidence	0.06	0.14	0.25	0.03

The relatively consistent Na/Si ratios between agglomerates formed under high and low steam indicates that sodium silicate mixtures are present in all agglomerates from the spouted bed experiments, regardless of gasification conditions. The variation of Na/Ca and Na/Al elemental ratios however indicates that calcium and aluminosilicate species are

proportionally lower in the agglomerates formed at high steam compared to low steam conditions. These trends are reflected by mineralogical analyses performed on agglomerates, which show that gehlenite ($Ca_2Al_2SiO_7$) is present in dominant (>60% of phases) to minor (5-20%) amounts in agglomerates from typical steam gasification conditions, while it is only present in minor to trace (<5%) amounts from high steam runs. Gehlenite has a liquidus temperature of 1590°C in air (Greig, 1927), which is significantly higher than the normal operating temperature range of a fluidised bed gasification system (i.e. 800 to 1000°C). Thus, it can be inferred that lower proportions of calcium aluminosilicate in the ash would result in a higher proportion of liquid silicate phase formation for a given temperature.

Total inorganic content of agglomerates, shown in Table 5.5, shows that agglomerates are composed of approximately 100% ash, indicating no significant organic fraction present. Given that the agglomerates are completely inorganic in nature, this infers that any amorphous phase detected in the agglomerate structure must be inorganic rather than organic.

Table 5.5. Total inorganic content of agglomerates, calculated as sum of oxides analysed via XRF.

Run	Inorganic content wt%
B02	101.8
B05	101.4
B08	101.1
A03	102.1
A04	101.3
A05	100.4
A06	101.2
C01	103.4
C02	104.2
C03	100.4
C05	100.5

Under low steam gasification conditions (i.e. Runs A01 to A06), calcium and magnesium silicates are predominant in agglomerates. Quartz is the dominant mineral species in all agglomerates. Gehlenite is found as a co-dominant species alongside quartz. Forsterite (Mg_2SiO_4) is found in sub-dominant quantities in three runs, and minor in the remaining run. Augite is detected in minor quantities in three runs, and sub-dominant in one run.

Nepheline is found in minor amounts, while monticellite was detected in minor quantities in one run only (A04 at 967°C). Thenardite was only detected as a trace mineral in one run, forming the only occurrence of sulphur minerals in the agglomerates. Magnetite was present in minor amounts, while hematite was detected as a trace compound in one run. No amorphous glass phase was detected.

Under medium steam gasification conditions (i.e. 14 to 17 wt% steam in the fluidising gas), quartz again is the dominant species, although was detected in minor amounts in one run. Gehlenite/akermanite was found in dominant proportions in the latter run, while the other runs yielded sub-dominant proportions. Augite was detected in similar proportions to low steam gasification conditions, in sub-dominant to minor proportions. Monticellite also appeared in minor to trace amounts. Periclase was present in trace amounts in all agglomerates (not detected in low steam gasification agglomerates), while lime (CaO) was present in minor to trace amounts. The presence of these oxides indicate that reaction rates of calcium and magnesium to form silicates and aluminosilicates are decreased in comparison to those under low steam gasification conditions.

Nepheline was only detected in the agglomerates from one run in trace quantities. Thenardite was also detected in the same run in minor amounts. An amorphous phase was present in minor amounts in the remaining two runs, with no other sodium compound detected. As the preceding silicate compounds have melting temperatures ranging from approximately 1280°C for nepheline to as high as 1890°C for forsterite (Hall and Insley, 1947), it is probable that none of these minerals would individually cause molten ash formation at the temperatures operated at under typical gasification conditions. Thus, by process of elimination, the amorphous phase is the likely phase responsible for particle growth and agglomeration in the bed. The sodium disilicate-quartz eutectic, identified by Kosminski (2001) as the primary cause of agglomeration in a gasification environment, readily forms an amorphous glass (Morey and Ingerson, 1938; Rawson, 1980), and therefore is not identifiable using the XRD technique. These findings indicate that sodium disilicate is a probable species forming in the ash under the spouted bed gasification conditions, and is causing the initiation of agglomeration.

Under high steam gasification conditions, quartz is again a dominant mineral in the agglomerated ash. An amorphous phase is also detected in dominant quantities in two runs,

with sub-dominant to minor quantities in the remaining runs. Meanwhile, silicate minerals are present in significantly lower quantities than in agglomerates produced under lower steam conditions. Gehlenite/akermanite is detected only in minor to trace amounts. Augite is present in minor to trace quantities, while monticellite is detected only in trace quantities. Nepheline is detected in all runs at trace quantities only. The high level of amorphous material in comparison to other crystalline silicates infers that the amorphous phase is a silicate mixture itself, with SiO_2 preferentially forming a glass phase rather than crystalline structures.

Agglomerates formed under high steam gasification conditions appear enriched in sulphur compounds in comparison to agglomerates from lower steam conditions. Oldhamite and anhydrite are both present in minor to trace quantities, mirroring the increase in total sulphur observed in elemental analysis of agglomerates. Evidence of unreacted oxides is present, with lime and periclase detected in trace quantities in one run (C05). Magnetite (minor) and hematite (trace) are also detected, in quantities consistent with the elevated content of iron in agglomerates produced under high steam conditions.

Coated Mineral Chemical Structure

Coated mineral particles were obtained in runs from typical steam gasification conditions (i.e. <20 wt% steam in the fluidising gas), as indicated in Chapter 4. Scanning electron microscopy with energy dispersive spectrometry (SEM-EDS) was employed to analyse the structure and composition of the coated mineral particles. The coating of each particle shown does not appear to have formed from direct reaction with the mineral particle itself, but rather has become coated in ash from a source external to the particles. However, some level of interaction is observed between the mineral particle and other components in the coal.

A section of a coated particle is shown in Figure 5.7. The coating surrounding the mineral particle is separated from the quartz particle by a definite border, with an empty space between the particle and coating. The reason for the space may be due to the sample preparation step, which involves immersing the particle in resin and subjecting it to a vacuum furnace to remove air bubbles. It is possible that part of the coating may have been drawn away from the surface of the quartz particle by the vacuum effect. No increase of

quartz content from the outer surface of the coating towards the mineral was observed, indicating no direct reaction of coal inorganics with the mineral occurred.

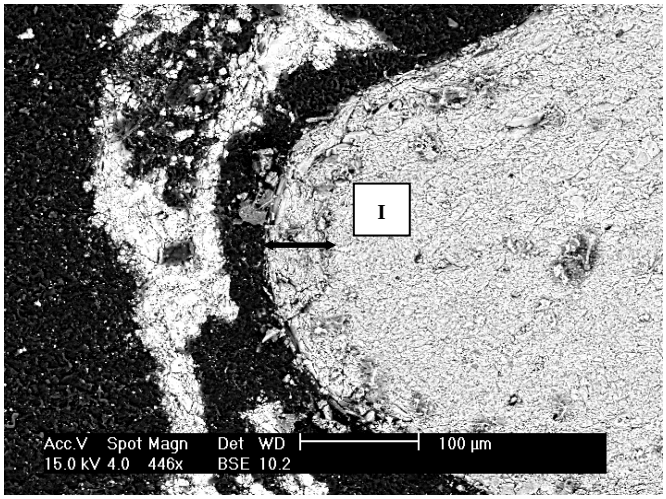

Figure 5.7. Enlargement of area highlighted in 4.3a (I – Path of Electron-Dispersive Spectrometry analysis of SiO2 surface.)

Although the coated minerals do not appear to have contributed to formation of the ash coating surrounding them, evidence was found that inorganic species from the coal were interacting with the surface of the minerals to a certain extent. Elemental analysis via EDS was performed at selected points from the surface of the silica particle to the centre, as indicated in Figure 5.7. The results of the analysis are shown in Figure 5.8. The linear analysis perpendicular to the edge of the silica particle demonstrates that sodium is interacting with the surface of the silica particle. A thin layer of sodium silicate, approximately 50-microns thick, is shown to have formed at the surface of the quartz particle. The immediate surface of the silica grain is composed of approximately 22.5% Na_2O, with the remainder being SiO_2. The sodium composition then decreases in prevalence towards the centre of the silica grain until silica is the only element detected (at approximately 50-microns from the surface). No other inorganic species was detected on the quartz particle surface, indicating that sodium was the favoured reactant with silica.

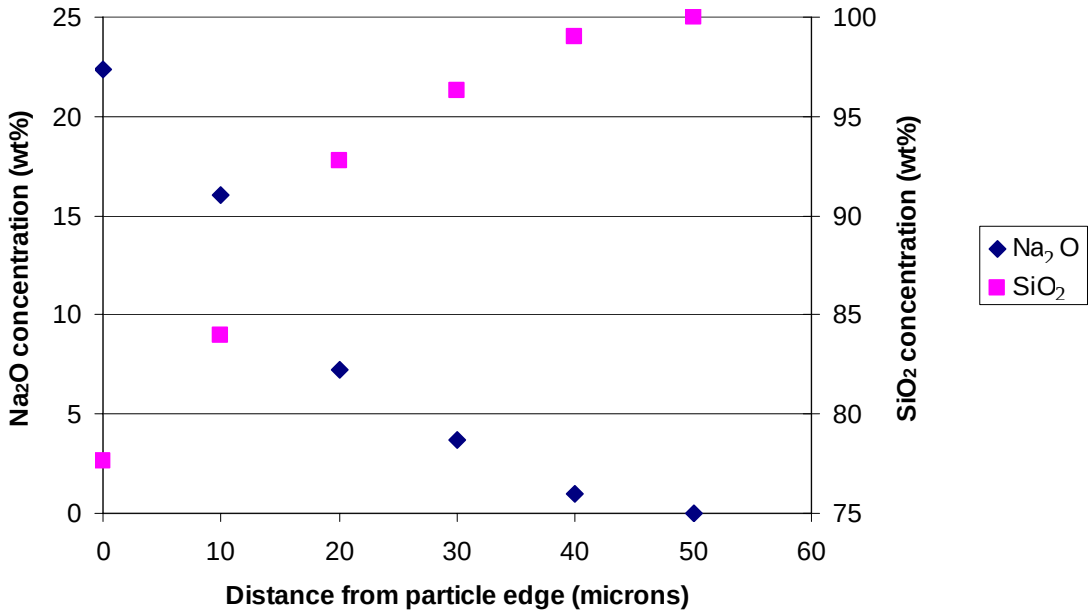

Figure 5.8. Electron-Dispersive Spectrometry analysis, performed in 10-micron increments, from the edge of the silica grain in Figure 5.7 toward its centre.

The maximum sodium content of 22.5% Na_2O at the immediate surface of the silica particle in Figure 5.7 corresponds closely with the sodium silicate eutectic composition of 25.8% Na_2O, which melts at 789°C (Kracek, 1939). Coincidentally, 789°C corresponds to the maximum operating temperature of the lowest temperature run in Set B (i.e. Run B06), which also showed some evidence of coated particles, and hence evidence of molten ash formation. The cross-sectional view in Figure 5.7 provides no conclusive evidence that the immediate surface of the silica particle had been molten during gasification, indicating that the formation of the sodium-silicate mixture may have been a result of sodium diffusing into the silica. While not impacting upon the overall composition of the silica grain to a large degree, it would be expected that smaller quartz fragments in the bed could completely convert into sodium silicate mixture via reaction with sodium.

X-ray mapping (XRM) of selected coated mineral samples was conducted to determine distribution of elements in the coated particle structure. Examples of XRM micrographs are shown in Figure 5.9 and Figure 5.10. Both images show clearly that the surface of the quartz particles contains a thin layer of sodium-rich silicate, with no other significant content of other elements. The surrounding coating appears to contain a similar proportion of sodium based on intensity of pixels in the image. The coating also contains high levels

of calcium, magnesium, and to a lesser extent aluminium, reflecting the calcium and magnesium silicates and aluminosilicates detected in the agglomerate structures. The sodium layer directly on the surface of the mineral particles provides direct evidence that even in gasification environments with relatively low amounts of steam, sodium-silica reactions take place to form potentially low melting-point ash.

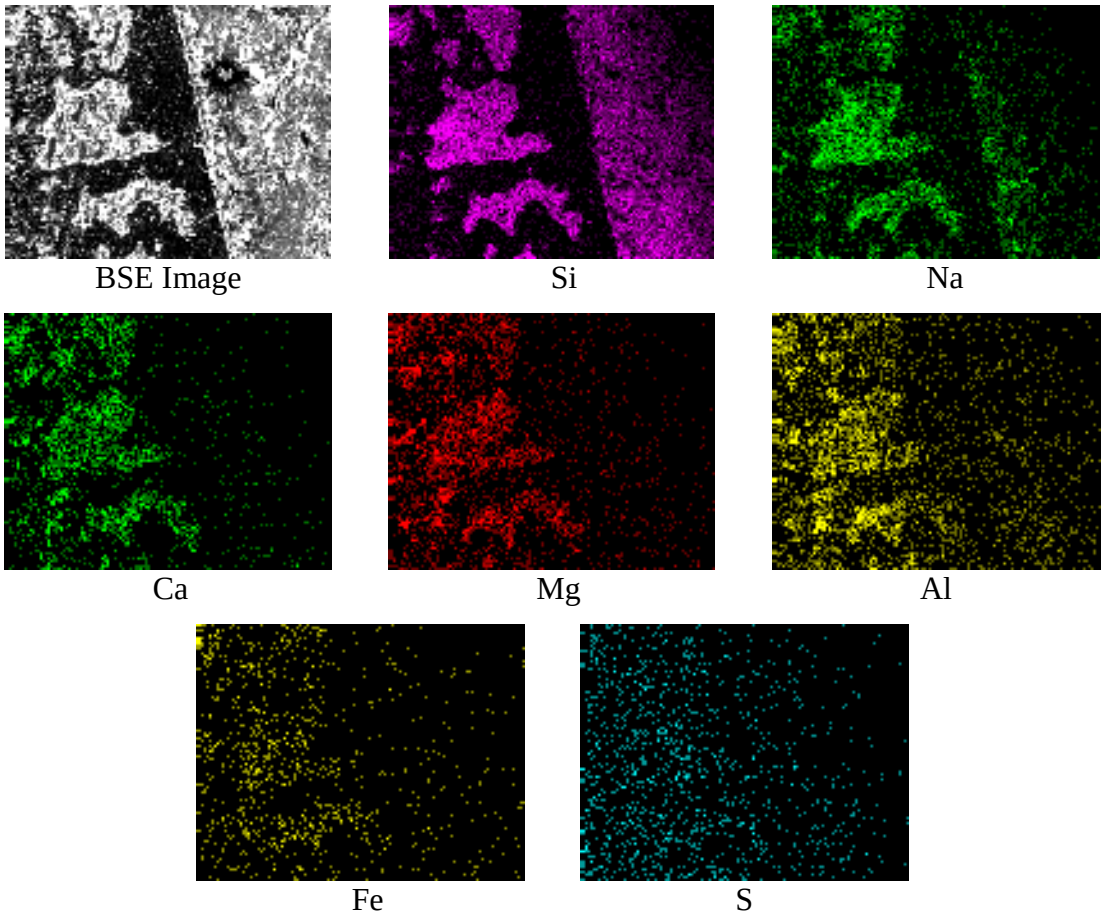

Figure 5.9. X-ray maps of major elements in section of coated mineral particle, from Run A04.

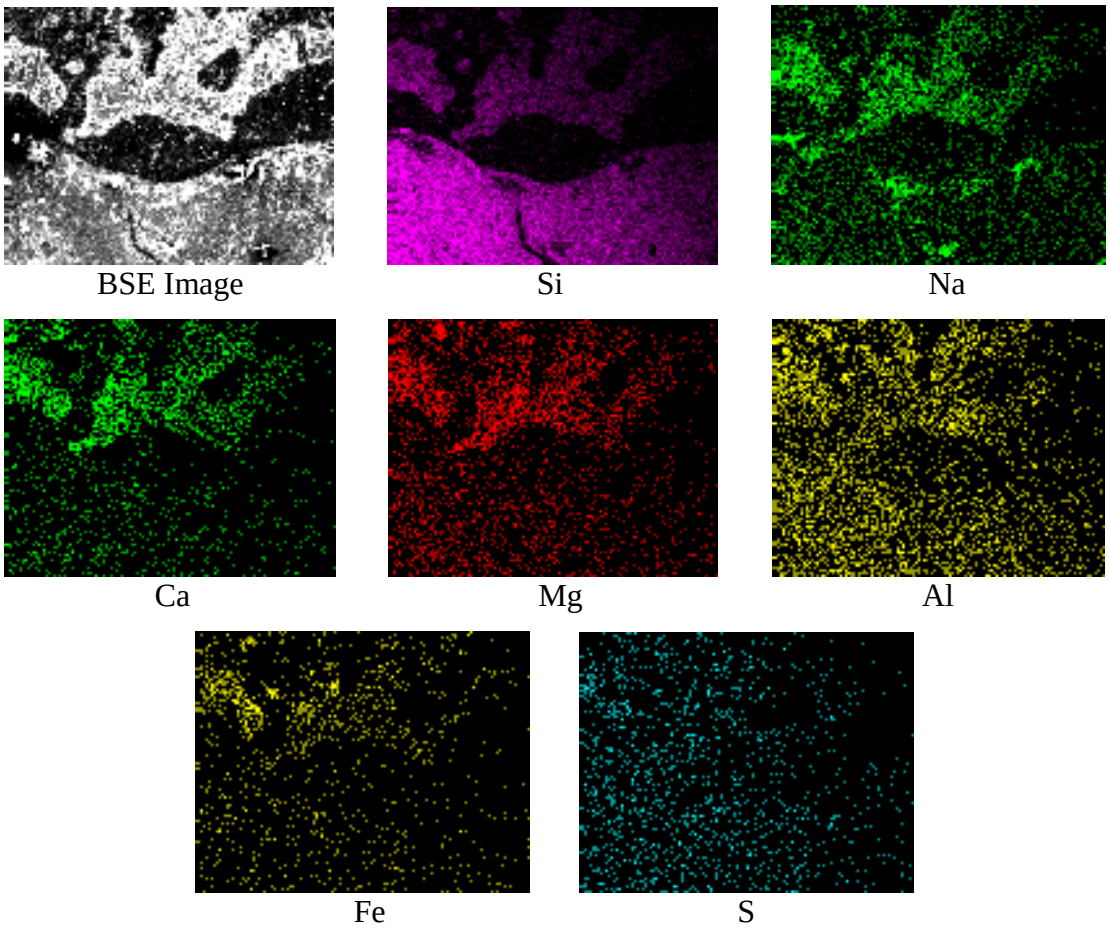

Figure 5.10. X-ray maps of major elements in section of coated mineral particle, from Run B03.

Agglomerate Chemical Structure

Examination of the agglomerates showed structures composed of solid minerals embedded in a silicate matrix, as detailed in Chapter 4. Chemical analysis was performed on agglomerate cross-sections using the X-ray mapping (XRM) function of the scanning electron microscope. This technique provides a qualitative analysis of the dispersion of each selected element throughout the body of ash, with higher content of each element represented by brighter coloured pixels.

Embedded minerals in agglomerates formed under low steam gasification conditions were surrounded by a thin layer of sodium-rich silicate phase from agglomerates. Figure 5.11 and Figure 5.12 show X-ray maps of typical agglomerate cross-sections from low steam gasification conditions (Run A03 and Run A05, respectively), indicating major element distribution. The greatest silicon content is collected in the area of the embedded particle, indicating a quartz particle. Surrounding the embedded particle in each case is a relatively

even spread of silicon, suggesting silicate compounds surrounding the particle. Aluminium also shows a strong distribution surrounding the quartz particle, indicating aluminosilicate minerals. Calcium, sodium, and magnesium show patchy distributions throughout the surrounding silicate matrix. Combined with aluminium, this indicates aluminosilicate minerals such as gehlenite and nepheline, and, to a lesser extent, silicates such as augite and monticellite making up the bulk of the agglomerate matrix. Other elements, such as iron and sulphur, show a weak dispersion throughout the agglomerate matrix, with only localised areas of significant content.

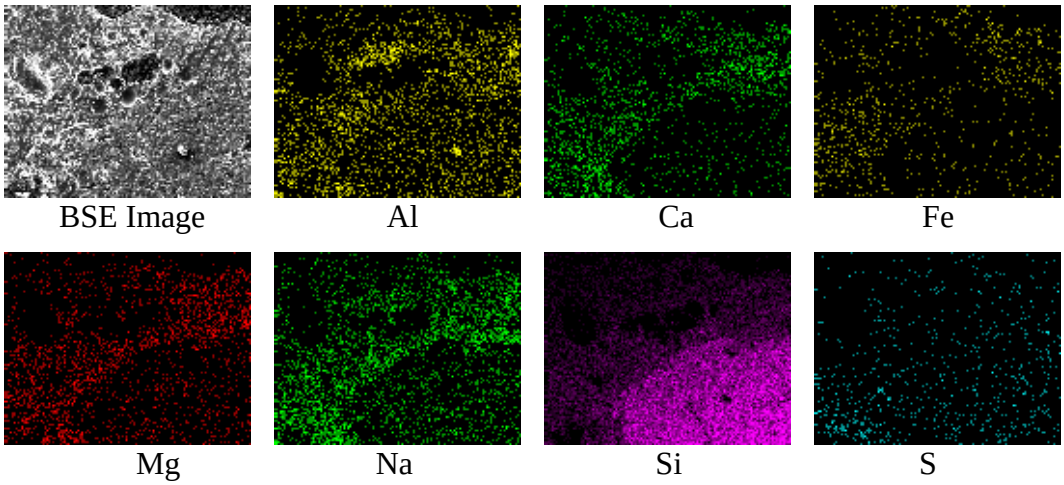

Figure 5.11. X-ray map of agglomerate cross-section collected from Run A03, showing major elemental inclusions.

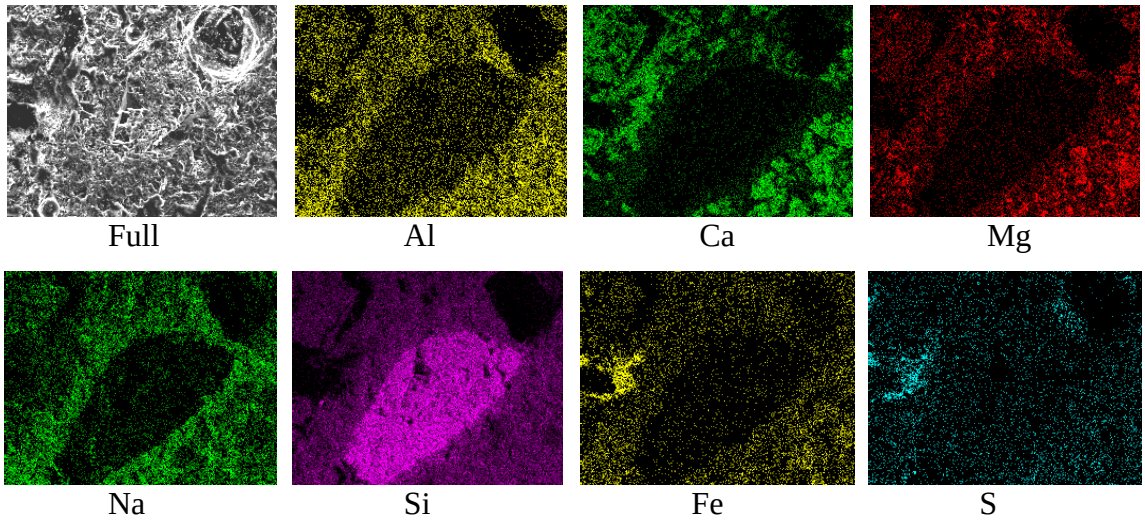

Figure 5.12. X-ray map of agglomerate cross-section collected from Run A05, showing major elemental inclusions.

At the immediate surface of the embedded silica grains in Figure 5.11 and Figure 5.12, there is a significant concentration of silicon and sodium in combination, without significant inclusion of any other major element. Both calcium and magnesium are clearly absent from this area, forming outside the sodium-rich layer. Aluminium does appear to contravene this area, indicating nepheline formation. However, Figure 5.13 shows silicon, aluminium and sodium maps from Figure 5.12 overlayed against each other, which indicates a very thin layer at the immediate surface of the silica particle consisting of only sodium and silicon. This thin layer is an indication of sodium disilicate-quartz eutectic formation, which would produce a sticky surface on the silica particles at temperature conditions used for the particular runs.

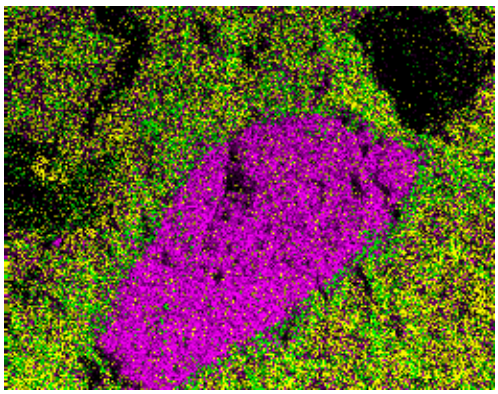

Figure 5.13. X-ray map overlays from Figure 5.12, showing distribution of Si (pink), Al (yellow), and Na (green).

Figure 5.14 shows quantification of sodium and silicon concentrations of the sodium-rich layer in each respective image from Figure 5.12. Using the XRM software package, a specific range of approximate compositions could be selected for each individual image, which displays the range via highlighted pixels on the image in question. This procedure was conducted on silicon and sodium images to display the sodium-rich area surrounding the quartz particle. The corresponding ranges of compositions for each element were 9 to 13% Na and 20 to 40% Si (not including oxygen). These selected percentage ranges represent the highest concentration of sodium in the image, and the highest silicon concentration outside the quartz grain itself. In comparison, the sodium disilicate-quartz eutectic mixture is composed of approximately 19.1% Na and 34.7% Si (remainder oxygen) on an elemental basis. These values correspond well with the measured values surrounding the embedded silica grains in the sintered agglomerates, providing firm

evidence of sodium disilicate-quartz eutectic formation in the ash under gasification conditions.

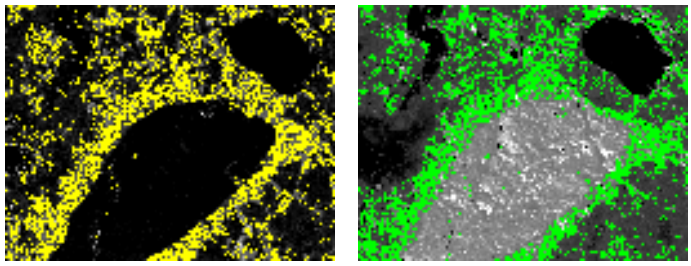

(a) (b)

Figure 5.14. Embedded silica particle in Figure 5.12 showing areas of selected composition ranges of each element. (a) 9 to 13 % Na, (b) 20 to 40 % Si.

This distribution of sodium throughout the agglomerate matrix appeared to be more prevalent in agglomerates formed under medium steam gasification conditions (i.e. 14 to 17 wt% steam in the fluidising gas), when compared to those from low steam gasification conditions (10 to 13 wt% steam in the fluidising gas). Figure 5.15 shows X-ray maps of an agglomerate cross-section from Run B05. This shows another embedded silica grain, similarly surrounded by a matrix composed of aluminium, calcium, magnesium and sodium. Sodium shows a strong, distinct outline around the edge of the silica particle. Conversely, calcium, magnesium and aluminium appear depleted at the very edge of the quartz particle, and grow stronger in composition further away from the particle. In contrast to the analysis in Figure 5.11 and Figure 5.12 however, the intensity of the pixels does not fall greatly moving away from the particle edge into the bulk matrix. This may signify a more even dispersion of sodium disilicate eutectic throughout the bulk agglomerate matrix, and suggest a more significant presence in agglomerates from medium steam conditions than from low steam gasification conditions. This is supported by mineralogical analysis, showing an amorphous phase in minor amounts in Set B agglomerates, while no amorphous presence was specifically detected in Set A runs.

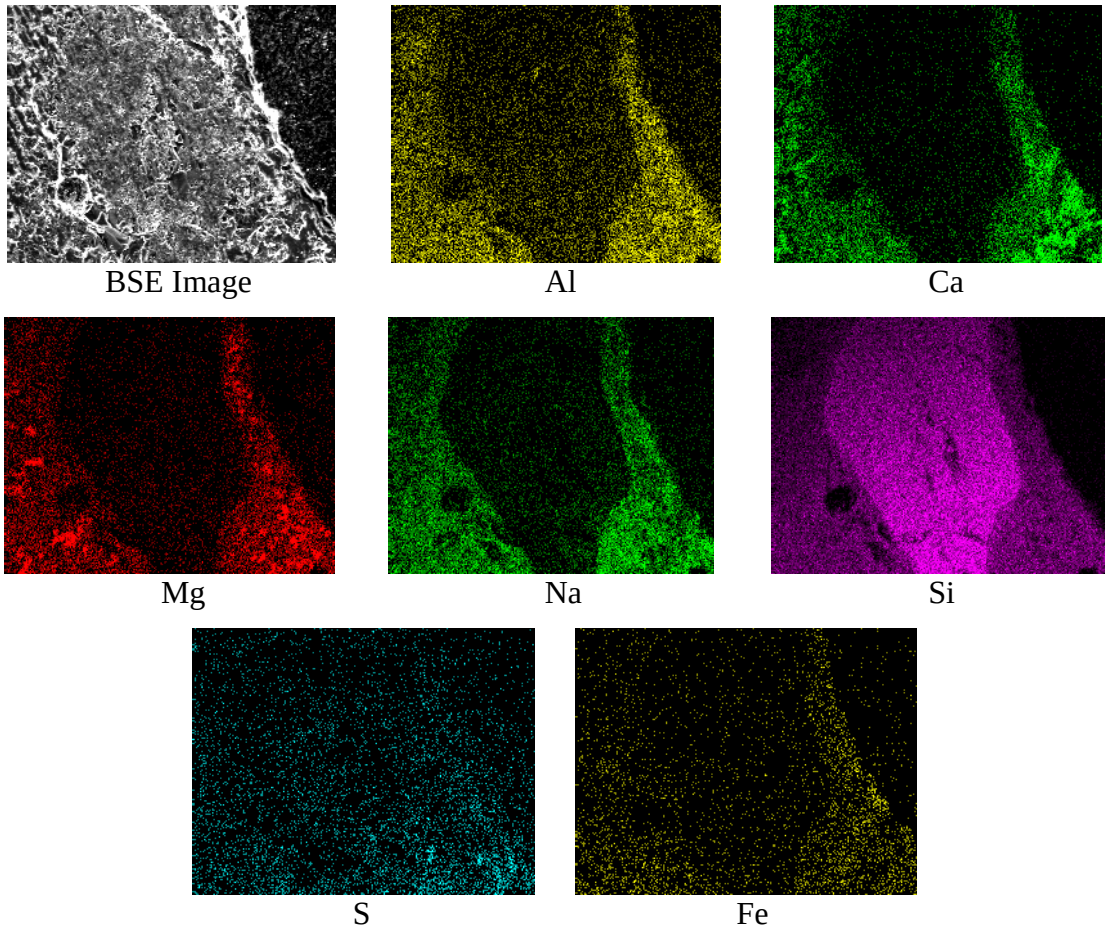

Figure 5.15. X-ray map of agglomerate cross-section collected from Run B05, showing major elemental inclusions.

The chemical structures of agglomerates from high steam experiments possess significant differences to agglomerates from runs conducted at more typical gasification conditions. X-ray maps of a typical agglomerate cross-section (Run C03) are shown in Figure 5.16. Two round quartz particles are shown bound by a layer rich in sodium. Calcium and magnesium are almost non-existent in the analysed area, except for an area of calcium in the top left corner of the image. Sulphur is also strong in this area, with no oxygen present, suggesting oldhamite. Aluminium is present in the lower part of the image, indicating nepheline. In the remaining material surrounding the silica particles however, sodium and silicon are the main components, providing further strong evidence of sodium disilicate-quartz eutectic. Furthermore, the quantity of this sodium-rich silicate phase in the coating suggests that steam does enhance the level of sodium-silica reaction, as per findings by Kosminski (2001).

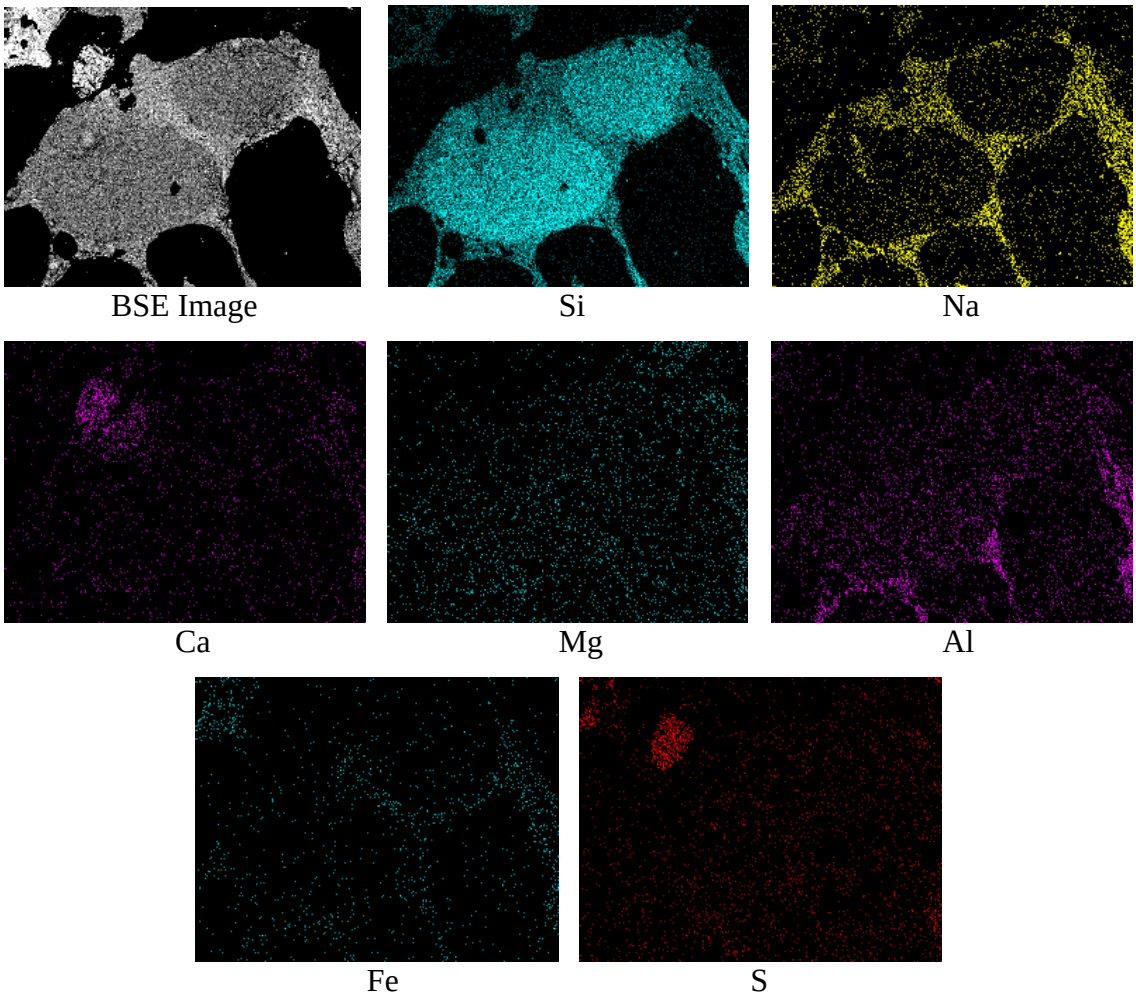

Figure 5.16. X-ray mapping of agglomerate cross-section, Run C03.

Similar occurrences are also apparent in Figure 5.17 and Figure 5.18, showing strong sodium silicate signals surrounding quartz and other mineral particles in agglomerates formed under high steam conditions. Figure 5.17 shows a cross-section of an agglomerate from Run C05. A spherical quartz particle is surrounded by a consistent sodium-rich silica phase. In the upper left corner of the image, aluminium shows a strong signal, indicating nepheline present as a discrete particle in the agglomerate matrix. Calcium only shows a significant presence in the lower right corner of the image, which corresponds to a strong sulphur composition, indicating CaS. A small particle of magnesium is also attached to the right hand edge of the CaS particle, which appears to be periclase in the absence of any significant silicon content in the area.

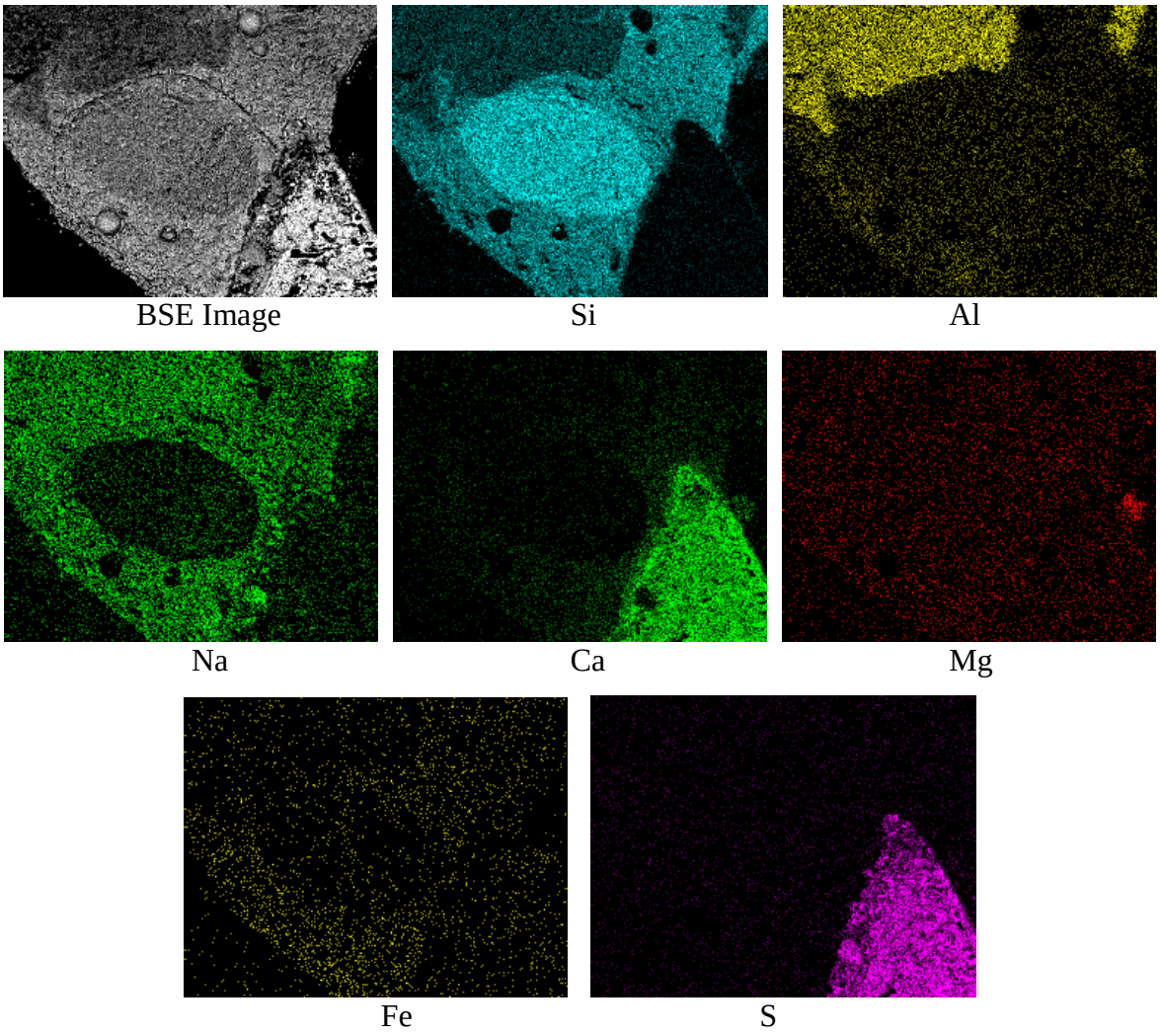

Figure 5.17. X-ray mapping of agglomerate cross-section, Run C05.

Figure 5.18 shows a cross-sectional view of an agglomerate from Run C02. Unlike the previous images from agglomerates formed under high steam conditions, the embedded silica particles do not possess strong boundaries, indicating the quartz has partially dissolved into the surrounding silicate mixture. Sodium is again prevalent throughout the silicate matrix, with calcium and magnesium present in only minor amounts. Aluminium is present as a separate compound, most likely as nepheline based on sodium prevalence in combination with the aluminium phases. Iron occurs as a separate entity to the other elemental inclusions, suggesting magnetite and/or hematite. As mentioned previously, much of iron content in the ash from high steam runs was likely a result of stainless steel from the reactor corroding under the severe reducing conditions and entering the ash. This makes it possible that the iron inclusions seen in the agglomerate matrix were a result of iron flaking from the inside surface of the reactor and entering the ash. Sulphur compounds

are also apparent, dispersed throughout the matrix. These appear to be thenardite compounds, as sodium composition is higher at the respective high sulphur locations, while no calcium is apparent in sufficient quantities to be either CaS or $CaSO_4$.

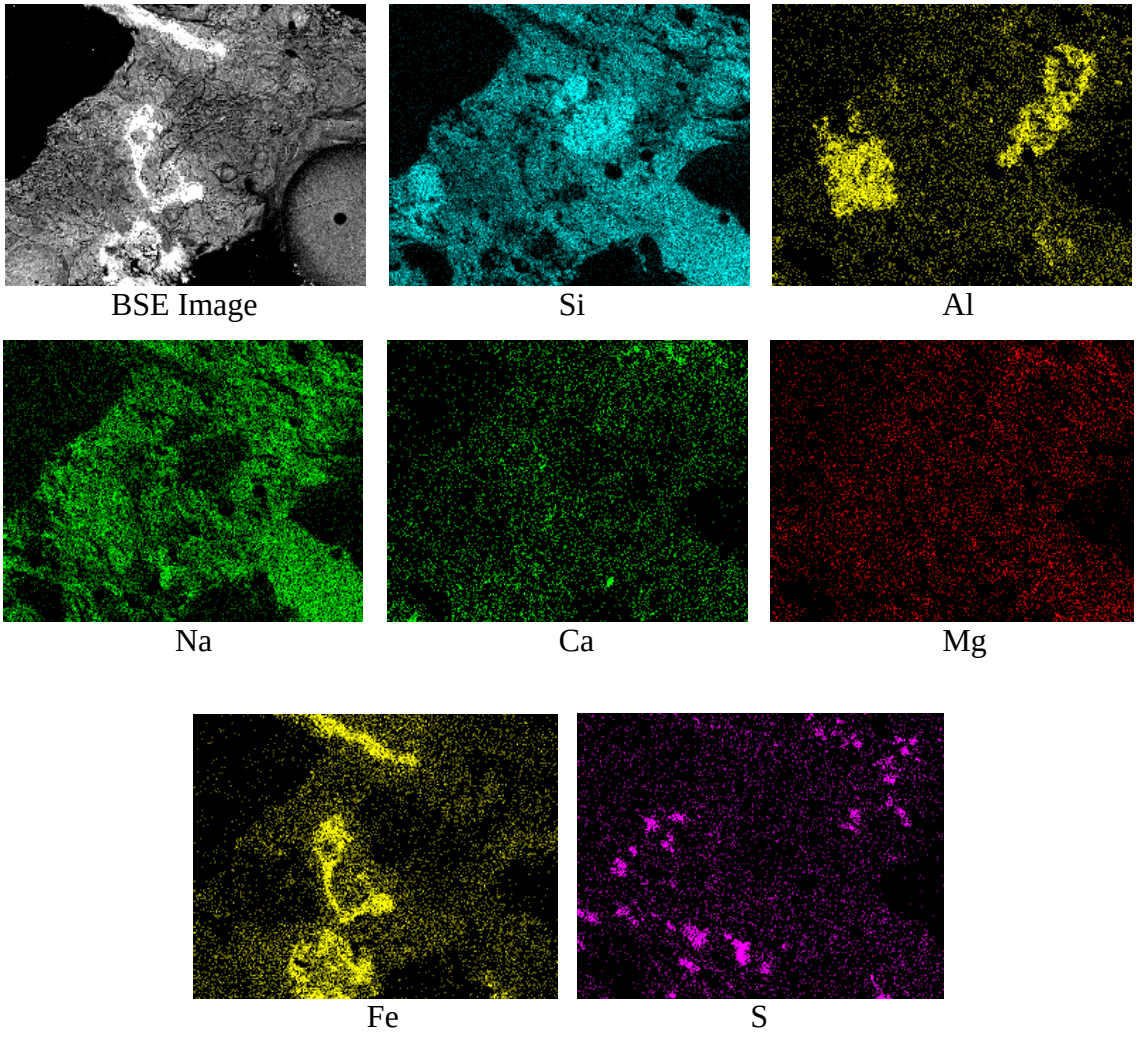

Figure 5.18. X-ray mapping of agglomerate cross-section, Run C02.

5.3.5 Gas Inlet Deposits

Minor amounts of ash (typically less than 1 g) were found to deposit around the gas inlet, as shown in Figure 5.19. The inlet deposits were found to some extent in each run of typical gasification conditions, regardless of whether defluidisation and agglomeration occurred. No such deposit was found in any of the high steam gasification runs. These observations indicate that these ash deposits represent inorganic reactions occurring in the combustion zone of the spouted bed gasifier. The deposits are thus formed by deposition of these reaction products at the base of the bed (i.e. in the oxidising region of the bed). Given

that only a small portion of these deposits were collected after each 4-hour experiment, it can be inferred that the remainder reaction products may further react in the upper reducing area of the bed, forming more reduced forms of the compounds created.

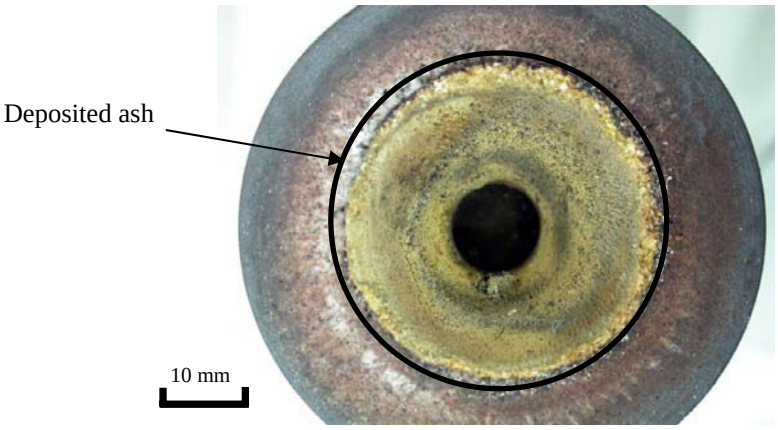

Figure 5.19. Top view of ash deposit formed around gas inlet (Run A03).

The ash deposits consisted of a yellow-coloured layer of ash that varied in level of sintering by temperature at the bottom of the bed. For instance, at lower temperatures of operation, the deposits were powdery, and relatively easy to remove from the conical distributor via scraping. Higher temperatures appeared to yield deposits that were more sintered in nature, and were removed in flakes from the distributor. Elemental and mineralogical analysis of the deposits was thus undertaken to elucidate whether chemical changes were responsible for the different deposit characteristics.

Figure 5.20 shows a plot of deposit weight versus average temperature measured at the bottom of the bed. Indicated on the plot is the state of sintering of each deposit, namely 'powdered' or 'sintered'. Powdery deposits were collected in reasonably consistent masses, at approximately 0.1 to 0.3 g, as temperature increased up to 760°C. Beyond this temperature however, the deposit mass begins to increase between about 760°C to 800°C. In this zone, the level of sintering appears to enter a transitionary phase, with both powdery and sintered characteristics observed. Further increase in temperature results in two different deposit behaviours being observed. When no agglomeration or defluidisation occurs, the deposit mass seems to maintain a relatively constant value of approximately 0.4 to 0.7 g. When agglomeration and defluidisation is an issue however, the mass increases to

1.0 to 1.2 g at approximately 800°C, and subsequently decreases sharply to below 0.2 g as the temperature approaches 900°C. This information implies that deposit formation is affected by both bed operating temperature, and whether agglomeration and defluidisation occurred.

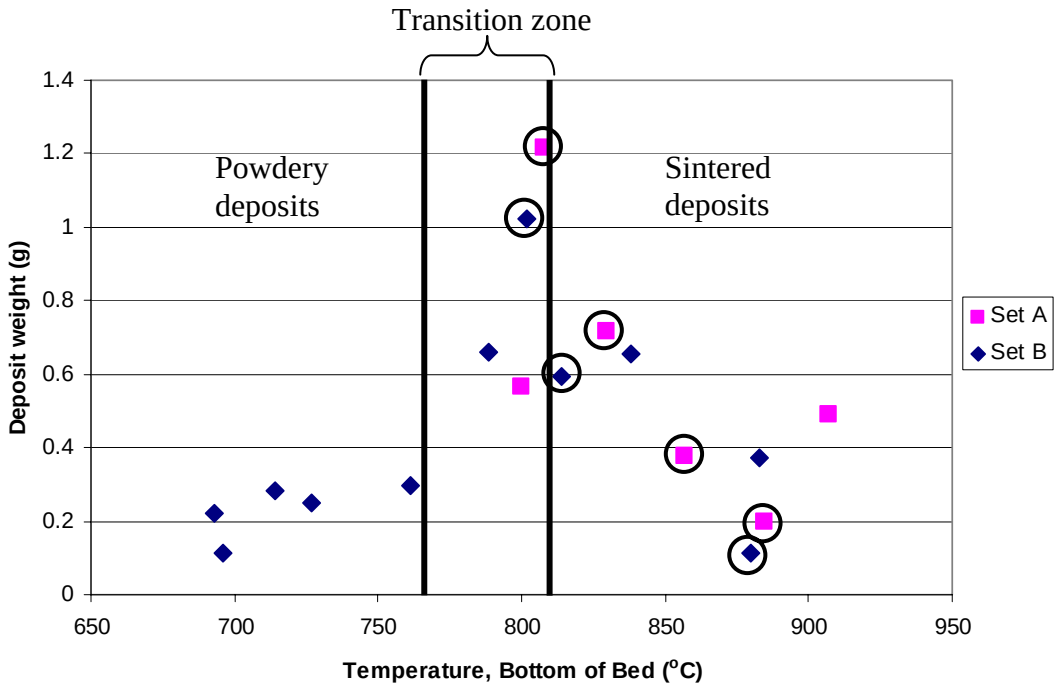

Figure 5.20. Variation of gas inlet ash deposit weight versus temperature measured at TC2. Circled data points indicate agglomeration and defluidisation was encountered.

Compositional analysis suggests that the inlet deposits are of similar composition to bed material coating detected in fluidised bed combustion studies (Manzoori, 1990; Bhattacharya et al., 1999). A summary of XRF analysis results on gas inlet deposits is shown in Figure 5.21. In general, sulphur dominates the deposit chemistry, with average composition at approximately 32 to 37 wt%. This high sulphur content reflects the yellow colouring for each collected deposit. Sodium is the next most prevalent element, with average compositions at 17 to 20 wt%. Calcium is present at 10 to 13 wt%, magnesium at 9 to 12 wt%, and aluminium at 6 to 8 wt%. Unlike bed ash compositions, silicon is present in only minor amounts, at 9 to 10 wt%. Iron is present in the smallest quantities of the major elements, at approximately 5 wt%. Chlorine is also present in significant, but highly variable, quantities – from 0.1 wt% up to over 4.0 wt%.

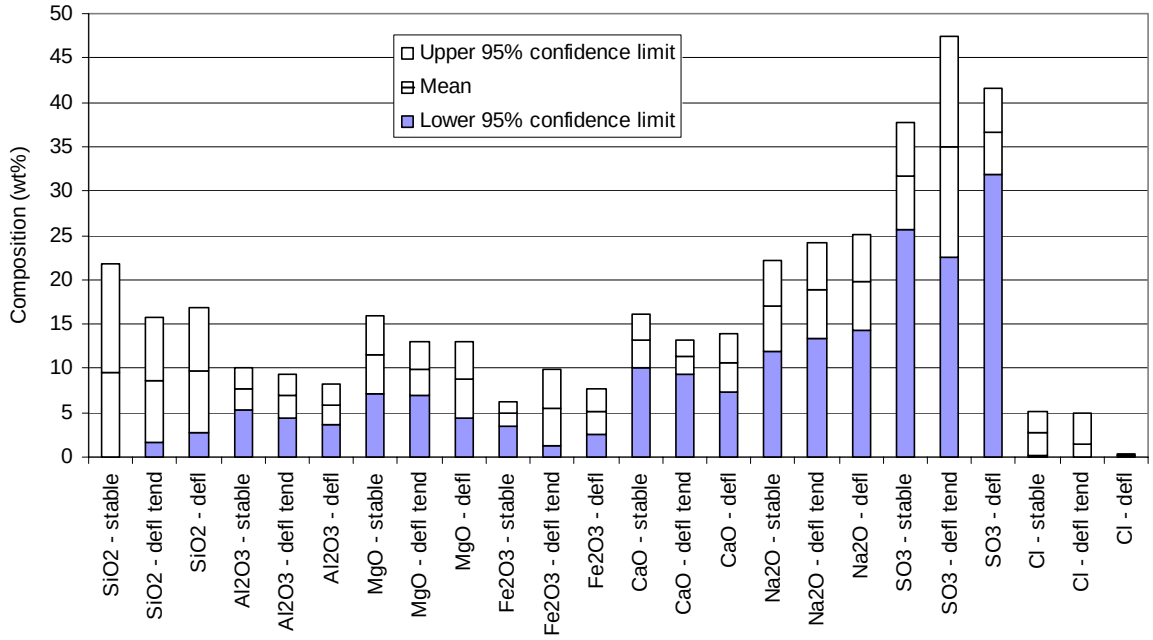

Figure 5.21. X-ray fluorescence analysis of gas inlet deposits from stable spouting runs; runs that showed possible defluidisation tendencies; and runs which showed agglomeration and defluidisation behaviour. Mean overall composition and 95% confidence limits are indicated.

Iron composition in the gas inlet deposits again appears to be elevated due to material from the stainless steel spouted bed vessel entering the deposit samples. Figure 5.22 shows the variation of NiO and Cr_2O_3 with iron content in the deposited ash. This indicates that as iron content increases, so too does the relative contents of nickel and chromium, up to 14,000 ppm Cr_2O_3 and 6,000 ppm NiO at an iron content of approximately 8.5 wt%. While leaching may contribute to elevated iron content in the samples, the method of sample removal may also contribute to this. Samples are scraped from the surface of the removable conical distributor using a spatula, which would be likely to remove any corroded iron on the surface of the distributor with the samples.

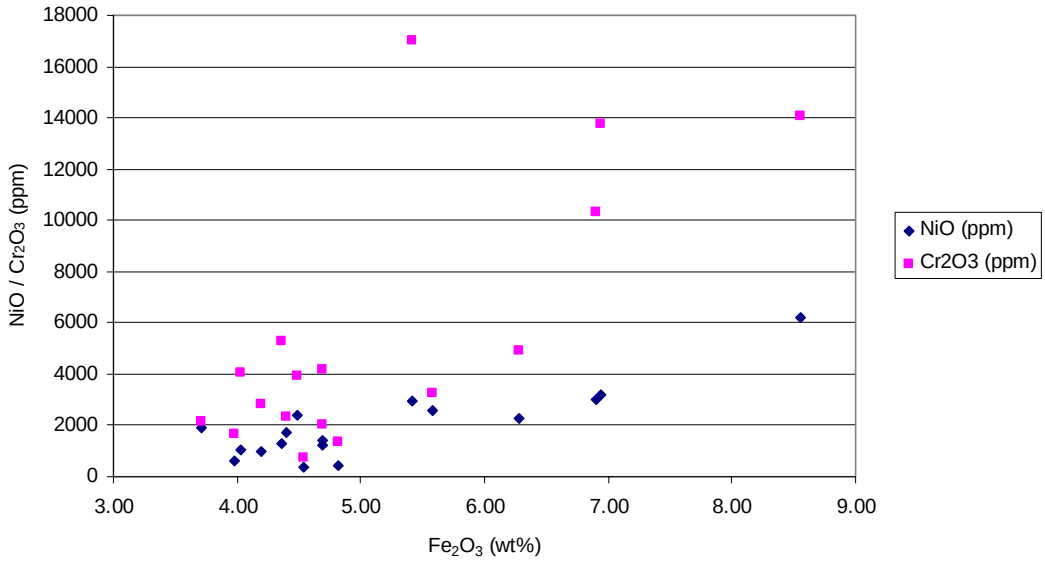

Figure 5.22. Variation of nickel and chromium with iron in gas inlet deposits.

Deposit compositions are relatively consistent across experiments, with minor differences in certain element compositions existing between deposits collected from stable and defluidisation runs. Figure 5.21 indicates the relative compositions of stable, possible defluidisation, and actual defluidisation experiments. Note that while differences are observed in the average compositions, the variations for each average value make these differences statistically insignificant, and thus variations should only be taken as indicative. Sulphur content from stable runs is 31.6±3.0 wt%; 35.0±6.2 wt% in experiments demonstrating particle growth; and 36.7±2.4 wt% in deposits from defluidisation runs. Sodium also shows a minor increase; at 17.0±2.5 wt% under stable runs; 18.8±2.7 wt% in experiments exhibiting defluidisation tendencies; and 19.7±2.7 wt% from runs showing agglomeration and defluidisation. On the other hand, aluminium, calcium, and magnesium show decreases in compositions from stable to defluidisation runs. Silica maintains a relatively constant value across the experiment groups, inferring that it is present mainly as quartz rather than associated with calcium, magnesium and aluminium in silicate form. Iron also maintains a relatively constant average value across the experiments.

Chlorine is present in significant quantities in deposits collected from stable runs, at 2.7±1.2 wt%. Chlorine content reduces to 0.21±0.12 wt% under defluidisation conditions,

seemingly a direct result of vaporisation under higher temperatures. Figure 5.23 shows the content of chlorine in each deposit versus the corresponding maximum average bed temperature. This plot indicates a gradual decrease of chlorine as bed temperature increases, from approximately 42,000 ppm at 800°C, decreasing to 1160 ppm at approximately 970°C. The chlorine concentration appears to level out below 5,000 ppm after approximately 850°C, which corresponds with findings by Kosminski (2001) that almost all of the chlorine in coal containing sodium chloride is released during gasification at 850°C.

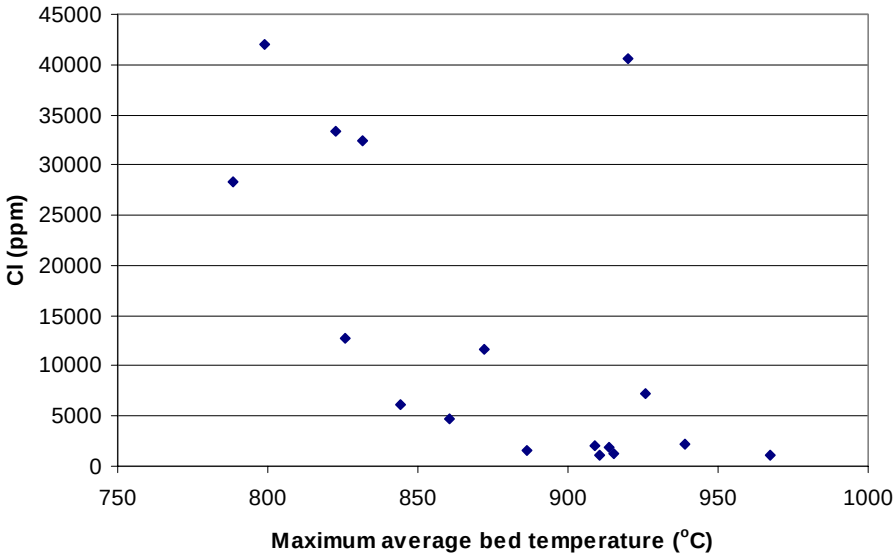

Figure 5.23. Variation of chlorine content (in ppm) of gas inlet ash deposits with maximum average bed temperature (°C).

Mineralogical analysis (Table 5.6) indicates that sulphates are the most significant constituents in the deposit make-up. Under stable conditions, anhydrite is present in dominant quantities. Thenardite is also present in minor quantities in 4 of 6 samples, and present in dominant to sub-dominant amounts in the remainder. A range of mixed sulphates are also present in the deposits, including: sodium calcium sulphate ($Na_4Ca(SO_4)_3$), detected in sub-dominant to minor quantities; calcium magnesium sulphate ($CaMg_3(SO_4)_4$), present in trace amounts; blodite ($Na_2Mg(SO_4)_2.4H_2O$), detected in minor to trace amounts; and eugsterite ($Na_4Ca(SO_4)_3.2H_2O$), present in minor to trace quantities. These mixed sulphate species correspond to the sodium-calcium-magnesium sulphate eutectics held responsible for agglomeration under spouted bed combustion conditions (Manzoori, 1990). These detections suggest a similar mechanism exists for deposit

formation in the oxidising conditions of the gasifier gas inlet as it does for coating of bed particles in a fluidised bed combustor.

Table 5.6. X-ray diffraction analysis of gas inlet ash deposits, including type of sample (i.e. powdery, sintered, or combined characteristics of powdery and sintered). Samples distinguished by 'stable runs', 'possible defluidisation', and 'actual defluidisation'.

Run	Dominant	Sub-dominant	Minor	Trace
Stable Runs				
B01[p]	Anhydrite, gehlenite	Sodium calcium sulphate	Halite, periclase, thenardite, eugsterite, monticellite	Calcium magnesium sulphate, quartz
B06[p]	Anhydrite, halite	Gehlenite, periclase	Thenardite, sodium calcium sulphate, monticellite	Calcium magnesium sulphate, quartz,
B07[p]	Anhydrite, halite	Na Ca sulphate, gehlenite	Periclase, thenardite	Calcium magnesium sulphate, quartz, eugsterite, magnetite
B09[p]	Anhydrite, thenardite	Halite	Gehlenite-akermanite, periclase, eugsterite, blodite	Quartz, magnetite
B10[ps]	Quartz, anhydrite	-	Gehlenite-akermanite, periclase, magnetite, thenardite, eugsterite	Halite, blodite
B11[p]	Anhydrite	Thenardite	Gehlenite-akermanite, periclase, eugsterite	Magnetite, halite, blodite
Stable with Particle Growth				
A01[sp]	Anhydrite	-	Periclase, spinel, magnetite, blodite, thenardite, eugsterite	Quartz, halite
A02[s]	Anhydrite	-	Quartz, periclase, magnetite, blodite, thenardite, halite, eugsterite	-
B03[s]	Na Ca sulphate	Thenardite, gehlenite, monticellite	Periclase, anhydrite	Halite, calcium magnesium sulphate, quartz, eugsterite, magnetite
B12[p]	Na Ca sulphate, thenardite	-	Anhydrite, periclase	Quartz, magnetite, eugsterite
Actual Defluidisation				
A03[s]	Na Ca sulphate, periclase, thenardite	-	Quartz, anhydrite, magnetite, eugsterite, glauberite	-
A04[s]	Na Ca sulphate, periclase, thenardite	-	Magnetite, eugsterite	Quartz, anhydrite, glauberite
A05[p]	Anhydrite	-	Sodium calcium sulphate, quartz, periclase, magnetite, thenardite	Eugsterite, glauberite, nosean
A06[sp]	Na Ca sulphate, periclase, thenardite	-	Quartz, anhydrite	Magnetite, eugsterite, glauberite, nosean
B02[s]	Thenardite	-	Quartz, anhydrite, periclase, eugsterite	Gehlenite-akermanite, magnetite
B05[s]	Na Ca sulphate, gehlenite, thenardite	-	Halite, periclase, anhydrite, eugsterite, monticellite	Calcium magnesium sulphate, quartz, magnetite
B08[s]	Na Ca sulphate	Anhydrite	Halite, periclase, thenardite, gehlenite, monticellite	Calcium magnesium sulphate, quartz, eugsterite, magnetite

[p] powdery deposit
[s] sintered deposit

Periclase is present in sub-dominant to minor quantities, suggesting magnesium did not react to the same extent as calcium and sodium. Magnetite is detected at minor to trace quantities, although its presence is likely to be mainly a result of inclusion from the stainless steel vessel, as mentioned previously. Halite (NaCl) was present in all runs, covering the full range of quantities from co-dominant to trace amounts.

Silicate species are detected in deposits under stable conditions, although in significantly smaller quantities to those in ash agglomerates. Quartz was detected in only trace amounts, although one run (B10) contained quartz as a co-dominant phase. Gehlenite/akermanite was also identified in sub-dominant to minor compositions. Minor detections of monticellite were made in two runs (B01 and B06). In general however, sulphates dominate the mineralogical composition of gas inlet deposits formed under stable conditions.

Runs that showed particle growth but no defluidisation indicate a generally higher content of sulphate species than deposits formed under stable runs. Differences in composition are also observed between deposits formed under low steam gasification conditions, and those formed under medium steam gasification conditions. At low steam gasification conditions, the dominant sulphate remains anhydrite, with thenardite, eugsterite and blodite in minor proportions. Unlike deposits from stable runs under typical conditions however, no mixed sulphates are present. Conversely, under medium steam gasification conditions, sodium calcium sulphate is the dominant species, with thenardite in dominant to sub-dominant quantities. Under the same conditions, anhydrite is present in minor amounts, and both calcium magnesium sulphate and eugsterite are present in trace quantities.

The reason for the differences in sulphate composition between the separate experimental conditions appears to be related to the amount of moisture in the gas more so than temperature. Runs A02 and B12 were operated with equivalent temperatures at the bottom of the bed, at 879°C and 883°C, respectively. However, sodium calcium sulphate and thenardite were present as co-dominant phases in Run B12, while thenardite and eugsterite were only present in minor amounts in Run A02. Conversely, anhydrite dominated the mineral phases in A02, yet was only a minor phase in Run B12. Additionally, Run A02 contained minor halite, while no chloride was detected in Run B12. This provides evidence that thenardite is forming via reaction of halite with sulphate from the coal, as per the

reaction mechanisms presented in Chapter 2, Equations 2.4 and 2.5 (Manzoori, 1990; Manzoori and Agarwal, 1992), namely:

$$CaSO_4 + 2NaCl + H_2O \rightarrow Na_2SO_4 + 2HCl + CaO \quad (2.4)$$

$$MgSO_4 + 2NaCl + H_2O \rightarrow Na_2SO_4 + 2HCl + MgO \quad (2.5)$$

These mechanisms indicate that water molecules take part in the formation of thenardite from calcium sulphate and magnesium sulphate associated with the coal. Steam flow rate used in Run A02 is at 5.0 g/min, and at 7.4 g/min in B12, or approximately 50% more steam in the case of Run B12. Thus the above reactions would be expected to proceed more favourably in the case of Run B12, as indicated by the analysis results.

Silicate minerals were not prevalent in the deposits from 'potential defluidisation' runs. Only one run (Run B03) showed silicate minerals, in the forms of gehlenite and monticellite, in minor amounts. Quartz is detected in minor to trace quantities, and periclase was detected in minor quantities in all of the deposits, suggesting that silicate reactions did not proceed to a significant extent in the reaction conditions. Minor spinel ($MgAl_2O_4$) was detected in Run A01 however.

Deposits from agglomeration and defluidisation runs showed a predominance of sodium calcium sulphate eutectic mixtures in all conditions. Under low steam gasification conditions, sodium calcium sulphate was detected in co-dominant proportions in 3 of the 4 runs. In these runs, thenardite and periclase were also co-dominant, and anhydrite was present in only minor to trace quantities. In the remaining run, anhydrite was the dominant species, while sodium calcium sulphate, thenardite, and periclase were all minor. Other sulphates were present in minor to trace quantities, including eugsterite and glauberite ($Na_2Ca(SO_4)_2$).

No silicate-containing compounds were detected other than trace amounts of nosean ($Na_8Al_6Si_6O_{24}SO_4$). The presence of nosean infers that reaction between Na_2SO_4 and aluminosilicate is occurring within the bed. This may be an intermediate compound for the formation of nepheline, taking part in an alternate reaction mechanism to that shown in Equations 5.1 and 5.2. However, given that nosean was not identified in the bed or agglomerate samples, it appears that this reaction is only applicable to oxidising conditions.

Similar deposit compositions to the low steam gasification experiments were found under medium steam conditions, with a few minor exceptions. Trace levels of calcium magnesium sulphate were detected in addition to the other sulphates identified in the preceding paragraph. Silicates were represented by gehlenite/akermanite, which ranges from co-dominant to trace quantities. Halite was also present in minor amounts, which was not detected in any of the low steam gasification runs. The presence of halite contradicts the preceding theory that higher steam contact results in a more complete reaction of NaCl to form Na_2SO_4.

Observing the deposit compositions in the various runs, in general the highly sintered deposits coincide with compositions containing sodium calcium sulphate in dominant quantities, while powdery deposits generally result from anhydrite dominance. This demonstrates the impact of the sodium calcium sulphate eutectics on agglomeration under combustion conditions, where sintering takes place at a rapid rate where such eutectics are able to form. Given that no calcium-sodium-magnesium sulphate mixtures are detected in bed char, cyclone dust or agglomerate samples however, it appears that the formation of sulphate eutectics is limited to the oxidising conditions of the combustion zone within the gasifier.

5.4 Impact of Gasification Environment on Inorganic Reactions

In all gasification conditions, sodium silicate mixtures were detected in close association with silica minerals from the coal. Indications are that sodium is reacting with the silica from the coal to cause molten ash formation required to initiate particle growth and agglomeration. Compositions of these sodium silicate mixtures are consistent with sodium disilicate-quartz eutectic, as per findings by Kosminski (2001). Sodium disilicate-quartz eutectic formation also appears to be enhanced in the agglomerate structures under higher steam gasification conditions. Under these higher steam conditions, minimum agglomeration temperature is reduced by approximately 50 to 100°C from typical gasification conditions, which further enhances the validity of the conclusions by Kosminski.

The chemical reason for the differences in minimum agglomeration temperature between typical gasification conditions and high steam gasification conditions appears to be due to two competing reaction mechanisms:

- formation of sodium silicate eutectics; and
- formation of high melting point calcium and magnesium silicates and aluminosilicates.

The formation of species such as gehlenite, augite and monticellite appear in predominant amounts under typical gasification conditions. Under these conditions, sodium disilicate is present, but primarily located at the surface of quartz particles and infused between the calcium, magnesium and aluminium silicates. Conversely, high steam gasification conditions showed a dominant proportion of sodium silicate making up the agglomerate structure, with isolated magnesium and calcium inclusions. Also, rather than these species existing in silicate and aluminosilicate form, these inclusions are mainly present in forms such as CaS and MgO, suggesting a lower reaction rate between these species and silicate material.

Kosminski (2001) states that reaction between silica and sodium chloride will only take place within a gasification environment containing steam. Furthermore, steam has an inhibitory effect on vaporisation of sodium chloride, which occurs readily under air. Thus, the elevated sodium silicate content of agglomerates from high steam conditions may be due to more extensive reaction between sodium chloride and silica, in addition to the effect of steam on lowering sodium carbonate melting point.

Dominant sulphur reactions appear to be located primarily in the oxidising conditions in the combustion zone of the bed. Although agglomerates do contain sulphides and sulphates of calcium and sodium, these minerals are present mainly as discrete minerals in the agglomerate matrix. The deposits found at the gas inlet indicate that formation of sulphate eutectics may be relevant to ash agglomeration and deposition problems at oxygen injection points in a full-scale gasification system. The high temperatures generated at such injection points may be sufficient for silicate chemistry to dominate however – as in pulverised fuel-fired combustion plants – which would make the possibility of sulphate ash causing problematic deposition negligible in relation to the effect of molten silicate formation.

Given the evidence presented, formation of agglomerates relates directly to the formation of sodium silicate species, which forms the 'glue' causing solid ash particles to cohere. Where there is sufficient presence of high melting point species, particularly earth alkali silicates, the minium agglomeration temperature is raised despite sodium silicate formation.

5.5 Summary

Ash from gasification of high-sodium, high-sulphur low rank coal is distributed throughout the gasification system in a number of forms. Other than inorganics retained in the char, primary forms of inorganics include fines elutriated from the bed, ash deposits on the walls of the vessel, and ash agglomerates under the applicable defluidisation conditions.

Under stable gasification conditions, calcium forms a number of primary components in the char. Calcium sulphide (i.e. oldhamite) and sulphate (anhydrite) are the major mineral phases forming. Calcium aluminosilicate (i.e. gehlenite) is an equally dominant phase, with lesser amounts of calcium and magnesium silicates also forming within the bed. Sodium does not combine with the calcium and magnesium silicates, instead forming sodium aluminosilicate (nepheline). The additional presence of sodalite (sodium aluminosilicate chloride) suggests that nepheline is formed via reaction of sodium chloride with aluminosilicate clay in the coal.

As agglomeration begins to impact upon stable operation of the gasifier, the sulphur forms of calcium reduce in quantity, while the silicate and aluminosilicate minerals increase. This effect can be attributed to the operating temperatures of the agglomeration runs, which are up to approximately 150°C higher than under stable conditions. The higher temperatures may result in higher release of sulphur into the gas phase, given that sulphur in the cyclone dust does not vary appreciably from stable to defluidisation runs. High temperatures also facilitate reaction of CaO and MgO with silica and aluminosilicate, providing the higher silicate proportion.

Steam is the most significant influence on sodium-silica reactions. High steam gasification operation (i.e. 90 wt% steam in the fluidising gas) results in agglomerates consisting of

high inorganic amorphous phase formation, determined to be a sodium silicate glass with composition corresponding to the sodium disilicate-quartz eutectic. Little calcium and magnesium silicates are found in agglomerate structures formed under these conditions, which may be primarily due to the lower operating temperatures under the high steam gasification runs. Sodalite structures (i.e. sodium-silicate-chlorine compounds) existing in the ash also suggest that reaction of sodium, in both chloride and carbonate forms, with silica is occurring to a more significant extent under the high steam gasification conditions. This corresponds to the findings by Kosminski (2001), which suggest that steam exacerbates agglomeration under gasification conditions.

Given the above information, agglomeration and defluidisation with high sodium coal should be avoided by limiting both the amount of steam in the gasification environment and the bed temperature. The presence of calcium and magnesium silicates and aluminosilicates also correspond with higher agglomeration temperatures, suggesting that increasing the amount of calcium and magnesium present in the bed may increase the extent of formation of these high melting point minerals, and consequently reduce the impact of agglomeration and defluidisation on gasifier operation. Further work in a pilot scale fluidised bed gasifier will determine whether such measures are effective in controlling ash related problems in a commercial scale process.

CHAPTER 6

AGGLOMERATION AND DEFLUIDISATION BEHAVIOUR OF LOW-RANK COAL IN A PILOT-SCALE FLUIDISED BED GASIFIER

6.1 Introduction

In this chapter, the agglomeration and defluidisation behaviour of South Australian lignite is investigated in a pilot-scale gasification unit. The investigation was conducted, in part, to validate the findings from 77-mm spouted bed gasification experiments. A gasification trial using Lochiel coal was performed by the CRC for Clean Power from Lignite in the Process Development Unit (PDU) gasification system (Bhattacharya, 2005a). A summary of the system and its operation is provided in the following chapter, along with detailed analysis of agglomerates collected from the gasification trial.

6.2 Process Development Unit

The PDU gasification system is a 300-mm I.D High Temperature Winkler (HTW)-type pressurised fluidised bed gasifier. The unit operates at pressures up to 8 bar, temperatures up to 1000°C, coal feed rates up to 240 kg/hr, and superficial velocity from 0.60 to 1.20 m/s (Beaupeurt, 2001). Either air-blown gasification, or oxygen-enriched air-blown gasification, can be performed. In the latter case, oxygen is injected into the bed to supplement oxygen in the air. No external heating to the vessel is supplied, other than via

an air pre-heater, with bed heat during operation generated by exothermic combustion reactions.

The PDU is characterised by a conical base, as per the HTW-type design. Operation of the PDU is unlike the spouted bed however, with a gentle bubbling motion instead of vigorous spouting. Where O_2-enriched air gasification is required, oxygen flows into the bed via jets located on the walls of the conical base. Elutriated solids are returned to the bed via a recirculating leg, which aids in increasing carbon conversion of the process. Further details of the gasification system are described elsewhere (Beaupeurt et al., 2002; Bhattacharya et al., 2002).

6.2.1 Experimental Program

Independent operators from the CRC for Clean Power from Lignite conducted a limited set of tests in the PDU. A total of six experiments were performed using air-dried Lochiel coal, which was obtained from the same source as that used for the spouted bed experiments described in the present study. Approximate ranges of experimental parameters are displayed in Table 6.1.

Table 6.1. Experimental operating conditions for validating results from spouted bed gasification experiments in the PDU (Bhattacharya, 2005b)

NOTE: This table is included on page 176 of the print copy of the thesis held in the University of Adelaide Library.

Gasification was performed with steam-air mixtures at 8 bar pressure. Experiments were each carried out over a 4-hour duration, unless halted prematurely by agglomeration. Mode of operation was varied from air-blown gasification (17 vol% O_2 in air-steam mixture) and O_2-enriched air-blown gasification (35 vol% O_2 in gas mixture). Air-to-Fuel ratios ranged from 2.0 to 2.2, and S/F was varied from 0.1 to 0.3, with the higher steam content required for O_2-enriched air gasification tests to provide additional heat sink for the greater heat produced from combustion. In contrast, A/F ratios in the spouted bed varied between 2.0 and 3.5 under typical steam gasification conditions, with S/F maintained between 0.4 and

0.5. The comparatively lower ratios used in the PDU is a result of the significantly higher coal throughput achievable in the high-pressure environment of the PDU.

Two initial experiments were operated at temperatures ranging from 800 to 850°C. These tests were operated using pure char beds. After operating problems were encountered in each case, a number of operating changes were implemented for the remaining runs (Runs 3-6). The main process changes included:

- introducing dolomite to the char to give a Ca/S ratio of 2.0 (i.e. approximately 20% of the bed); and
- reducing operating temperature from 800-850°C to 780-800°C.

Dolomite was added primarily to capture sulphur in the product gas, with approximately 3500 ppm H_2S detected in the output gas of the pure char gasification. These changes resulted in stable operation over the 4 hour run period of each test. Agglomerate samples were collected from the bed at the conclusion of applicable experiments and subjected to analysis similar to that of the samples generated in spouted bed experiments.

6.3 Summary of Bed Behaviour During Gasification

Stable operation in the PDU was characterised by stable bed temperatures and pressure drop (gas inlet to freeboard). Gas composition remained relatively constant throughout the tests. Experiments were conducted in both air-blown and oxygen enriched air-blown modes of gasification. Typical gas composition for each mode of operation is shown in Table 6.2. Reported concentrations are as-measured, uncorrected values (wet basis).

Table 6.2. Typical gas composition from PDU experiments, air-blown and O_2-blown composition (Beaupeurt et al., 2004)

Gas Component	Air-blown composition (mol%)	O_2-enriched air composition (mol%)
CO	10-20	15-24
H_2	11-15	15-24
CH_4	0.7-2.5	1-4
C_2H_y	~1	~1
H_2O	10-16	10-18

Production of combustible species is enhanced with oxygen-enriched air-blown gasification. Hydrogen shows the largest increase in yield from O_2-enrichment, with production increased from 11-15 mol% up to 24 mol%. Carbon monoxide and CH_4 yield increased up to 50% from air-blown composition. Dolomite addition to the bed was effective in reducing H_2S in the gas to below detection limits.

Stable operation was achieved only in Runs 3-6. Runs 1 and 2 were terminated prematurely owing to uncontrolled excursions in observed operating parameters during gasification. The specific observations that inferred unstable operation included:

- gradual loss of temperature measured at thermocouple locations;
- measurable increase in fluctuation of pressure drop from gas inlet to freeboard; and
- obstruction of the bottom ash screw.

The preceding observations can be accounted for by ash deposition and agglomeration in the reactor vessel during gasification. Decreasing temperature indicates that fouling of the thermocouples was occurring. Visual observations confirmed this, with ash deposits found on the walls in the bed region of the vessel, in particular at the air injection points (Beaupeurt et al., 2004). Large agglomerates, up to 30 cm in diameter, were also found in the bed, attributed to breakage of ash deposits attached to the walls. These ‘floating deposits’ were responsible for creating pressure drop fluctuations across the bed, and causing obstruction of the ash screw (Bhattacharya, 2005b). In particular, termination of the applicable experiments was necessary to allow removal of the bottom of the reactor and the obstruction.

The preceding visual observations of ash deposition in the PDU suggest that ash agglomerates and deposits are primarily formed on the walls of the reactor. This corresponds to agglomeration experienced in spouted bed experiments, which was found to occur in the annulus section of the bed. Free agglomerates are consequently only formed following breakage of these deposits. Bed temperature appears to be the main reason for deposit formation, with the largest mass of deposited ash found localised at combustion locations (i.e. air injection points).

Agglomeration in the PDU occurred at temperatures lower than the minimum temperature of agglomeration experienced in the spouted bed gasifier for typical steam gasification

conditions (i.e. 860°C in Run B05). This observation conflicts with the expectation that laboratory-scale reactors result in more pronounced agglomeration than in a pilot-scale process, as identified under fluidised bed combustion conditions (Manzoori, 1990; Bhattacharya et al., 1999). Operating pressure is the main difference in operation between PDU experiments and those conducted in the spouted bed, which may be responsible for this discrepancy.

Increasing operating pressure in a steam environment is known to decrease the melting point of sodium silicate mineral mixtures. Morey and Ingerson (1938) showed that the liquidus temperature of pure sodium disilicate decreases with increasing steam pressure. At a pressure of 8 bar (approximately 115 psi), the liquidus temperature of sodium disilicate decreases by approximately 20°C, from 874°C at atmospheric pressure to approximately 855°C at 8 bar. Thus, a 20°C reduction in minimum agglomeration temperature from atmospheric conditions would result in agglomeration occurring at approximately 840°C, which is within the operating temperature range of PDU Runs 1 and 2.

6.4 PDU Ash Agglomeration

6.4.1 Agglomerate Formation

The physical structure of agglomerates obtained from the PDU showed similarities with agglomerates from spouted bed experiments. Figure 6.1 shows a photo of a 15-cm diameter agglomerate collected from inside the reactor vessel following completion of Run 1. The sample is typical of agglomerates formed in Runs 1 and 2. No evidence of individual sintered coated mineral particles is apparent on the surface of the agglomerate, which was a feature of agglomerates formed in the spouted bed, as shown in Figure 6.2a. Instead, the agglomerate has a smoothed, yet porous, appearance (refer to Figure 6.2b), suggesting the extent of sintering of ash in the PDU was greater than that experienced in the spouted bed. Embedded mineral particles are apparent on the surface however, in the form of light coloured flecks.

Figure 6.1. Photo of agglomerate (150 mm diameter) collected from bed of Run 1

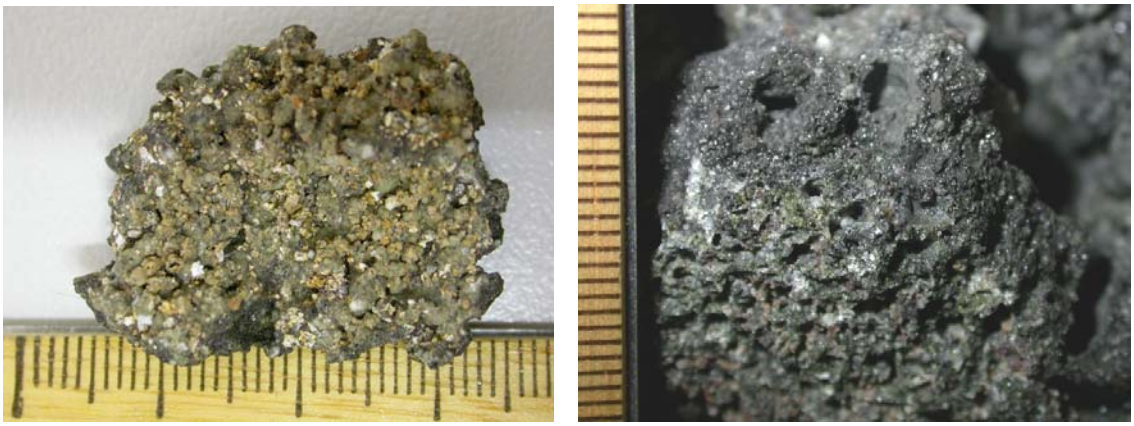

(a) (b)

Figure 6.2. Photos of agglomerate surfaces; (a) agglomerate collected from spouted bed experiment Run B05; and (b) close-up of the PDU agglomerate shown in Figure 6.1.

The light coloured mineral particles found on the surface of the PDU agglomerates are finely dispersed throughout the bulk ash matrix. The agglomerate cross-section shown in Figure 6.3 illustrates the dispersal of mineral particles throughout the matrix. The agglomerate matrix itself has a glassy appearance, suggesting the possibility of sodium silicate glass as identified in spouted bed agglomerates.

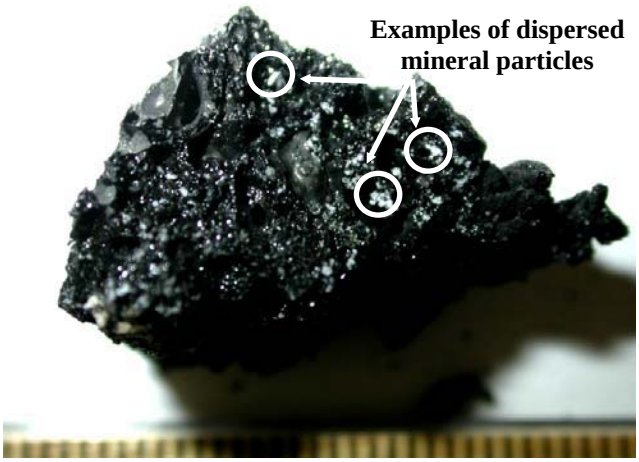

Figure 6.3. Photo of agglomerate cross-section collected from bed of Run 1, showing mineral particles dispersed throughout structure

The bulk ash matrix of the PDU agglomerates differs in colour to the agglomerates collected from typical steam gasification spouted bed experiments, yet appears similar to the agglomerates formed under high steam gasification conditions. Agglomerates formed under high steam spouted bed gasification conditions and in the PDU have a black, glassy matrix. In contrast, agglomerates formed under typical gasification spouted bed conditions are of a dark brown colour. This colour difference may be due to compositional differences, with sodium silicate glass prevalent in the high steam spouted bed agglomerates, while calcium and magnesium silicates and aluminosilicates are predominant under typical steam spouted bed gasification conditions. This indicates that sodium disilicate may also be more prevalent than calcium and magnesium silicates in the PDU agglomerates.

6.4.2 Inorganic Chemistry

Bed Char Chemistry

Bed char from PDU tests shows an overall lower composition of inorganic constituents than that in bed char from spouted bed experiments. Table 6.3 shows general analysis results of bed char from the PDU tests along with analyses from the spouted bed gasification experiments for comparison purposes. The analyses presented relate only to runs in which agglomeration was avoided.

Table 6.3. Composition of inorganic constituents of bed char from PDU, compared with results for typical steam gasification (<20 wt% steam in the fluidising gas) and high steam gasification (90 wt% steam in the fluidising gas) experiments from the spouted bed gasifier (SBG). Does not include bed char from runs in which agglomeration and defluidisation occurred.

Component	Bed Char		
	PDU[a] (Runs 3-6)	SBG – Typical steam gasification	SBG – High steam gasification
	wt%	wt%	wt%
SiO_2	6-13	13-36	17.2
Al_2O_3	0.5-0.7	2.8-6.5	4.7
Fe_2O_3	0.7-1.3	2.0-5.0	2.5
MgO	3.5-6.5	3.2-9.0	6.2
Na_2O	1-1.5	3.7-6.4	4.7
CaO	5.5-7	6.0-15.0	7.6
Cl	0.5-0.8	0.2-0.8	0.5

[a] Results from Bhattacharya (2005b).

Two significant process differences between the PDU tests and the spouted bed experiments are likely to have resulted in the differences exhibited between the compositions of inorganic constituents of the bed char in each case. These differences include:

- Continuous bed material removal, at a rate of 6% of the incoming solid feed (Beaupeurt et al., 2004); and
- Addition of dolomite to the bed at a rate of 20% of the feed.

The continuous removal of bed material from the PDU tests also removes ash from the bed. In contrast, no bed removal (other than by elutriation) is performed in spouted bed experiments, resulting in the higher observed inorganic compositions in Table 6.3. Dolomite was also added to the beds of stable, non-agglomerating PDU runs, resulting in an increase in the calcium and magnesium contents of the bed char from that of a bed of pure char.

Approximate elemental ratios in the bed char from the PDU tests are shown in Table 6.4, with comparison to ratios from bed char from spouted bed gasification experiments. Average ratios for the spouted bed experiments were calculated using XRF analytical data (Table D.1, Appendix D). The Ca/Si and Mg/Si ratios show that the contents of calcium and magnesium in the bed char from PDU tests are significantly higher than in the spouted bed runs, due to the addition of dolomite to the PDU tests. The Na/Si ratios do not appear statistically different between PDU and spouted bed runs, indicating similar levels of

sodium retention in the bed char between the experimental conditions. However, a lower Al/Si ratio and significantly higher Na/Al ratio in the bed char from the PDU tests indicates a reduced aluminosilicate content in the PDU bed char compared to the bed char from the spouted bed runs. The reason for the lower proportion of aluminium in the bed char from PDU tests is unclear. The Na/Cl ratio is the only other ratio in Table 6.4 showing a statistically significant difference between PDU and spouted bed tests, showing a slightly lower value than that of the typical steam spouted bed gasification runs, and significantly lower than the high steam spouted bed gasification runs. These differences in ratios suggests a high level of halide compounds in the inorganic matter in the PDU. The reason for high chlorine can be attributed to the reduced temperatures of operation in these tests, operated below 800°C.

Table 6.4. Elemental ratios of inorganic constituents in the bed char from PDU tests (Runs 3-6), compared with ratios in the bed char from typical steam (<20 wt% steam in the fluidising gas) and high steam (90 wt% steam) spouted bed gasification (SBG) runs.

Elemental Ratio	Bed Char		
	PDU[a] (Runs 3-6)	SBG – Typical steam gasification	SBG – High steam gasification
	wt/wt	wt/wt[b]	wt/wt[b]
Na/Si	0.13	0.19±0.06	0.21±0.08
Al/Si	0.06	0.16±0.06	0.19±0.11
Na/Al	2.08	1.20±0.31	1.10±0.38
Ca/Si	0.66	0.36±0.14	0.37±0.17
Mg/Si	0.53	0.20±0.10	0.24±0.17
Na/Ca	0.20	0.55±0.20	0.57±0.12
Fe/Si	0.11	0.13±0.08	0.17±0.11
Na/Cl	1.92	6.62±2.37[c]	32.9±43.3

[a] Elemental ratios based on the average of maximum and minimum values of ranges shown in Table 6.3.
[b] Average elemental ratios for spouted bed gasification runs include 95% confidence intervals.
[c] Na/Cl ratio for typical steam gasification spouted bed runs shown for stable (non-agglomerating) runs only.

The resulting high content of calcium and magnesium due to dolomite addition may have contributed to the stable operation of gasification tests in comparison to the pure bed char tests. Increased contents of calcium and magnesium may have increased the formation of higher melting point silicate and aluminosilicate species in preference to low melting point sodium species, thus reducing the amount of liquid phase in the ash for any given temperature. The Na/Ca ratio of the bed char from the PDU tests is significantly lower than

for the spouted bed char due to the addition of dolomite to the bed resulting in an increase in the calcium composition of the char. Thus, an increase in calcium composition of the ash may have been a significant contributor to the stable operation of the PDU tests where dolomite was added, in addition to the reduced bed temperature used in these cases.

Agglomerate Inorganic Chemistry

The PDU agglomerate composition corresponded to that of the agglomerates from spouted bed experiments. Table 6.5 shows the average elemental composition of agglomerates obtained from PDU Run 1 alongside compositions from typical and high steam gasification experiments. The PDU agglomerate composition is dominated by quartz, at 64.2 wt%. CaO is the next most prevalent component at 10.2 wt%, with Na_2O at approximately 9 wt%. Al_2O_3 is present at 3.2 wt%, indicating that the agglomerate composition is more prevalent in silicate than aluminosilicate species. Sulphur is also present only in low concentration, at 2.8 wt%.

Table 6.5. Oxide analysis of PDU agglomerate via XRF analysis technique, with comparison to agglomerates from spouted bed gasification (SBG) experiments – typical steam gasification (<20 wt% steam in the fluidising gas), and high steam gasification (90 wt% steam in the fluidising gas)

Component	Agglomerate Compositions		
	PDU	SBG – Typical steam gasification	SBG – High steam gasification
	wt%	wt%	wt%
SiO_2	64.2	47.6±2.1	53.8±4.5
Al_2O_3	3.2	7.6±0.7	4.6±0.6
MgO	4.8	9.4±1.1	3.7±1.3
Fe_2O_3	4.9	5.6±0.9	10.3±3.0
CaO	10.2	15.4±1.1	10.5±1.5
Na_2O	8.8	9.2±0.5	10.3±0.8
K_2O	0.15	0.17±0.04	0.22±0.03
TiO_2	0.81	1.34±0.07	0.55±0.21
SO_3	2.8	2.8±0.8	4.7±2.1

Certain similarities exist between analysis results from PDU and spouted bed agglomerate compositions, particularly between PDU and high steam gasification tests. Compositions of silica (64.2 wt%), aluminium (3.2 wt%), magnesium (4.8 wt%), and calcium (10.2 wt%) in the PDU agglomerate sample all corresponded to the same component compositions

under high steam spouted bed conditions, namely 53.8±4.5 wt% SiO_2, 4.6±0.6 wt% Al_2O_3, 3.7±1.3 wt% MgO, and 10.5±1.5 wt% CaO. In contrast, aluminium (7.6±0.7 wt%) and magnesium (9.4±1.1 wt%) were approximately double the composition of the PDU agglomerate, and CaO (15.4±1.1 wt%) was 50% greater than the same PDU composition. Sodium maintained a relatively constant level in all of the agglomerate samples, while sulphur composition in the PDU agglomerate was approximately half that of the high steam spouted bed agglomerates. Iron content in the PDU agglomerate was also half that of the spouted bed agglomerate, although this discrepancy is most likely due to corrosion of the stainless steel spouted bed vessel, as mentioned in Chapter 5. These findings imply that the formation of high melting point phases (e.g. gehlenite, monticellite and augite) are more predominant in the typical steam gasification conditions of the spouted bed than in the PDU.

Mineralogical composition of the PDU agglomerate indicates that sodium-rich inorganic glass is a significant contributor to the agglomerate composition. Table 6.6 shows mineralogical composition of the PDU agglomerates. An inorganic amorphous phase is detected in minor quantities (5-20% of the total mineral phases). None of the other detected minerals contain sodium, which infers that the amorphous phase is a sodium-based glass mixture. Sulphur may also be represented by the amorphous phase, with amorphous FeS favoured to form in the presence of H_2S (Harmandas and Koutsoukos, 1996; Anderko and Shuler, 1997). The other detected minerals, which include gehlenite ($Ca_2Al_2SiO_7$), monticellite ($CaMgSiO_4$) and augite ($Ca(Mg,Fe)Si_2O_6$), are detected in minor to trace amounts. In the spouted bed however, these minerals are detected in dominant to minor compositions under typical steam gasification conditions, suggesting that the amorphous phase has a more significant impact on ash behaviour than in the spouted bed.

Table 6.6. Mineralogical analysis of PDU agglomerate via XRD analysis technique

Dominant >60%	Sub-dominant 20-60%	Minor 5-20%	Trace <5%
Quartz	-	Gehlenite, cristobalite, amorphous	Monticellite, augite

Silica (SiO_2) is detected in two different crystalline forms, namely cristobalite and quartz. Quartz is the low temperature form of silica, while the cristobalite typically forms at temperatures greater than 1470°C (Hall and Insley, 1947). The high temperature of cristobalite formation indicates that the ash was subjected to significantly higher temperatures than those experienced in the spouted bed experiments during agglomerate formation.

At temperatures conducive to cristobalite formation, liquid phase in the ash is expected to be high, and therefore result in the high rate of sintering that would have contributed to the smoothed appearance of the agglomerates from the PDU. Such high temperatures would likely be a result of localised temperature excursions in the bed due to low relative movement of particles at the walls, where deposition occurred. Similar conclusions were reached during combustion tests in a CFBC pilot plant with Lochiel coal (Bhattacharya et al., 1999). In that situation, low melting point sulphate-rich ash deposited on bed material particles (i.e. sand) causing poor fluidisation and localised hotspots within the bed.

Agglomerate Chemical Structure

Agglomerate structure consists of embedded mineral particles in a bulk ash matrix, similar to those collected from spouted bed experiments. Typical back-scattered electron (BSE) micrographs from PDU agglomerate cross-sections are shown in Figure 6.4 and Figure 6.5. Electron dispersive spectroscopy (EDS) analysis was performed on selected points on each image in order to identify the various mineral phases, as shown in Table 6.7 and Table 6.8, respectively.

As identified in the bulk mineralogical and elemental analyses in the preceding section, silicate chemistry dominates the agglomerate composition. Dark-grey areas in each of the BSE images indicate silica particles embedded in the agglomerate structure, with Analysis Points 1 and 4 in Table 6.7, and Point 4 in Table 6.8 showing approximately 50-60% silicon, with the remainder being oxygen. Visually, the agglomerate cross-sections appear to contain a higher proportion of embedded silica particles in the agglomerate matrix than from agglomerates formed under typical steam spouted bed gasification conditions, which also corresponds to the comparison of elemental analyses, although this is not quantifiable in the images.

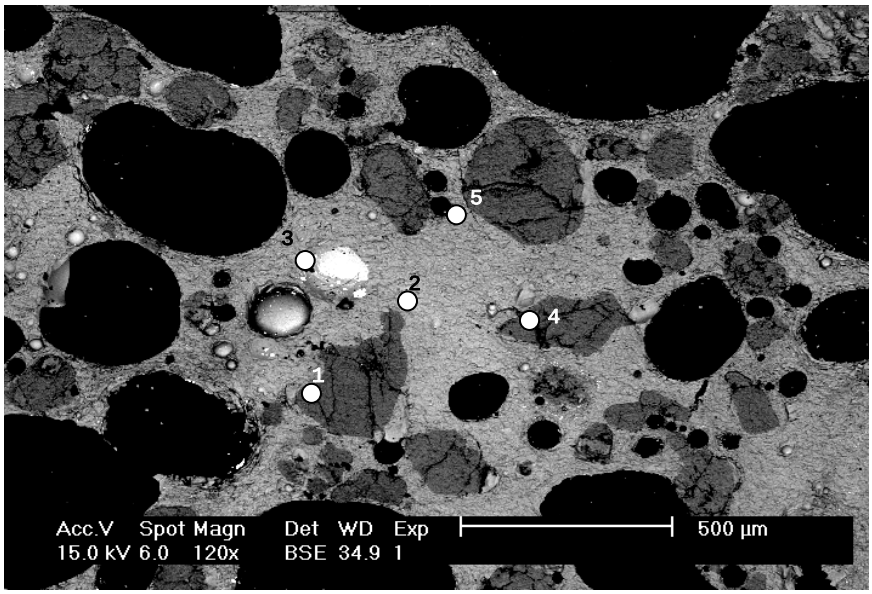

Figure 6.4. Backscatter electron image, cross section of PDU agglomerate, Analysis Area 2

Table 6.7. Energy dispersive spectroscopy results, Analysis Area 2

Element	1	2	3	4	5
	wt %	wt %	wt %	wt %	wt %
O	50.58	41.84	27.88	42.77	45.51
Na	-	9.56	6.76	-	9.02
Mg	-	2.98	2.75	-	2.44
Al	-	2.52	2.61	-	1.6
Si	49.42	32.48	30.37	57.23	33.49
S	-	-	6.5	-	-
Ca	-	5.88	4.58	-	4.55
Fe	-	4.74	18.56	-	3.38
Total	100	100	100	100	100

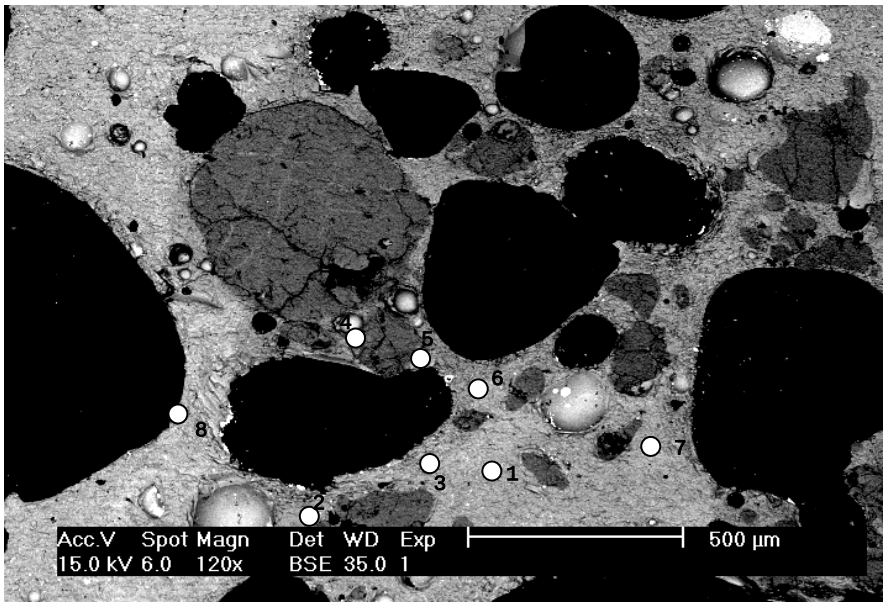

Figure 6.5. Backscatter electron image, cross section of PDU agglomerate, Analysis Area 3

Table 6.8. Energy dispersive spectroscopy results, Analysis Area 3

Element	1	2	3	4	5	6	7	8
	wt %	wt %	wt %	wt %	wt %	wt %	wt %	wt %
O	44.02	43.36	39.03	46.71	35.7	45.08	44.8	42.93
Na	9.49	7.6	9.16	-	5.96	10.0	8.2	9.92
Mg	2.79	2.56	2.58	-	1.93	2.99	3.05	3.83
Al	1.51	1.48	1.8	-	2.08	2.14	2.42	2.73
Si	34.24	38.37	33.48	53.29	42.19	33.2	34.09	27.45
S	-	-	1.9	-	-	-	-	0.84
Cl	-	-	-	-	1.29	-	-	0.94
Ca	5.58	4.35	6.58	-	7.48	4.29	4.6	7.22
Fe	2.37	2.28	5.47	-	3.36	2.31	2.84	4.13
Total	100	100	100	100	100	100	100	100

The light-grey area surrounding the embedded mineral particles is a heterogeneous mixture consisting of approximately one-third silicon in combination with sodium, calcium, magnesium and aluminium. In each of the analysis point concerning the bulk agglomerate matrix (i.e. Points 2, 3 and 5 in Table 6.7, and Points 1-3 and 5-8 in Table 6.8), Al is detected at 1.5 to 2.7 wt%, while Si is present at 27 to 42 wt%, suggesting that much of the matrix is silicate rather than aluminosilicate material. Sodium (6.8 to 10.0 wt%) is generally more prevalent than calcium (4.3 to 7.5 wt%) or magnesium (1.9 to 3.8 wt%), indicating a significant presence of sodium silicate glass in the agglomerate matrix. Inclusions of iron-sulphur minerals are also present, designated by white areas in the

agglomerate structure. Point 3 in Table 6.7 shows a composition high in iron (18.6 wt%) and sulphur (6.5 wt%), indicating possible FeS formation.

Analysis of elemental distribution confirms that sodium silicate is prevalent throughout the bulk agglomerate matrix. Figure 6.6 and Figure 6.7 show X-ray maps of elemental distributions within PDU agglomerate cross-sections. In Figure 6.6, Na has a strong, evenly dispersed composition in the agglomerate matrix, as does silicon. Unlike agglomerates formed in spouted bed experiments, sodium is not concentrated around the embedded silica particles. Conversely, Ca, Mg and Al distributions show generally weaker signals throughout the matrix, appearing more prevalent towards the edge of the agglomerate (i.e. right-hand edge of images in Figure 6.6). Similar trends are also observed in Figure 6.7, although Ca, Mg and Al show a stronger presence, particularly at the edges of the agglomerate cross-section, closest to the exposed areas (i.e. black areas). These observations suggest that the formation of calcium and magnesium silicates and aluminosilicates are favoured by oxidising conditions, while reducing conditions within the agglomerate structures are conducive to sodium disilicate formation.

The general absence of calcium, magnesium silicates and aluminosilicates within the agglomerate structure suggest strongly that addition of dolomite to the bed in the remaining tests provided a benefit to operation other than simply sulphur capture. Additional calcium and magnesium in the bed may have resulted in preferential formation of high melting point silicates/aluminosilicates, and consequently suppressed the formation of low melting sodium disilicate-quartz eutectics to an extent. With reduced liquid content within the ash, and the lower temperature of operation, deposition of ash, and formation of hot-spots, was avoided. Equilibrium thermodynamics support the effect of increasing ash melting point with dolomite addition. Equilibrium phase diagrams indicate that increasing calcium content of a sodium silicate mixture above 5% of total composition increases the liquidus temperature of the mixture by approximately 100°C (Morey and Bowen, 1924). Thus, by using calcium-rich additive with high sodium, high-sulphur content lignite, the minimum agglomeration temperature of the bed may also be increased. Thus, in an industrial process, the use of high-sodium lignite may be dependent on the ability for additives such as dolomite to be added to the bed, thus avoiding the ash-related problems of agglomeration and defluidisation.

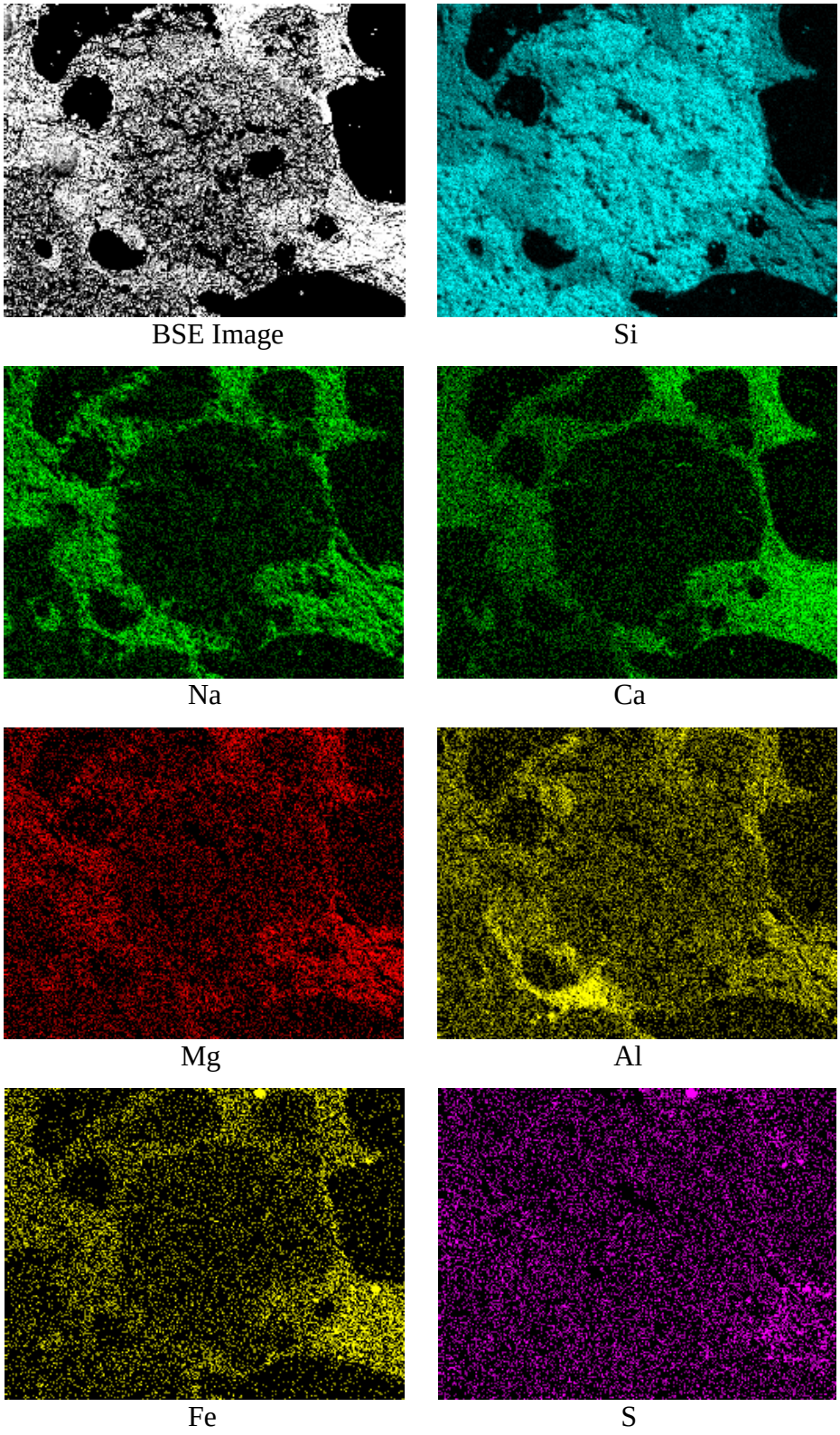

Figure 6.6. X-ray maps showing elemental distribution throughout PDU agglomerate cross-section

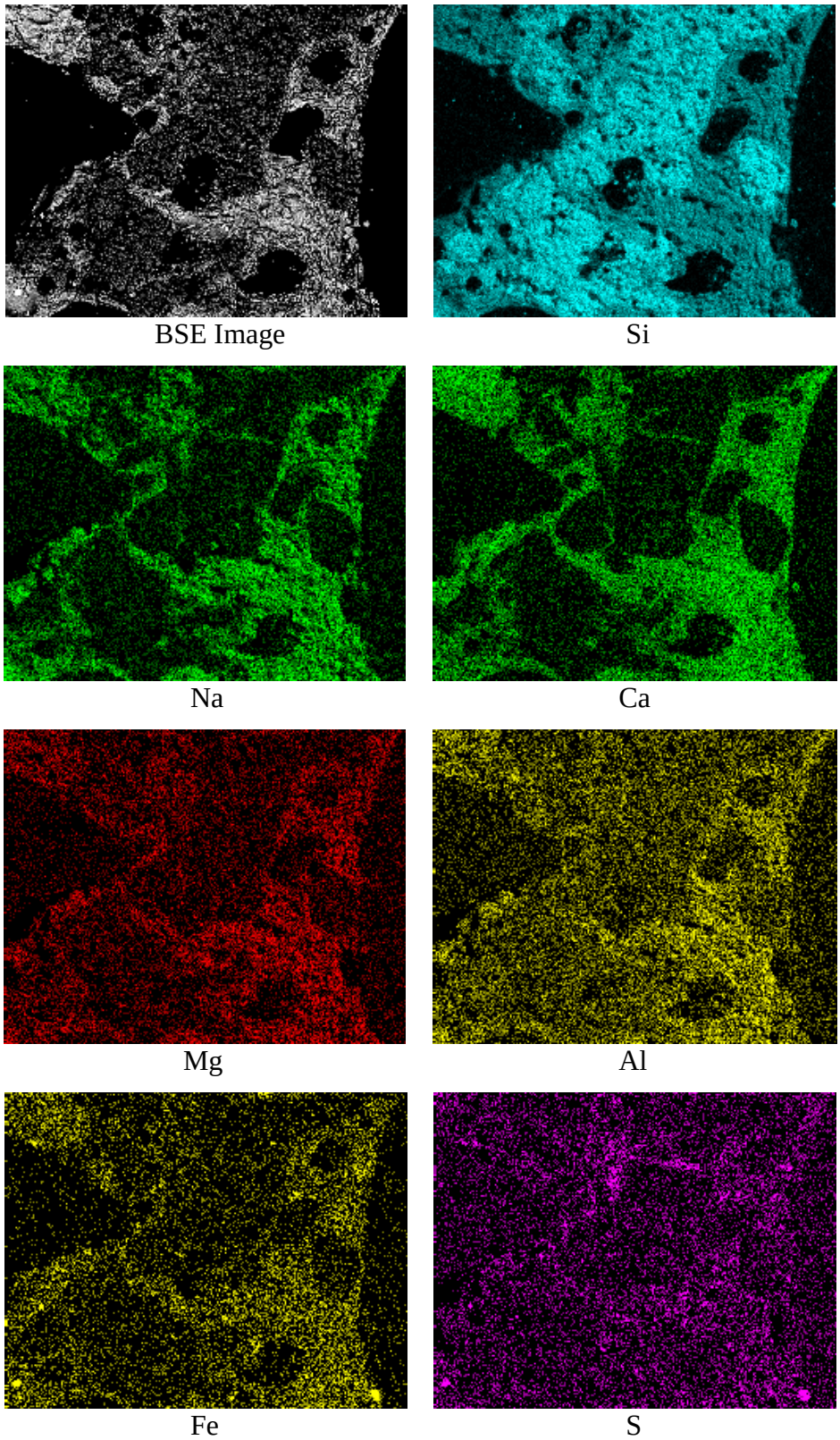

Figure 6.7. X-ray maps showing elemental distribution throughout PDU agglomerate cross-section

6.5 Significance of results to agglomeration and defluidisation behaviour during gasification of high-sodium, high-sulphur content lignite

The trials conducted in the PDU validated a number of conclusions arising from the spouted bed gasification experiments, which include:

- agglomerate structure is based on mineral particles embedded in a silicate matrix;
- agglomeration occurs via deposition of molten ash at the walls of the reactor;
- a key component in agglomerate structures formed from Lochiel coal is an amorphous, sodium-rich silicate mixture, which forms via reaction of sodium with silica from the coal;
- minimum temperature of agglomeration is reduced via the addition of steam to the reactant gas, or in the case of the PDU, increase in the pressure of steam; and
- preferential formation of calcium and magnesium silicates and aluminosilicates over sodium silicate mixtures enables operating temperature to be increased before agglomeration begins to impact upon stable operation.

In the PDU tests, reduction of bed operating temperature is likely to have provided the largest benefit to operation between tests that agglomerated, and those which operated in a stable manner for the entire operating time. Significantly better process control was achieved when the bed was operated below 800°C (Bhattacharya, 2005b). Dolomite addition to the bed may have also been responsible for improving operation of the PDU however, with the formation of calcium and magnesium silicate species. A similar effect of improvement of operation via additives was observed in circulating fluidised bed combustion (CFBC) tests with Lochiel coal, with dolomite additive resulting in greater $CaSO_4$ formation in the ash, thereby raising sintering temperature of coating forming on bed material (Bhattacharya et al., 1999).

The measures described above for reducing agglomeration propensity with Lochiel coal – namely, lowering bed temperature and raising calcium and magnesium content of the bed – may each have resulted in more stable operation of the PDU. No tests were conducted observing the impact of running with pure char below 800°C, or running above 800°C with dolomite additive, in order to separate the relative effects of each measure. Further work would be beneficial for assessing the relative effects of these measures in mitigating agglomeration propensity during gasification of high-sodium lignite.

In fundamental terms, the problematic deposition of ash at the walls of the gasification reactor is dependent on the formation of liquid phase in the ash. Once this occurs, localised 'hot spots' in the bed create self-sustaining conditions for deposit growth. Thus, the key to controlling ash agglomeration/deposition problems is to operate at conditions that limit liquid phase formation in the ash, and hence avoid initiation of deposition in the first place. The ability for the use of additives in the bed to improve operation is a commercial and availability consideration, and may not be viable in a large-scale continuous process. Lowering bed temperature to avoid agglomeration may also not be viable, depending on the output gas composition that is required for the process. Another option for control of agglomeration that was not investigated in the PDU is to operate at pressures closer to atmospheric. Evidence presented in the preceding sections shows that agglomeration occurred at lower temperature compared to spouted bed tests, with higher steam pressures lowering the liquidus temperature of sodium disilicate. Thus, provided gas output is acceptable under lower pressure conditions, control of agglomeration could also be achieved by operating under atmospheric conditions.

6.6 Summary

Tests were conducted in the HTW-type Process Development Unit in order to validate conclusions developed from spouted bed gasification tests. Results confirmed that deposition of ash occurs via the coating of minerals in a heterogenous molten silicate mixture, and that the key component for liquid phase formation in the ash is the sodium disilicate-quartz eutectic.

Elevated operating pressure resulted in a reduction in the minimum agglomeration temperature from approximately 860°C under typical spouted bed gasification conditions to 800-850°C in the PDU. Reducing operating temperature to below 800°C resulted in stable operation, with no evidence of agglomeration. Addition of calcium- and magnesium-rich dolomite also coincided with improved operation, which both acted as a capture for sulphur in the output gas, and increased the content of calcium and magnesium in the bed. It is surmised that raising calcium and magnesium levels in the ash results in an increase in high melting point compounds in the ash, including calcium and magnesium silicates and aluminosilicates, thus reducing liquid phase formation.

Control methods suggested for limiting agglomerate formation were suggested, which include:

- reducing bed temperature below the minimum agglomeration temperature of the ash;
- reducing operating pressure to atmospheric conditions, or decreasing steam content of the fluidising gas; and
- addition of calcium to the bed (if viable).

By implementing the above measures, agglomeration and deposition of ash from high-sodium, high-sulphur content lignite could be minimised, and hence the use of such coal for commercial gasification processes will be possible.

CHAPTER 7

CONTROL OF AGGLOMERATION AND DEFLUIDISATION DURING FLUIDISED BED GASIFICATION OF HIGH-SODIUM, HIGH-SULPHUR LIGNITE

7.1 Introduction

In this chapter, an operational methodology for controlling agglomeration and defluidisation during gasification of high-sodium content lignite is presented. Experimental results pertaining to agglomeration and defluidisation behaviour of Lochiel coal are consolidated and discussed. The areas covered in the discussion include the operational behaviour of high-sodium lignite when subjected to 'agglomerating conditions', and the ash chemistry that contributes to this behaviour. The findings from the experimental data are subsequently used to suggest operating methodology for effective control of agglomeration and defluidisation during gasification of high-sodium, high-sulphur content lignite.

7.2 Mechanism of agglomeration and defluidisation behaviour of high-sodium lignite under gasification conditions

7.2.1 Introduction

In both the spouted bed experiments and the PDU validation tests, stable operation was defined by stable pressure drop and bed temperatures for the duration of operation.

Behaviours characterising agglomeration and defluidisation during gasification, as per analysis from both the spouted bed and PDU experiments, include:

- Growth of particles in the bed during operation via coating of solid mineral particles by molten ash;
- A loss of effective fluidisation in the bed, which is characterised by reduction of pressure difference measured between the top of the bed and the distributor;
- Generation of hot spots within the bed due to impeded particle movement, resulting in bed temperature excursions, thereby raising the rate of ash sintering and exacerbating the extent of agglomeration; and
- Consolidation of molten ash particles as deposits at the walls of the reactor vessel, where relative movement of char and bed particles is lowest.

Of these behaviours, the growth of particles via molten ash formation initiates the problems of agglomeration and defluidisation, as it results in destabilisation of the fluidisation in the bed.

To satisfy the objectives of the present study, identification of the lowest melting point species forming in the ash is required. This inorganic species creates the molten properties exhibited by the ash as the bed temperature increases beyond the 'initial sintering temperature', and hence causes the particle growth leading to agglomeration and defluidisation. By identifying this species, implementation of control methods to limit its formation in a fluidised bed gasifier is possible. The following section summarises experimental results from all gasification conditions, namely:

- 'Low' steam spouted bed gasification (10-13 wt% steam content in the fluidising gas);
- 'Medium' steam spouted bed gasification (14-17 wt% steam in the fluidising gas);
- 'High' steam spouted bed gasification (approximately 90 wt% steam in the fluidising gas); and
- PDU gasification tests.

These results are used to determine the problematic species contributing to agglomeration and defluidisation during gasification of high-sodium lignite, and identify the physical mechanisms in the bed resulting in defluidisation.

7.2.2 Inorganic Behaviour Contributing to Agglomeration

Table 7.1 summarises the semi-quantitative analysis of ash agglomerate mineral phases via the XRD technique in each set of steam gasification conditions. Mineral phases detected in more than one semi-quantitative category across experiments from similar steam gasification conditions are indicated.

Table 7.1. Summary of mineralogical analysis of agglomerates distinguished by gasification conditions.

Mineral phase dominance	Spouted bed			PDU
	Low steam (10-13 wt% steam in fluidising gas)	Medium steam (14-17 wt% steam in fluidising gas)	High steam (90 wt% steam in fluidising gas)	
Dominant (>60%)	Quartz*, gehlenite	Quartz*, gehlenite*	Quartz, amorphous*	Quartz
Sub-dominant (20-60%)	Quartz*, forsterite*, augite*	Gehlenite*, augite*	Amorphous*	-
Minor (5-20%)	Nepheline, augite*, magnetite, monticellite, forsterite*	Amorphous, augite*, magnetite, quartz*, lime*, thenardite, monticellite*	Magnetite, gehlenite*, oldhamite*, augite, anhydrite	Gehlenite, cristobalite, amorphous
Trace (<5%)	Hematite, thenardite	Anhydrite, oldhamite, lime*, periclase, nepheline, magnesite, monticellite*	Gehlenite*, periclase, nepheline, hematite, oldhamite*, thenardite, lime, monticellite	Monticellite, augite

* Indicates agglomerate mineral phases appearing in more than one semi-quantitative category under the same experimental conditions.

The major silicate phases identified in Table 7.1 all possess melting temperatures significantly greater than the minimum temperatures at which defluidisation was detected under each set of gasification conditions. Table 7.2 shows the empirically determined melting temperatures of each silicate mineral species. None of the mineral species possess liquid temperatures below approximately 1280°C (i.e. nepheline), which is well above the measured operating temperatures used in any of the gasification runs. Based on this analysis, none of these mineral species are expected to have initiated defluidisation via molten phase formation in the ash.

Table 7.2. Mineral species and the temperatures at which they become completely liquid. Adapted from phase diagrams presented by Hall and Insley (1947)

The prevalence of silicon-based minerals detected in agglomerates (other than quartz) appears to decrease as steam content of the fluidising gas increases. Gehlenite is detected in dominant proportions in agglomerates from low steam gasification conditions, and is present in sub-dominant quantities in agglomerates from the medium steam gasification tests. However, gehlenite is present in only minor to trace amounts in agglomerates from high steam gasification experiments. Other calcium silicate phases, including augite and monticellite, are present in sub-dominant to minor quantities in low steam gasification agglomerates, and in minor to trace quantities under high steam conditions. Forsterite, a magnesium silicate, is only present in the 'low' steam gasification conditions at sub-dominant to minor proportions, while magnesium is present as periclase (MgO) in trace quantities under medium and high steam spouted bed gasification conditions. Agglomerates from the PDU, which formed at a temperature between 800 to 850°C, possess a composition similar to that of high steam gasification agglomerates. Under these conditions, gehlenite is present in only minor amounts, while monticellite and augite are only present in trace quantities. Neither periclase nor forsterite are present in agglomerates from PDU tests.

The variation in content of alkaline earth silicates and aluminosilicates with steam gasification conditions is reflected in overall composition of agglomerates. Figure 7.1 shows data presented in Figure 5.6, Chapter 5 (excluding SiO_2 and Fe_2O_3), with comparison made to analysis data from agglomerates formed in the PDU. Compositions of aluminium, calcium, and magnesium in the agglomerates are all greater under low steam

gasification conditions in comparison to those formed under high steam conditions. As indicated by the mineralogical analysis, the composition of agglomerates formed in the PDU tests more closely resembles the composition of high steam runs, with the exception of sulphur content, which is closer to the content observed in typical steam gasification runs. In contrast, no significant variation in sodium content is observed between the different gasification conditions.

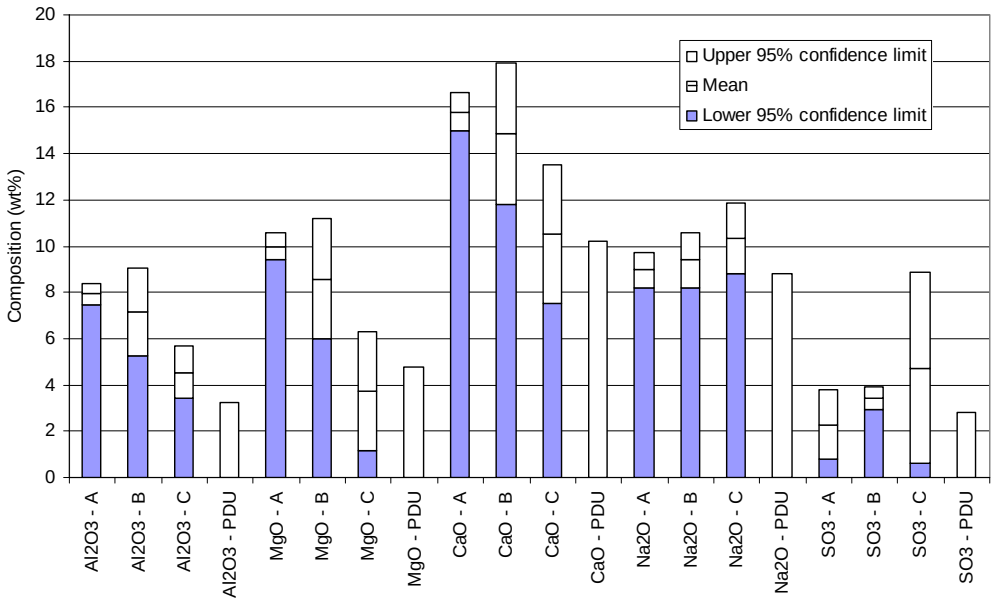

Figure 7.1. Variation of Al, Mg, Ca, Na and S content in agglomerates from gasification conditions used in experimental program. A - low steam gasification (10-13 wt% steam in the fluidising gas); B – Medium steam gasification conditions (14-17 wt% steam in the fluidising gas); C – High steam gasification conditions (90 wt% steam in the fluidising gas); and PDU – Pilot scale tests (confidence intervals for data values not included).

Although calcium, magnesium, and aluminium content in the agglomerates all decrease as steam content in the fluidising gas increases, the analysis data does not indicate a corresponding increase in these elements in either the bed char or cyclone dust to account for the discrepancy. Figure 7.2 and Figure 7.3 show the ash composition of bed char and cyclone dust, respectively, for the runs in which agglomeration occurred. Only sulphur shows variation to any significant extent, with average retention of sulphur in the agglomerates and bed char increasing with increasing steam content, and correspondingly decreases in the cyclone dust. Note however that the large variation in sulphur in the analysed samples does not make these trends of sulphur content statistically significant. Other components, including calcium, magnesium and aluminium, remain relatively consistent across the analysed bed char and cyclone dust samples.

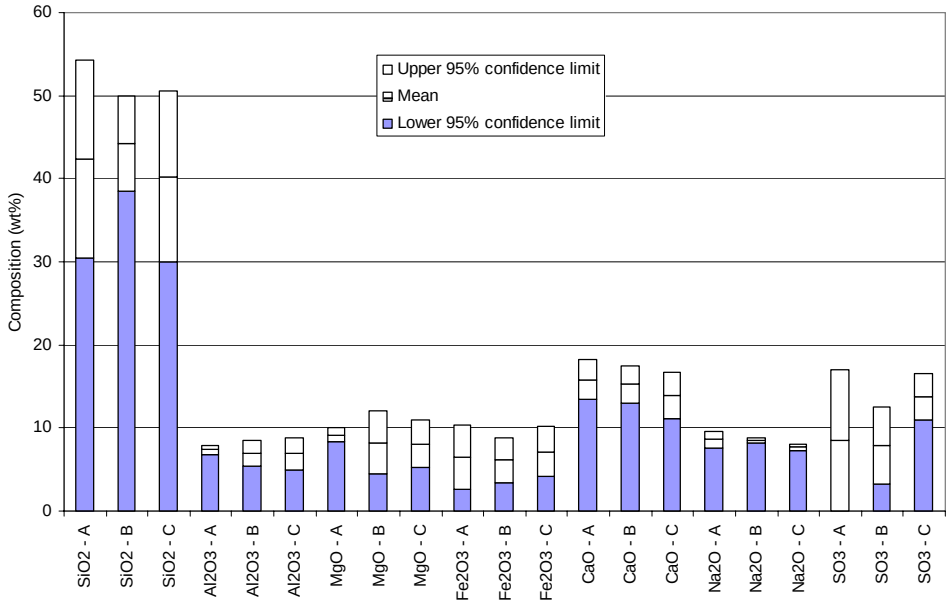

Figure 7.2. Bed char ash analysis for low, medium, and high steam gasification runs.

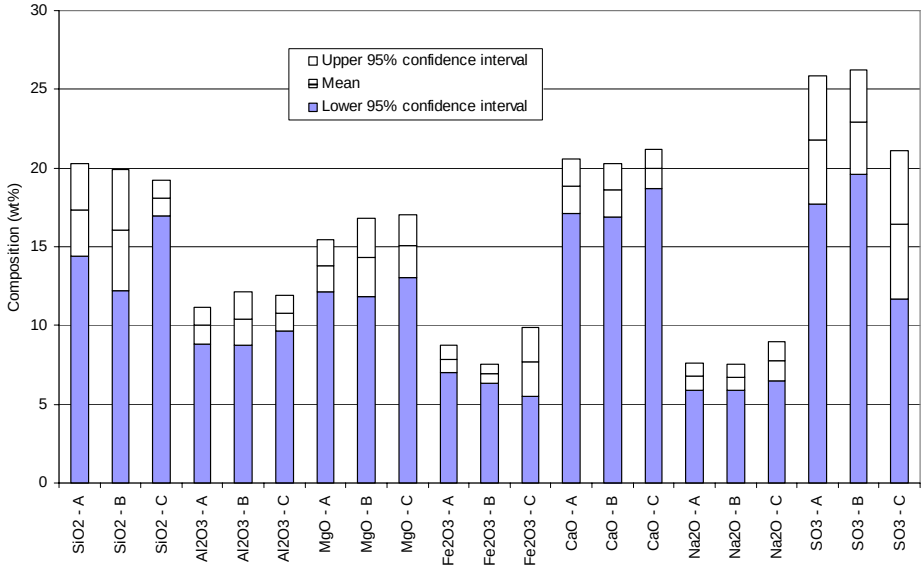

Figure 7.3. Cyclone dust ash analysis for low, medium, and high steam gasification runs.

The lack of variation of composition in the bed char from spouted bed experiments may be a result of the fact that coal continues to be fed into the reactor even following bed defluidisation, until the pre-defined 4 hour run length is reached. Defluidisation effectively prevents further circulation of char through the bed as agglomerates form in the annulus of the spouted bed, indicating that additional char entering the reactor would sit on top of the bed. At the completion of experiments in which defluidisation occurred, it was often

observed that very little bed char would exit the reactor following removal of the removable conical distributor, until manual breakage of the agglomerates was performed. Once this occurred, the char would flow freely from the bottom of the reactor and be collected for further analysis. This observation suggests that the assumption of additional char entering the reactor and forming a bed on top of the original defluidised bed is correct. Thus, analysis of char composition from a bed in which extensive agglomeration occurred would not necessarily represent the composition of char in the bed at the time of defluidisation, but rather the composition of char that had not taken part in the agglomeration process.

One possible reason for the relative consistency of the elemental compositions in the cyclone dust across all gasification conditions is that a certain proportion of the coal feed may have been elutriated from the vessel before entering the bed. Although fines below 1 mm were removed from the coal prior to feeding to the bed, some breakage of the coal particles may have occurred in the screw feeder. Manzoori (1990) observed that a small increase in fines was encountered using the same screw feeder during spouted bed combustion experiments due to such breakage. Thus, with a portion of fine material from the coal feed passing directly to the cyclone upon entering the spouted bed vessel, some dilution of the fines elutriated from the bed would be expected. This would account for sulphur content of the cyclone dust from typical steam gasification conditions being present at approximately 20 to 25 wt%. In the Run-Of-Mine coal, 27.5 wt% of the ash was present as sulphur (refer to Table 3.1, Chapter 3). Even with elutriation of fines, partitioning of elements is evident, with only 15 to 20 wt% of the cyclone dust ash present as silica, compared to 31.4 wt% silica in the coal ash, and approximately 40 to 45 wt% silica in the bed char. Thus, the continued elutriation of feed coal fines directly to the cyclone may have masked any increase of calcium, magnesium or aluminium in the cyclone dust ash with increasing steam content of the fluidising gas.

As the content of alkaline silicate and aluminosilicate mineral species in the agglomerates decreases with increasing steam content, the amorphous, non-crystalline phase tends to increase in proportion. The highest proportion of amorphous material detected in agglomerates is found under high steam conditions, in dominant to sub-dominant proportions (Table 7.1). Under medium steam conditions, the amorphous phase is present in minor amounts, while no amorphous material was detected under low steam conditions.

All agglomerates were composed wholly of inorganic material, indicating that the amorphous phase is an inorganic species. In addition, quartz (SiO_2) is present in dominant quantities in agglomerates from all conditions. Elemental analysis conducted in Chapter 5, Section 5.3.4, also indicates that compositions of silica in the agglomerates are not significantly different between the relative steam gasification conditions. Thus, even though the detection of silicate and aluminosilicate minerals using XRD showed a decrease in composition with increasing steam content of the fluidising gas, the total content of silica remained relatively constant in the agglomerates. It can therefore be surmised that the reduction of silicate mineral prevalence in the agglomerate structure is a result of more silicate content being present in amorphous form (i.e. as a silicate glass).

Sodium in particular appears to be a component of the amorphous phase. In agglomerates with an amorphous phase present, only trace quantities of sodium compounds were detected, in the form of nepheline, and thenardite in some cases. In the case of the agglomerates from the PDU, no sodium species were detected at all. However, Figure 7.1 shows that sodium content does not vary significantly between gasification conditions, providing evidence that the remaining sodium was present in other non-crystalline forms that were unidentifiable by XRD analysis. Given that the amorphous phase appears to contain silicate matter, this suggests that sodium silicate glass is a significant component of the amorphous mixture. This assessment agrees with the conclusions from the study conducted by Kosminski (2001) that sodium disilicate forms in the ash under steam gasification conditions.

Visual analysis via SEM indicates that glass is present in the agglomerate structures. Two examples of agglomerate cross-sections from high steam runs, analysed using SEM-EDS, are shown in Figure 7.4 and Figure 7.5. These figures show significant areas of smooth, glass-like appearance, indicating that these areas were likely molten during gasifier operation. These smooth areas were not cut during sample preparation, having passed sufficiently below the cutting plane to avoid being affected, and thus represent the surface of the agglomerates. Also evident are quartz particles embedded in the glassy phase, as indicated by the enclosed area in Figure 7.4. The quartz particles can be distinguished from the glass along the cutting plane by a definite difference in texture, with quartz exhibiting a rough appearance, and the glass phase retaining a more smoothed texture.

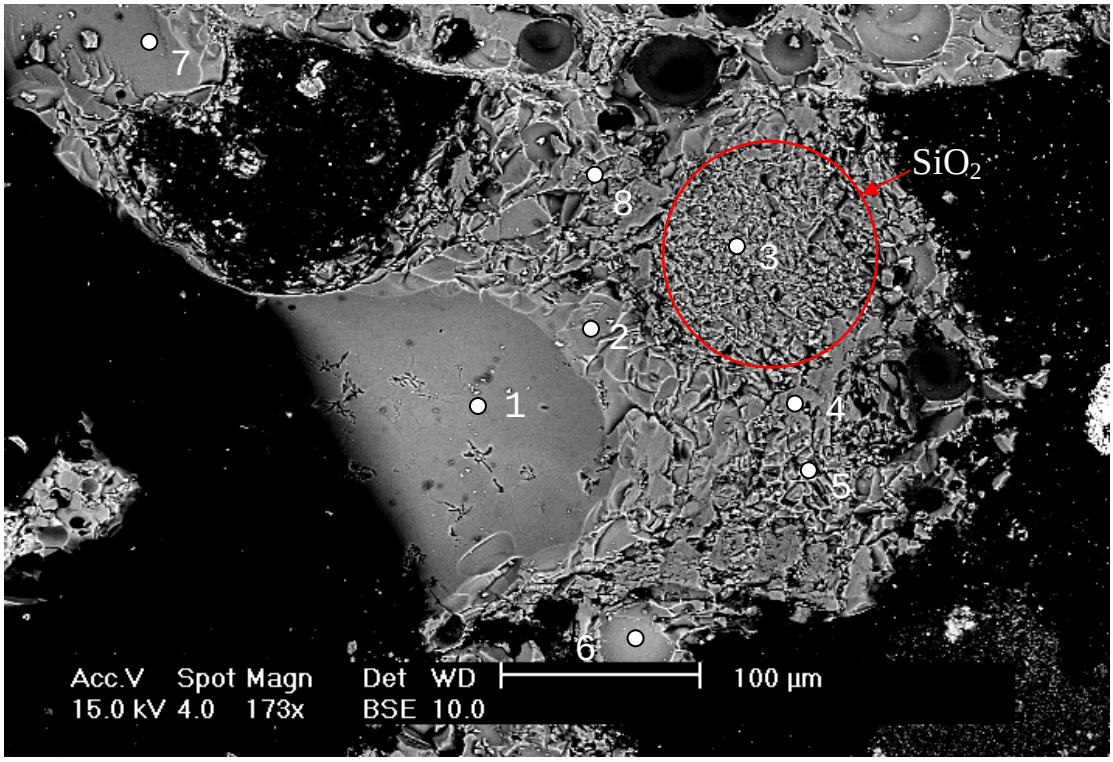

Figure 7.4. Backscattered-electron (BSE) micrograph image of an agglomerate cross-section from a high steam run (C03). Points 8 to 15 represent the points where electron dispersive spectrometry was carried out for elemental analysis, the results of which are presented in Table 7.3.

Table 7.3. Elemental analysis results of electron dispersive spectrometry, carried out on agglomerate cross-section depicted in Figure 7.4.

Point	O	Na	Mg	Al	Si	S	Cl	Ca	Ti	Fe	Total
1	38.7	6.00	-	-	51.9	-	-	-	-	3.34	100
2	44.8	10.9	-	-	44.3	-	-	-	-	-	100
3	27.0	-	-	1.06	71.9	-	-	-	-	-	100
4	17.8	5.87	-	1.06	69.9	-	2.86	2.47	-	-	100
5	46.4	10.1	-	-	38.6	1.43	-	1.73	-	1.66	100
6	30.4	7.42	1.38	-	45.5	-	1.58	4.81	4.62	4.30	100
7	33.4	4.49	-	-	52.9	-	1.35	4.20	-	3.70	100
8	45.9	12.0	-	-	41.0	-	1.05	-	-	-	100

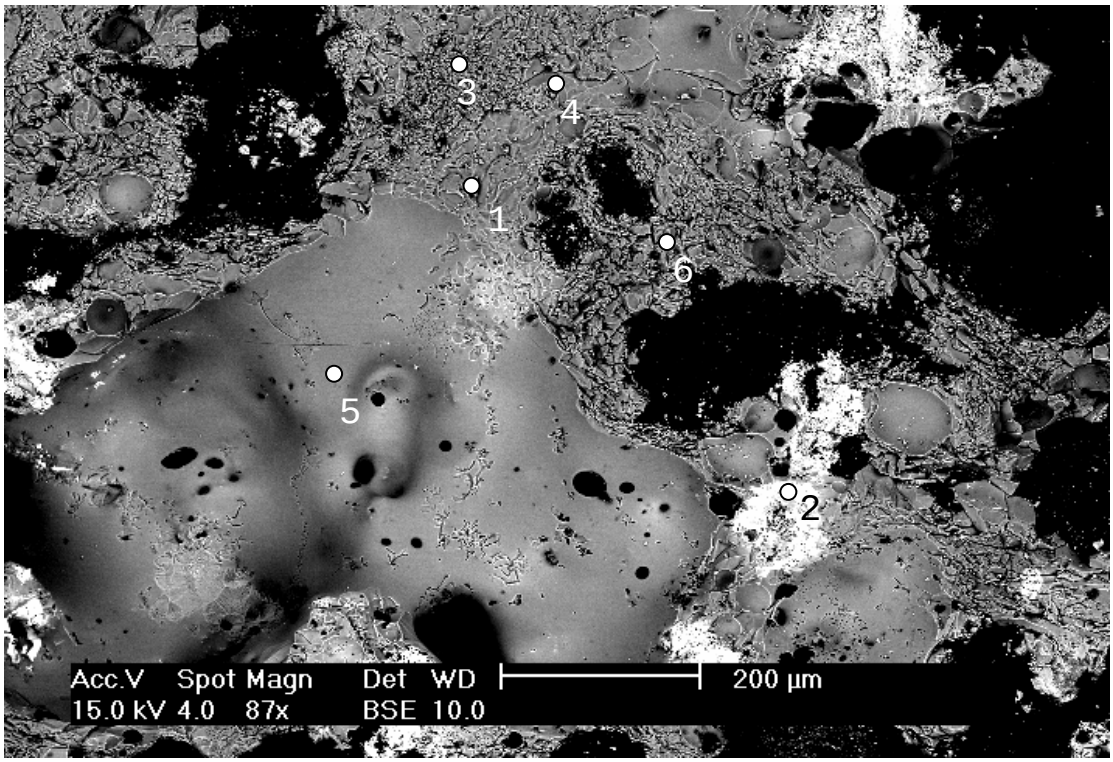

Figure 7.5. Backscattered-electron (BSE) micrograph image of an agglomerate cross-section from a high steam run (C03). Points 16 to 21 represent the points where electron dispersive spectrometry was carried out for elemental analysis, the results of which are presented in Table 7.4.

Table 7.4. Elemental analysis results of electron dispersive spectrometry, carried out on agglomerate cross-section depicted in Figure 7.5.

Point	O	Na	Al	Si	Cl	Ca	Ti	Fe	Total
1	22.5	7.82	1.12	58.5	1.72	2.76	-	5.59	100
2	25.7	1.81	-	3.59	-	-	-	69.0	100
3	42.1	1.13	-	56.7	-	-	-	-	100
4	36.5	9.87	-	45.6	1.70	1.81	1.59	2.94	100
5	36.4	10.6	1.10	41.4	1.35	2.55	3.00	3.54	100
6	48.4	11.2	-	26.5	-	4.44	6.32	3.17	100

Analysis of the glass areas shows areas that range in composition from 5.9 to 12.0% Na and from 26.5 to 69.9% Si, with only trace inclusions of other elements in some cases (refer to Table 7.3 and Table 7.4). Given that the elemental composition of the sodium disilicate-quartz eutectic is 19.1% Na and 34.6% Si and the remainder oxygen (Kracek, 1939), this demonstrates that the glass is higher in silica than would constitute the pure eutectic composition. This agrees with experimental observations by Morey and Bowen (1924), which suggest that sodium-silicate mixtures with greater silica present than the sodium-disilicate-quartz eutectic are the most difficult to crystallise from a glass state of all

sodium-silica compositions. The sodium-silica phase diagram developed by Kracek (1939) indicates that some liquid silicate phase would be present in equilibrium with quartz at temperatures above 789°C (in air) for compositions above the sodium disilicate-quartz eutectic composition. Therefore, the glass compositions detected above are well within the range of liquid phase formation for the temperatures used in the high steam gasification experiments, and thus further enhances the claim by Kosminski (2001) that sodium disilicate-quartz mixtures are the major binding phase contributing to agglomeration in high-sodium lignite.

The amorphous phase does not appear to be a homogenous mixture of sodium silicate however, with inclusions such as calcium, magnesium, iron and aluminium observed in analysed agglomerate cross-sections. Figure 7.6 shows a cross-section of an agglomerate from the high steam gasification runs, with analysis results presented in Table 7.5. Analysis point 2 shows a probable quartz particle, with 55.7% consisting of Si. Points 1, 3, 5 and 6 appear to indicate the bulk matrix surrounding the quartz phase, with sodium present in significant contents (8.6-11.7%), indicating that the amorphous phase is primarily a sodium silicate mixture. Other elements such as Ca, Mg, Al, Fe and even S are detected in varying amounts at these points, such that the matrix cannot be considered a pure mixture of sodium disilicate. Such inclusions in a silicate mixture can result in a decrease in its melting point, as indicated by equilibrium phase diagrams (Hall and Insley, 1947).

Point 4 of Table 7.5 shows a white coloured area high in iron (76.6%) with only a small amount of oxygen present (7.9%), suggesting iron in reduced form. A small amount of sulphur is present at this location (2.6%), although not in large enough quantity to indicate iron sulphide. FeS is known to form an amorphous phase in a reducing environment, when iron-rich minerals such as hematite react with reducing gases, in particular H_2S (Berner, 1964; Wiggering, 1990). Such a species was only observed to form as isolated inclusions in the agglomerate structures however, and is unlikely to form a large proportion of the amorphous phase given that hematite and magnetite are detected in amounts up to minor quantities (5-20% of the total mineral phases), and iron under typical gasification conditions is only detected at approximately 5 wt% of the agglomerate composition.

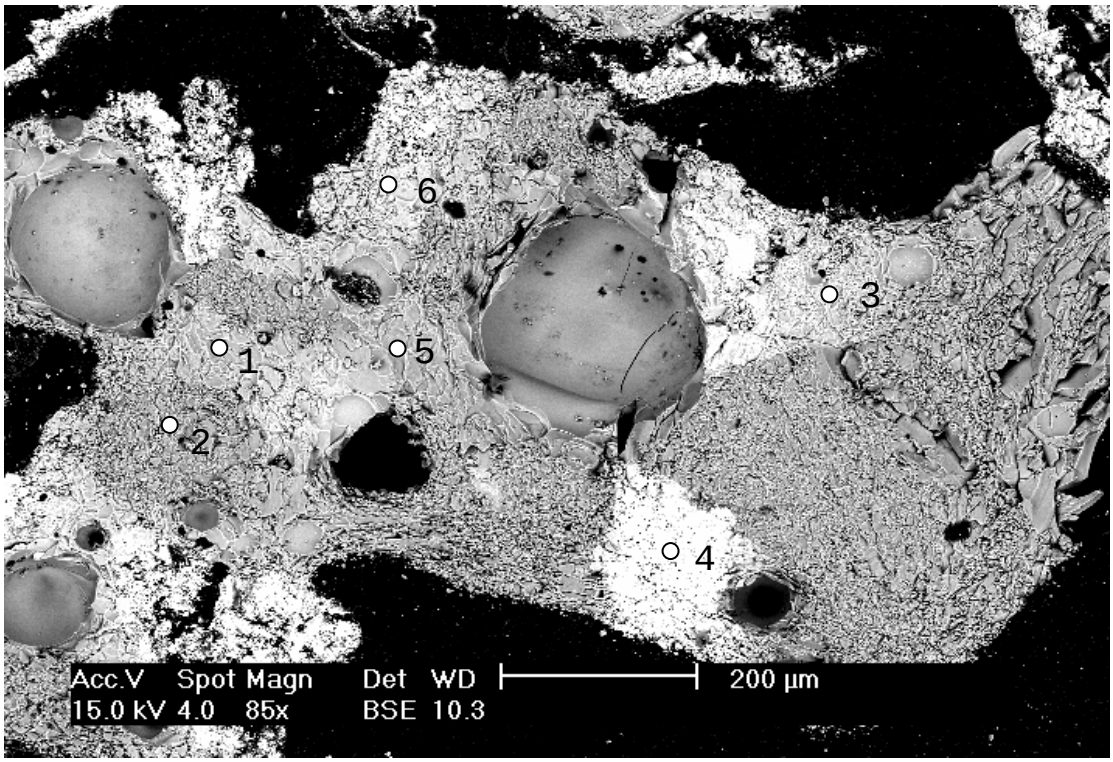

Figure 7.6. Backscattered-electron (BSE) micrograph image of an agglomerate cross-section from a high steam gasification run (C01). Points 1 to 6 represent the points where electron dispersive spectrometry was carried out for elemental analysis, the results of which are presented in Table 7.5.

Table 7.5. Elemental analysis results of electron dispersive spectrometry, carried out on agglomerate cross-section depicted in Figure 7.6.

Point	O	Na	Mg	Al	Si	S	Ca	Fe	Total
1	40.8	11.7	-	-	34.9	-	2.31	3.84	100
2	34.4	-	-	-	55.7	1.16	-	-	100
3	41.8	8.63	3.08	2.35	26.9	1.31	5.01	5.46	100
4	7.91	1.81	-	-	6.36	2.55	-	76.6	100
5	45.8	11.5	-	-	33.0	-	1.25	1.50	100
6	41.3	9.44	-	-	33.1	-	5.15	7.03	100

Analysis of agglomerate structures indicates that sodium reacts with silica preferentially to other species, providing a reason for the relatively constant Na_2O/SiO_2 ratio maintained in all agglomerates from gasification experiments. Figure 7.7 to Figure 7.9 show comparisons of sodium and calcium contributions of agglomerate cross-sections obtained from low steam, high steam, and PDU gasification conditions. Figure 7.7a gives the clearest indication of the mode of agglomerate formation during gasification, with the sodium-silicate phase concentrated around the quartz mineral phase. The bulk agglomerate matrix surrounding the silica particle is composed of predominantly calcium (Figure 7.7b), likely

to be in the form of high melting temperature mineral species such as gehlenite, augite and monticellite, with lesser amounts of sodium. These observations add further weight to the assessment that a sodium-rich silicate phase is forming a molten amorphous phase in the bed, thereby acting as the glue between solid mineral particles.

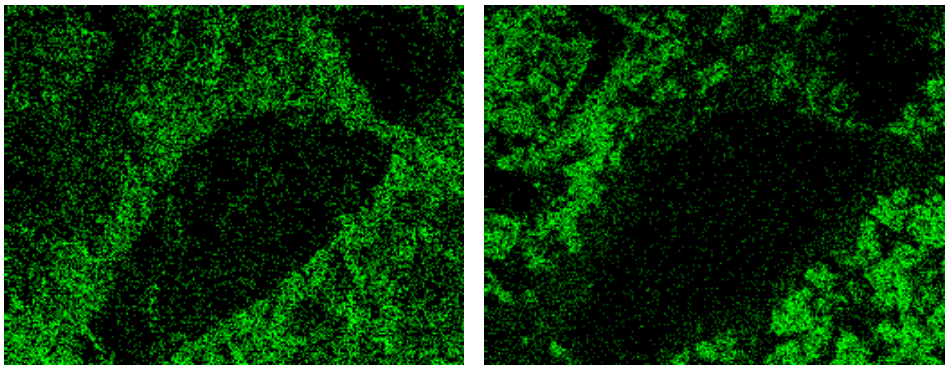

(a) (b)

Figure 7.7. Elemental distributions in an agglomerate cross-section from Run A04. (a) Na; (b) Ca.

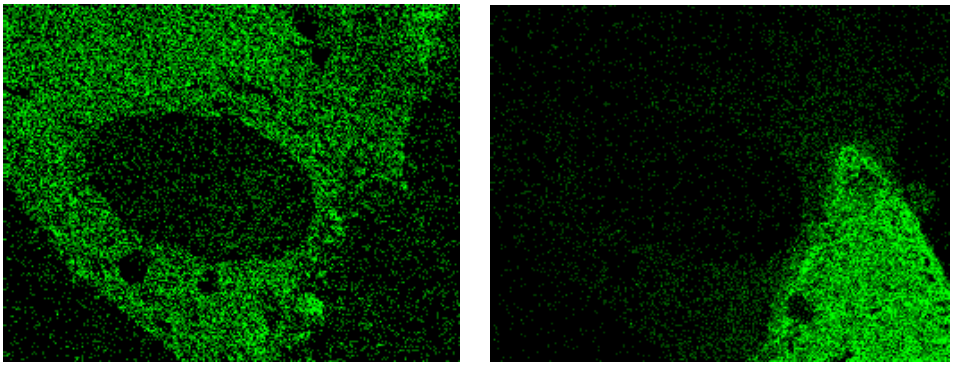

(a) (b)

Figure 7.8. Elemental distributions in an agglomerate cross-section from Run C05. (a) Na; (b) Ca.

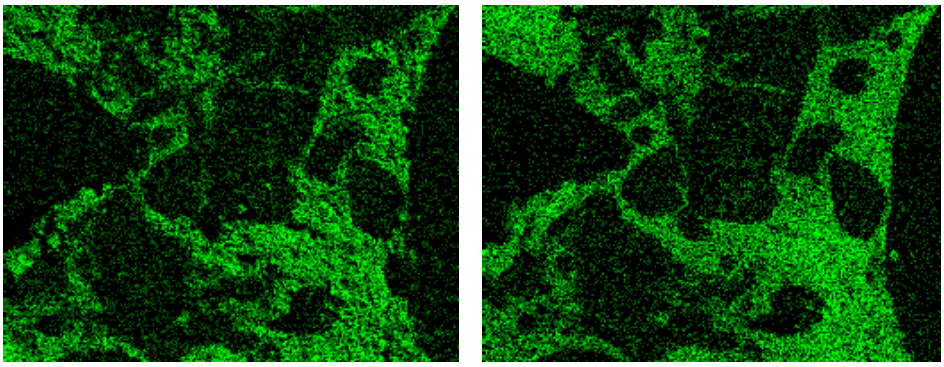

(a) (b)

Figure 7.9. Elemental distributions in an agglomerate cross-section from the PDU. (a) Na; (b) Ca.

Sodium distribution is distributed more evenly throughout the bulk ash matrix under high steam gasification conditions. Figure 7.8a shows the majority of the area surrounding the

quartz particle consisting of a sodium-rich silicate phase. Calcium is collected in a discrete area (see Figure 7.8b), which also contained sulphur (not shown), suggesting an embedded CaS particle. The lower bed temperatures used in high steam gasification conditions may have resulted in less reaction between calcium (present as $CaSO_4$ in the ROM coal) and the sodium silicate phase. This is reflected in mineralogical analysis results (Table 7.1), which show that gehlenite is present in reduced quantities, while elevated oldhamite (CaS) content is present in the agglomerates in comparison to typical steam gasification spouted bed experiments.

Elemental distribution of sodium and calcium in agglomerates from the PDU differs from both low and high steam gasification spouted bed experiments. Sodium (Figure 7.9a) and calcium (Figure 7.9b) are each distributed evenly throughout the agglomerate matrix, with silicon also spread evenly throughout this area (not shown). Mineralogical analysis shows that gehlenite and the amorphous phase are present at approximately 5-20% of the total mineral phase analysed, which corresponds with the seemingly similar composition of calcium and sodium silicate in the analysed area. Although the operating temperature in the PDU was held below the agglomeration temperatures for typical steam spouted bed gasification experiments, an enhance mixing of calcium and sodium phases is observed. The reason for this enhanced mixing may be due to temperature excursions in the bed following agglomeration, which would have increased the rate of diffusion of species within the ash. The presence of cristobalite in the agglomerate composition confirms that bed temperatures significantly greater than the recorded operating temperatures were reached. The temperature required for transformation of quartz to cristobalite (i.e. 1470°C; Hall and Insley, 1947) would have rendered silicates such as gehlenite, augite and monticellite as a liquid phase, thereby creating a more homogenous mixture.

Temperature excursions (or lack thereof) may account for the different elemental distributions, and the different mineralogical compositions, existing between low and high steam spouted bed gasification experiments. Table 7.6 shows the temperature conditions before and after defluidisation of runs in which agglomeration and/or defluidisation were detected. This shows clearly that the maximum bed temperatures of runs from typical steam gasification conditions (i.e. <20 wt% steam in the fluidising gas) reached significantly greater values than those under high steam gasification conditions (i.e. approximately 90 wt% steam in the fluidising gas), in which no apparent increase in bed

temperature occurred following defluidisation. Raising the temperature of the inorganic ash mixture would have the effect of increasing the proportion of liquid phase in the ash, and therefore enhance sintering and create a more uniform bulk ash matrix phase in the agglomerates.

An increase in bed temperature following defluidisation may also accelerate reactions taking place between ash species, resulting in more calcium silicate phases and less calcium-sulphur species in the agglomerate structure, as identified by mineralogical analysis. This effect is particularly noticeable with the detection of magnesium inclusions in the agglomerates. Periclase (MgO) is detected under high and even medium steam gasification conditions, but is only available in combination with silica in the low steam and PDU gasification tests, such as in forsterite, monticellite and augite species. The same issue with magnesium is observed in cement chemistry. Only a small amount of magnesium is able to dissolve in silicate phases, with excess magnesium crystallising as periclase (Eglinton, 1987). In contrast, periclase is not observed in blast furnace slag, which is produced at temperatures between 1300 to 1900°C (Dorin, 1992). Instead, magnesium reacts with silica and aluminium compounds under the higher temperature conditions of the blast furnace (Eglinton, 1987).

Table 7.6. Maximum bed temperatures before and after the onset of defluidisation (data for Sets A and B also included in Table 4.6, Chapter 4).

Experiment	Maximum Bed Temperature Before Defluidisation °C	Maximum Bed Temperature After Defluidisation °C
A02	920	954
A03	939	1055
A04	967	1036
A05	915	1042
A06	909	1034
B02	914	963
B05	861	954
B08	887	1023
C01	811	811[a]
C02	791	791[a]
C03	861	861[a]
C05	891	891[a]

[a] No temperature increase following defluidisation.

7.2.3 Operational Factors Contributing to Agglomeration and Defluidisation

Although molten ash formation is a prerequisite for agglomeration and defluidisation to proceed, other operational factors also contribute to these problems. Agglomeration and defluidisation only occurred under certain operating conditions during the 4-hour operating periods in spouted bed and PDU systems. These conditions include:

- Agglomeration and defluidisation was observed when the "high-temperature defluidisation limit" was exceeded, namely when the combination of bed temperature and fluidising gas velocity (hence particle momentum) created significant particle growth and consequently destabilised fluidisation.
- High inorganic content of the bed (>85 wt% of the bed) was present in all cases of typical spouted bed steam gasification conditions where agglomeration and defluidisation occurred.
- Increasing the steam concentration of the gas decreased the minimum temperature required for agglomeration to occur, and also decreased the inorganic content of the bed at which agglomeration was problematic (approximately 60 wt%).
- Operating at higher pressure within the gasifier resulted in agglomeration occurring at lower temperatures than under typical steam gasification conditions in the spouted bed (i.e. 800-850°C).
- No agglomeration was detected in tests in which addition of dolomite to the pure char bed was performed. These tests also coincided with operating temperatures below 800°C.

The mechanisms summarised above affecting the occurrence of agglomeration and defluidisation indicate that control of the phenomena is not dependent on one sole operating factor, but rather a combination of a range of factors that can be used to minimise the impact of agglomeration on gasifier operation. In summary however, successful control of agglomeration and defluidisation is dependent on two main factors, namely the minimisation of liquid phase formation in the ash, and maintaining adequate fluidisation in order to avoid ash sintering arising from low particle movement.

7.3 Control of Agglomeration and Defluidisation during Fluidised Bed Gasification of High-Sodium Content Lignite

Based on the information obtained from both spouted bed and PDU tests, the following set of control guidelines should be implemented to minimise the impact of agglomeration and defluidisation when gasifying Lochiel coal, process requirements permitting. These guidelines include operating:

1. at a maximum bed temperature below 850°C;
2. at operating pressures close to or at atmospheric;
3. with continued removal of ash from the system via a bottom ash screw;
4. with steam concentration of the fluidising gas below approximately 20 wt% (steam in air);
5. with S/F ratios as low as practicable (e.g. below 0.4 wt/wt), while limiting A/F ratio to below 2.5 wt/wt; and
6. with calcium-rich bed additives, such as dolomite.

Note that some of these guidelines may not be appropriate, or possible, to use as an agglomeration control mechanism, with other process requirements governing their ultimate values. The following sections discuss each guideline individually.

7.3.1 Control Factors Affecting Agglomeration and Defluidisation

Limiting Bed Temperature

Bed temperature is the most critical parameter for controlling agglomeration and defluidisation under gasification conditions, as it determines the amount of liquid phase formation occurring in the ash, and hence the viscosity of the ash. Under typical steam gasification conditions in the spouted bed, agglomeration, or at least significant particle growth, was observed in most cases in which maximum bed temperature exceeded 860°C. By operating below approximately 850°C, agglomeration and deposition behaviour of ash during gasification may be avoided, without adverse impact upon output gas composition.

Although operating below 850°C may minimise particle growth under atmospheric pressure gasification, gasifying Lochiel coal at 8 bar pressure in the PDU tests showed agglomeration occurring between approximately 800 and 850°C. Operating at 8 bar in the presence of steam lower the liquidus temperature of sodium disilicate from 874°C to approximately 855°C (Morey and Ingerson, 1938). Thus, operating at higher pressures

may require adjustment of the maximum bed temperature to approximately 800°C in order to avoid agglomeration and defluidisation.

Limiting Operating Pressure

Limiting gasifier pressure to atmospheric conditions will provide a number of benefits to operation. Firstly, as indicated in the preceding section on temperature control, high operating pressure in a steam environment decreases the melting temperature of sodium disilicate. Given that sodium disilicate is a major component of the amorphous phase detected in the agglomerates, the melting point of this species can be maximised by decreasing the operating pressure close to atmospheric pressure. Secondly, high operating pressure increases the cost of auxiliary equipment such as coal feed systems and monitoring equipment (e.g. pressure sensors), and creates additional Occupational Health and Safety issues over those under atmospheric conditions.

A major issue against the use of atmospheric operating pressures is that high operating pressure enables greater coal conversion than that achievable under atmospheric pressure. Lowering operating pressure to atmospheric pressure may therefore not be economically viable for the control of agglomeration and defluidisation for a commercial process. However, operating at a lower pressure of 4 bar yields a sodium disilicate melting temperature of approximately 865°C, while a pressure of 2 bar only reduces the melting temperature to approximately 870°C (Morey and Ingerson, 1938). By operating at these lower pressures, successful operation above atmospheric pressure can be achieved without adversely affecting the liquidus temperature of sodium disilicate. Actual operating pressure will be dependent on required process conditions and economics, but a pressure of between 2 to 4 bar is recommended to ensure that the liquidus temperature of sodium disilicate is maintained sufficiently above the operating temperature of the gasifier.

Limiting S/F and A/F Operating Ratios

Controlling S/F ratio to below 0.4 wt/wt limits the amount of available steam for contributing to formation of low melting point species. As indicated in the chemical analysis of Section 7.2.2, high steam gasification conditions resulted in defluidisation at temperatures significantly below the minimum temperature of defluidisation under typical steam gasification conditions. Air-to-fuel ratio should correspondingly be controlled to

below 2.5 wt/wt in order to avoid agglomeration behaviour of high sodium content coal. Increasing A/F ratio has two main effects, which include:

- increasing the bed temperature; and
- increasing the level of oxygen available to react with the char surface.

Bed temperature has a major impact on whether agglomeration will proceed, and should be controlled to a low level wherever possible. Additionally, a greater reaction of oxygen with the char surface results in a greater rate of char consumption, and hence a greater release of ash into the bed. As noted by Kosminski (2001), ash forms uniformly throughout the char grain in a gasification environment, indicating that the more char consumption occurring, the greater the amount of ash exposed to the gasification environment. Limiting char consumption is not a viable method for controlling agglomeration and defluidisation however, as high char consumption is an important process requirement for optimising the gas yield from the gasifier.

Bed Additives

Adding a calcium- and magnesium-rich species, such as dolomite, to the bed of high-sodium content lignite may increase the sintering temperature of the ash formed in the fluidised bed gasifier by forming a greater proportion of high melting point calcium and magnesium silicates in the ash, and thus contribute to control of agglomeration and defluidisation behaviour. This was shown to be an effective measure in the PDU tests, with no agglomeration detected in any run in which dolomite was used. The additional benefit of using dolomite is that it is effective in sulphur capture from coal containing high sulphur content, which was also demonstrated in the PDU.

In work by previous authors, fine additives, such as aluminosilicate clay, were successfully introduced into a pilot scale fluidised bed combustion process using Lochiel coal in order to control agglomeration (Bhattacharya et al., 1999). This measure was reported to be successful in controlling agglomeration and defluidisation by the fine additives trapping molten ash from the coal in small multiparticle bodies, allowing elutriation of the problematic ash from the bed. Although this is a physical mechanism, and not dependent on the composition of the additive, evidence was found in a 77 mm I.D. spouted bed combustion reactor that showed a reaction was taking place between an aluminium-rich bed material and the Lochiel coal ash coating surrounding the bed particles, which contributed to raising the sintering point of the ash (Vuthaluru, 1999b). Thus, the effect of

additive use in a fluidised bed may control agglomeration via both physical and chemical mechanisms. Note that additives may create additional fines in the gasification system, thereby placing extra load on the gas filtration system, which may create operating problems downstream in the process.

Kosminski (2001) later suggested that addition of aluminosilicates to the bed of a fluidised bed gasifier, with sodium-rich lignite, would cause the sodium to favourably react to form sodium aluminosilicate species such as nepheline, in preference to sodium disilicate. This material may also be an option for additive control of agglomeration and defluidisation, although an aluminosilicate material such as kaolin does not have the same benefit for sulphur capture as does a calcium-containing mineral such as dolomite, making dolomite a preferential additive for gasifier operation with Lochiel coal.

In many fluidised bed systems, a bed material, such as silica sand, is used to assist with fluidisation of the bed and facilitate heat transfer. Such a measure in a fluidised bed gasification environment may be detrimental to gasifier operation with high-sodium lignite however, with the increase in silica content of the bed potentially resulting in a significant increase in silicate melt phase. Kosminski (2001) identified that formation of a sodium disilicate liquid species may dissolve additional silica into the melt phase, thereby forming the sodium disilicate-quartz eutectic mixture. Thus, the use of silica bed material should be avoided altogether, with the use of pure char beds the preferred method of operation.

7.3.2 Other Operational Factors Affecting Agglomeration and Defluidisation

Ash Removal

Bottom bed material removal is a common feature of fluidised bed gasification reactors to control bed height. It also has the added benefit of removing ash from the gasification environment, therefore limiting the amount of inorganic phase available to create particle growth. The ash build-up in the spouted bed gasification experiments may have forced agglomeration under certain conditions, where effective ash removal may have prevented or limited its occurrence. Note however that bed removal was performed in Runs 1 and 2 in the PDU, but were still both affected by agglomeration. In these cases, agglomeration was primarily located at the air/oxygen inlet jets as deposits (Bhattacharya, 2005b), which would have provided the most extreme conditions in the bed for temperature excursions to occur. While not specifically a method for controlling agglomeration and defluidisation,

ash removal from the bottom of the reactor still remains important in limiting the amount of free ash present in the bed.

Steam Concentration

Evidence presented from the spouted bed gasification tests suggests that increasing the content of steam in the fluidising gas, as opposed to S/F ratio, results in a decrease in minimum temperature required for agglomeration to occur. At extreme steam gasification conditions, namely 90 wt% steam in the fluidising gas, agglomeration and defluidisation occurred at bed temperatures approximately 70°C below that experienced in the spouted bed when gasifying with 10 to 20 wt% steam in the fluidising gas. The highest temperatures of agglomeration were recorded in Set A experiments, which were operated at 10 to 13 wt% steam in the fluidising gas. Steam concentration is not specifically a control variable for agglomeration and defluidisation however, but instead is determined by A/F and S/F ratios.

7.3.3 Discussion

Gasification experience with both the 77 mm spouted bed gasifier and the 300 mm PDU indicates that use of lignite that contains high levels of sodium and sulphur for gasification purposes is possible with appropriate manipulation of operating parameters. Of the control parameters used to minimise agglomeration behaviour, steam has the most significant impact on low melting point sodium disilicate formation. The use of steam should therefore be limited as much as practically possible where coals with high sodium content are used in order to control agglomeration and defluidisation behaviour. To further ensure that agglomeration does not occur at temperatures below approximately 850°C, calcium can be added to the bed to raise the viscosity of the ash and minimise particle growth. Thus, by controlling the chemical aspects of the ash, more effective operational control may be achieved with agglomeration and defluidisation behaviour minimised.

One issue that was not addressed in the experiments however was the time aspect of agglomeration and defluidisation. All runs were performed over a time period of approximately 4 hours duration, which was sufficient to observe agglomeration and defluidisation under most conditions. However, some tests that did not show defluidisation did indicate significant particle growth within the bed. It was surmised that such runs might have eventually defluidised if operated for an extended time. This raises the

possibility that other runs which did not show significant particle growth or defluidisation may have also eventually defluidised, although in the case of spouted bed experiments, this may be inevitable given that no bed material removal was performed other than by elutriation. Further, more extensive pilot scale testing should be performed in order to assess the frequency of fluidisation problems occurring over time, using the aforementioned guidelines to minimise agglomeration behaviour.

7.4 Summary

Fluidised bed gasification of high-sodium, high-sulphur content lignite is strongly affected by agglomeration and defluidisation. Agglomeration and defluidisation proceeds with initial particle growth via molten ash formation, which inhibits particle movement in the bed, creating hotspots which exacerbate the formation of extensive ash deposits at the walls of the vessel, and eventually destabilises fluidisation.

Agglomeration is initiated with formation of the sodium disilicate-quartz eutectic, which contains approximately 26 wt% Na_2O. Formation of this species is exacerbated by steam, which lowers the melting point of sodium carbonate – the primary form of organically bound sodium – and facilitates reaction with silica in the coal. Increasing steam content of the fluidising gas lowers the temperature required for agglomeration to proceed by allowing liquid sodium silicate to form at a lower temperature. Increased steam content also suppresses the formation of calcium silicates, which act to raise the viscosity of the ash.

An effective control methodology for minimising agglomeration and defluidisation when gasifying high sodium lignite was discussed. This methodology involves operating with the following settings:

- bed temperature below 850°C;
- operating pressure at 2 to 4 bar;
- steam content of the fluidising gas below 20 wt%;
- steam-to-fuel ratio not exceeding 0.4 wt/wt, and air-to-fuel ratio not exceeding 2.5 wt/wt;

- addition of dolomite to the bed, particularly in the case of lignite with high sulphur content; and
- ensuring that bottom ash removal is performed.

Many of these guidelines are unsuitable to use specifically for controlling agglomeration and defluidisation however, as other process requirements determine their ultimate values. Bed temperature, operating pressure (to a certain extent), and limiting steam in the fluidising gas as much as possible are the main parameters available for limiting molten phase formation in the ash. Additives containing calcium and magnesium species can also be used to raise the level of high melting point phases in the ash, although this measure is determined by cost and availability of the raw material. Adhering to these guidelines will ensure that agglomeration and defluidisation behaviour is minimised effectively, enabling lignite that is currently not utilised in South Eastern Australia to be used for power generation purposes.

CHAPTER 8

CONCLUSIONS AND RECOMMENDATIONS

8.1 Conclusions

8.1.1 Mechanism of Agglomeration and Defluidisation During Spouted Bed Gasification of a High-sodium, High-sulphur Content Lignite

The experimental program showed clearly that agglomeration and defluidisation impacts upon fluidised bed gasification with high-sodium lignite. The fundamental requirements for defluidisation to occur are low superficial velocities and/or high bed temperatures. Under these conditions, the formation of an inorganic liquid phase in the ash causes a sticky coating to form on solid mineral particles from the char, resulting in unstable particle growth. Once the Rosin-Rammler trend line gradient of the bed material reaches a value of between approximately 1.9 and 2.1, defluidisation begins to become an issue to operation.

In the spouted bed, defluidisation occurs with reduced particle movement in the annulus, or the close-packed region of the bed, due to inter-particle interactions between coated mineral particles. Reduced relative particle movement results in a reduction of measured pressure difference between the top of the bed and below the distributor. Hot-spots also form in the bed, and cause temperature excursions. As the bed temperature increases above the steady-state temperature, the rate of ash sintering increases, causing coalescence of ash particles into larger ash deposits that form at the walls of the bed. Thus, defluidisation is caused by an increase in particle size via agglomeration, which in turn causes agglomerates to coalesce into larger sintered ash bodies.

Aside from bed temperature and superficial velocity, other operating conditions also contribute to defluidisation in the fluidised bed gasification environment. Increasing operating pressure reduces the temperature required for defluidisation to occur. High-sodium, high-sulphur content lignite from the Lochiel coal deposit in South Australia demonstrated defluidisation behaviour under temperatures as low as approximately 860°C under atmospheric pressure conditions, and at temperatures in the range of 800 to 850°C under 8 bar pressures. Steam content of the fluidising gas also influenced the minimum temperature at which defluidisation occurred. At extreme gasification conditions, with the fluidising gas containing approximately 90 wt% steam, defluidisation occurred at temperatures as low as approximately 790°C.

The inorganic content of the bed also contributes to defluidisation, with increasing ash content resulting in a greater contact area for inorganic particles. All typical-steam runs exhibiting defluidisation behaviour in the spouted bed possessed bed char inorganic contents exceeding 85 wt%. The high inorganic content in the bed char, relative to the feed coal, is a result of ash build up in the bed due to the absence of a bed material removal mechanism. The inorganic content of bed char from high steam spouted bed runs that showed defluidisation behaviour was found to be as low as 60 wt% of the total bed mass, indicating that a lower contact surface area is required for agglomeration to occur as the melt phase in the ash increases.

The species responsible for initiating molten ash formation and defluidisation during gasification of high sodium, low-rank Lochiel coal differed from that causing agglomeration under fluidised bed combustion conditions. Eutectic mixtures of sodium-calcium-magnesium sulphate mixtures are responsible for coating bed material in fluidised bed combustion reactors, while agglomerates from the gasifier environment predominantly consist of silicate mixtures. Deposits containing high levels of sulphur were found in the spouted bed gasifier under typical steam gasification conditions, but only on the conical distributor at the gas inlet to the bed, and did not appear to take part in the agglomeration mechanism. These sulphate deposits were similar in composition to the bed material coatings found under combustion conditions (Manzoori, 1990), and demonstrated the impact of sodium on agglomeration under combustion conditions, with increasing sodium sulphate content in the deposits resulting in greater levels of sintering in the deposits.

In the gasification environment, sodium reacts with silica from the coal to form amorphous sodium silicate mixtures, consistent in composition with the sodium disilicate-quartz eutectic (approximately 76 wt% SiO_2). The reaction occurs as a result of sodium diffusing into the silica, creating a sodium silicate glass phase, and formed consistently under all gasification conditions tested in the study. Sodium/silica ratios in agglomerates and bed char remained consistent at approximately 0.2, regardless of gasification operating conditions, suggesting that the temperature of agglomeration does not decrease with increasing levels of sodium silicate. Instead, calcium, magnesium, and aluminium silicate species decrease in the agglomerate composition as the temperature of defluidisation decreases.

Sodium silicate glass mixtures containing similar compositions to the sodium disilicate-quartz eutectic were found to form extensively throughout the agglomerate structures from high steam gasification conditions (i.e. 90 wt% steam in the fluidising gas). Agglomerates from more typical steam gasification environments possessed higher contents of calcium and magnesium silicates and aluminosilicates, a result of greater reaction between SiO_2 and CaS/SO_4, MgO and aluminosilicate species in the coal. These silicates possess significantly higher melting points than that of the sodium silicate species, and as such are not likely to have initiated the agglomeration observed under the temperatures used in the experimental program.

The eutectic melting point of the sodium disilicate-quartz eutectic species is approximately 790°C. This temperature corresponds to the lowest temperature at which defluidisation was observed under the extreme steam gasification conditions, in which calcium and magnesium silicate species were relatively low in comparison to the sodium silicate species in the agglomerates. The identification of the sodium disilicate-quartz eutectic in agglomerate structures corresponds directly with findings by Kosminski (2001), who predicted that this species would cause agglomeration problems in a steam gasification environment.

8.1.2 Control of Agglomeration and Defluidisation During Spouted Bed Gasification of a High-sodium, High-sulphur Content Lignite

The influences on agglomeration and defluidisation, as indicated in Section 8.1.1, provide methods for controlling agglomeration and defluidisation during the fluidised bed

gasification of high-sodium lignite. Bed temperature is the critical parameter, which should be maintained as low as practicable, subject to process requirements. This in turn demands that air-to-fuel ratio should be maintained at lower values in order to limit the amount of oxygen reacting with the char, which creates heat in the bed. Bed temperatures below approximately 850°C (at atmospheric pressure) should be used in order to avoid unstable particle growth in the bed, which results in defluidisation.

In order to raise the minimum temperature of defluidisation of the bed, the formation of calcium and magnesium silicates in the coal ash should be promoted. This entails that steam-to-fuel ratio should be limited in cases where high-sodium coals are used, to allow reactions between calcium and magnesium species and silica to proceed to a greater extent, and correspondingly limit the proportion of low melting point sodium glass in the ash phase. A maximum steam-to-fuel ratio of approximately 0.4 wt/wt at atmospheric gasification conditions is an appropriate limit to achieve this aim. Another method that may prove successful in promoting calcium and magnesium silicate formation is via the use of bed additives such as dolomite. Dolomite contains high amounts of calcium and magnesium carbonate, which may promote reactions with silica in the coal to form high melting point species in the ash. The use of additives may be governed by other process considerations however, such as the handling of additional fines downstream in the filtration system. Given that silica contributes to melt phase formation in the gasification environment, the use of silica bed material to enhance fluidisation in the bed should also be avoided.

Operating pressure should be limited as much as possible to maximise the temperature of agglomeration with the fluidised bed gasification of high-sodium lignite, given that the melting point of sodium disilicate decreases with increasing pressure (Morey and Ingerson, 1955). Practical process considerations of maximising coal throughput may make such a measure unviable for controlling agglomeration however. Thus, if high pressures are required for the gasification process, maximum bed temperature should be maintained below approximately 800°C to avoid agglomeration and defluidisation.

Overall, fluidised bed gasification of lignite containing high levels of sodium in the ash appears to be viable for commercial gasification operations, although provides a major challenge for fluidised bed gasifier operators. Provided that the guidelines outlined in this

section are adhered to wherever process considerations permit, gasification with high-sodium lignite may be possible. This will enable currently unused reserves of lignite in South Eastern Australia to be utilised for efficient power generation, providing an extra valuable fuel resource for generations to come.

8.2 Recommendations

Future work arising from the current study should focus on more extensive pilot-scale testing of high-sodium lignite under gasification conditions. Experiments using dolomite as a bed additive should be performed over a wider range of bed temperatures, in particular at temperatures exceeding 800 to 850°C, in order to assess whether the additive does impart a chemical control mechanism for molten phase formation in the ash. More extensive variation of operating pressure should also be performed in order to properly assess the impact of pressure on the minimum temperature of agglomeration.

The findings of this study should also be applied to other lower-quality coal deposits, which may contain higher levels of sodium and sulphur, to determine whether the chemical mechanisms are altered with different sodium contents. The scope of the study could also be extended to other forms of fuels, such as biomass, which possess larger contents of potassium in the inorganic matter. The impact of steam on the minimum agglomeration temperature of biomass would be of particular benefit to its use in gasification reactors.